INVESTIGATION OF THE EFFECTS OF PROCESS PARAMETERS ON PERFORMANCE OF GRAVURE PRINTED ITO ON FLEXIBLE SUBSTRATES

A Thesis

Presented to

The Academic Faculty

by

Joel Emerson Neff

In Partial Fulfillment

of the Requirements for the Degree

Master of Science in Mechanical Engineering in the

Woodruff School of Mechanical Engineering

Georgia Institute of Technology

August 2009

INVESTIGATION OF THE EFFECTS OF PROCESS PARAMETERS ON PERFORMANCE OF GRAVURE PRINTED ITO ON FLEXIBLE SUBSTRATES

Approved by:

Dr. Shreyes Melkote, Advisor

School of Mechanical Engineering

Georgia Institute of Technology

Dr. Steven Danyluk

School of Mechanical Engineering

Georgia Institute of Technology

Dr. Samuel Graham

School of Mechanical Engineering

Georgia Institute of Technology

Date Approved: May 4, 2009

ACKNOWLEDGEMENTS

I would like to thank the many people who made completion of this thesis possible. First and foremost I would like to acknowledge my wife, Julie, who has given me unwavering support in my decisions, and given me counsel and encouragement when I most needed it. I would also like to thank my parents for always encouraging me to pursue my education and for always providing wisdom, love, support, and guidance throughout my life. I would also like to acknowledge my advisor, Dr. Melkote, for always being committed to helping me succeed. His patience and support have made my time at Georgia Tech a great experience, and it has been a pleasure to work with him. I want to thank Dr. Danyluk, for his continuing financial support of the research, and for the dedication he has shown to me, as he has to all of his students. Special thanks needs to be given to the Center for Organic Photonics and Electronics (COPE) for their partial funding of my research and for the people who have been willing to assist me in taking data and giving invaluable advice during the course of my research. I would like to mention specifically Dr. Kippelen, Canek Fuentes, and Michal Malicki for their invaluable assistance in gaining access to the required equipment, and for their time spent assisting me. I need to also acknowledge Dr. Kalaitzadou for her help in using the ARES, and for her advice and support. I also want to acknowledge Dr. Graham and Roderick Jackson for their insights, experience, and support. I want to thank Steven Sheffield for his help in many different aspects of my research, and for his advice and interest in my project. I finally want to thank the many others who have given their advice and support, and with whom I have gained a greater appreciation and perspective of engineering. This

includes my fellow students, the PV group, faculty members, and staff. These people are too numerous to mention but have made my experience at Georgia Tech richer and more enjoyable.

TABLE OF CONTENTS

LIST OF TABLES

LIST OF FIGURES

SUMMARY

Gravure printing is a conventional printing process used for printing graphics on products ranging from magazines and packaging to wallpaper and floor coverings. It is a versatile process that can be used to deposit a variety of fluid materials onto many different surfaces. It is also capable of very high speed deposition, with speeds up to 60 m/min being reported. Because of its versatility and high throughput capability, gravure is an attractive platform for the manufacture of devices composed of relatively thin layers of functional, electronic materials deposited onto flexible substrates. In many cases, these materials can be deposited in liquid form, in which case gravure printing can potentially be used. One such material that is commonly used is Indium Tin Oxide (ITO), a transparent, conducting ceramic material. It is commonly deposited onto flexible, transparent polyethylene terapthalate (PET) films that can be used in flexible displays, solar cells, and other devices requiring a transparent, conducting layer.

This thesis examines the effect of key process parameters on the physical and functional characteristics of a printed ITO nanoparticle layer. ITO layers were successfully printed that were between 300 and 1300 nm thick, with roughness R_a generally less than a few hundred nm. The sheet resistance values were relatively high, in the hundreds of kΩ/□. The transparency was relatively low, although the films were generally transparent. Several parameters were found to be significant in affecting the several different physical and performance measures, specifically solvent and ITO content, as well as cell geometry.

CHAPTER 1

INTRODUCTION

Electronic devices fabricated by depositing thin patterns of functional material onto a flexible substrate have the potential to replace many traditional electronic devices. These flexible electronic devices are more physically robust than their traditional counterparts and are finding use in ever-increasing numbers of applications. Furthermore, some of these devices can potentially be manufactured using high volume, low cost processes such as printing. High speed, continuous, roll-to-roll printing processes could be used to manufacture everything from RFID tags to organic solar cells and flat panel displays.

Attempts to manufacture thin film and flexible electronics currently employ high cost, low volume processes such as physical and chemical vapor deposition, sputtering, and spin coating. These methods typically give precise control of parameters such as thickness and surface morphology, and are capable of depositing high purity materials onto a substrate. However, these processes are often expensive or impractical for high volume production. Although using a lower cost process may not offer the same quality as the more traditional thin film processes, better materials are continually being developed and more robust designs are being presented. Thus it is conceivable that at least in some applications, a conventional high volume printing process could be used for deposition of certain materials and used to manufacture entire electronic devices. Furthermore, with a focus on printing processes as a manufacturing platform for electronics rather than graphic media, further advancements in process refinement and

control may be possible. One need only imagine a newspaper-type printing press rolling out sheets of functional electronic circuits or flat panel electronic displays at high speed to realize the transformational potential of using a printing platform to manufacture electronic devices.

The gravure printing process is one such high volume printing process that may be suitable as an electronics manufacturing platform. It is a commonly used process that is used for printing graphics on products ranging from magazines to floor coverings. It is capable of very high throughput and can be used to print various types of inks onto many different substrates. However, it has not traditionally been used to print functional electronic materials. Most previous work in gravure printing has been focused on issues relating to print quality in graphics printing, which may have little relation to the functional requirements for electronics manufacturing.

One of the primary characteristics of any printing process is the ink or material that is to be printed. The most obvious requirement for this material is that it must be a liquid and thus be able to flow at ordinary process temperatures. In addition, the material must be able to adhere to the surface it is being printed on, and have a mechanism for stabilization or solidification after deposition. In order to meet these requirements using a functional material, however, some tradeoffs may be required. For example, inorganic solids can be deposited in liquid form in the form of micro- or nanoparticles suspended in a liquid polymer solution, but the resulting printed layer will almost certainly not have the same functional properties of the bulk inorganic solid. In addition, additives that can improve printing in graphics printing inks may be detrimental to the performance of functional materials.

Indium tin oxide (In_2O_3:Sn, ITO) is a transparent, conductive oxide that is commonly used in the production of thin film solar cells, displays, and other devices which require a transparent yet conductive material. It typically functions as a transparent electrode in such devices. ITO is usually deposited using traditional thin film deposition processes such as sputtering. Deposited layer thickness generally ranges from a few tens to a few hundred nanometers thick. The sheet resistance ranges from a few to a hundred ohms per square. ITO has very good optical and electrical properties. However, it is also very brittle and is therefore more susceptible to cracking when deposited on flexible substrates. In order to reduce the processing cost of ITO thin films, several methods have been proposed. One method is to deposit ITO nanoparticles in solution in a thin layer using a liquid-based deposition process such as printing. The resulting ITO film is much cheaper to produce and can also be made less brittle than with traditional deposition processes, due to the resulting discontinuous material structure. The ITO could also be deposited with other materials such as a polymer that forms a robust, flexible matrix around the nanoparticles. However, the optical and electrical performance decreases significantly when using this approach.

1.1 Objectives

The objective of this research is to investigate the effect of certain process parameters in gravure printing on the properties of a printed ITO nanoparticle-based thin film. Key process parameters, such as process speed, gravure cell geometry, and ink parameters will be related to the properties of a deposited layer of ITO nanoparticles. The effects of the parameters on properties including thickness, roughness, transparency, and

conductivity will be investigated. A physical explanation of the effect of the various process parameters on printed ITO layer properties will then be presented, based upon prior work and observations encountered in this study.

1.2 Motivation

The primary motivation for this work came from the work currently being done in the field of organic photovoltaics (OPV). This is a nascent field with a lot of potential for growth as photovoltaic conversion efficiencies and device lifetimes improve. OPV is a broad term that refers to any of a variety of different technologies in which an organic, i.e. carbon based material such as a polymer is used to achieve the photovoltaic effect. Perhaps one of the greatest potential advantages of OPV is the possibility of low cost processing of the materials used to produce solar cells, including the potential to use low cost printing processes for manufacturing. Even if solar conversion efficiencies or device lifetimes do not meet those of traditional silicon-based solar cells, a dramatic decrease in the cost of these devices may compensate for those deficiencies. This would make solar power more competitive with traditional energy sources.

It should also be noted that there are many other types of electronics which may benefit from this research, including non-organic thin film PV technologies. However, since most inorganic materials used in electronics manufacture are metals or oxides that are not liquid at ambient conditions, these technologies require special adaptation. One goal of this thesis is to address some of these issues. Organic materials are more easily processed as liquids and therefore a wet processing method is more appropriate for

immediate implementation. In addition to PV, other thin film electronic devices such as displays, RFID tags, and even thin film transistors could potentially be printed onto flexible substrates using low cost processes such as gravure.

1.3 Outline

This thesis is organized as follows. Chapter 2 is a literature review that reviews the gravure process and contains a survey of the relevant research that has been done on gravure printing, and especially gravure printing of electronic materials such as ITO. Literature related to ITO and printed electronics in general is also reviewed. Chapter 3 includes a description of the experimental approach for a screening experiment and an explanation of process parameters and metrics, as well as measurement methods and general assumptions. It also contains the results of the screening experiment. Chapter 4 presents the approach and results of the main experiment and provides analysis of the data. Chapter 5 presents a further analysis of the data based on fundamental parameters not included in the experiments. Chapter 6 summarizes a mechanistic description of the gravure process that provides justifications for some of the explanations given in the analysis of the data. Chapter 7 includes discussion and conclusions of the research, as well as recommendations for further work.

CHAPTER 2

LITERATURE REVIEW

This chapter will provide an overview of gravure printing and previous research in the areas of both gravure printing and printed electronics. Previous work on ITO nanoparticle-based film will also be reviewed. As part of the motivation for this work was to investigate manufacturing platforms for photovoltaic technologies, an overview of organic solar cells and the use of ITO in such devices will also be presented.

2.1 Gravure Printing

Gravure printing is an *intaglio* printing process, meaning that the pattern to be printed is engraved into the surface of a printing form, so that the pattern to be printed is recessed below the surface. The pattern is filled with ink, and the surface subsequently wiped clean, or *doctored*, leaving ink only in the recessed image. Paper or other substrates are then pressed onto the inked image, and the ink from the pattern is then transferred onto the substrate [1]. The ink then dries or cures and the process can be repeated. This section will identify and explain the gravure process in more detail.

2.1.1 Gravure Printing Processes and Configuration

Rotogravure printing is the most common gravure based process in use today. In rotogravure, the pattern is engraved on a metal roller, allowing the pattern to be printed continuously. A schematic of the process is shown in Figure 2.1. A modern graphics press typically has at least four different printing heads for the traditional CMYK (cyan, magenta, yellow, key (black)) color separation, with the heads connected in series [1].

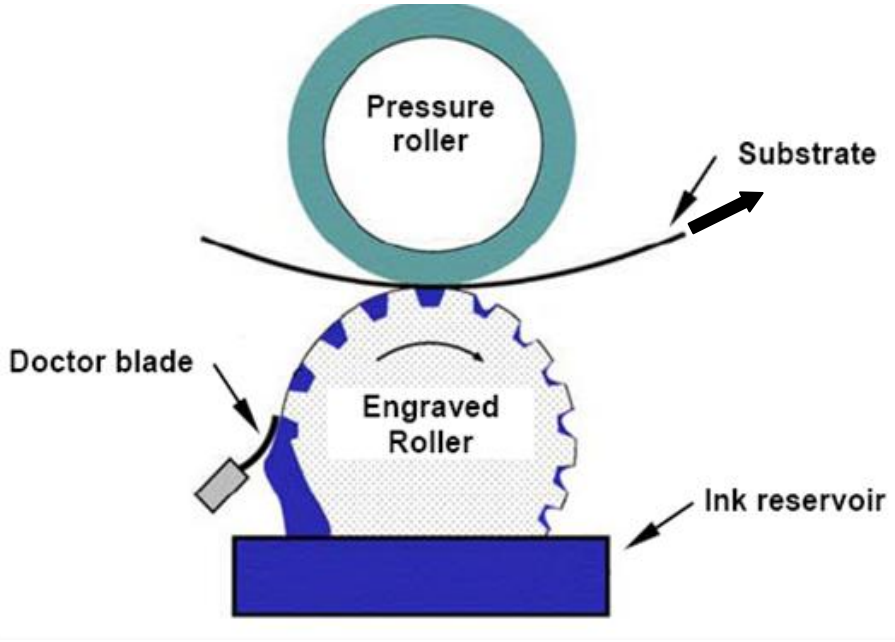

Figure 2.1: The gravure process in rotogravure configuration [2]

The engraved gravure roller typically picks up ink from a reservoir, which is then doctored by a flexible blade that is kept in contact with the roller. The blade also oscillates back and forth across the roller, ensuring uniform blade wear and complete doctoring. The substrate then comes into contact with the roller and the ink is printed onto the substrate. A soft impression roller is often used to force the substrate into intimate contact with the gravure roll. The gravure roller then rotates back into the ink reservoir, and the process continues [1].

The gravure printing process is relatively simple, yet quite versatile. A wide range of inks can be printed onto almost any substrate. In addition to traditional products, such as magazines and newspaper inserts, gravure has been used to print patterns on diverse products such as wallpapers, product packaging, and floor coverings. In all of these

applications, gravure is considered to be one of the highest quality printing processes, achieving high print quality consistently, even on lower quality paper and other substrates. However, because of the cost of engraving the gravure roll, it has traditionally been used on products with very large print runs, where the "per unit" cost can be reduced to an acceptable level. Further development in engraving technology may reduce this limitation [3].

There are several variations of gravure printing. One variation is gravure offset printing. In gravure offset, the image is printed onto an intermediate offset roller before being transferred to the substrate. The process is illustrated in Figure 2.2. The main advantage of this process is that it allows printing onto curved or other non-flat surfaces due to the flexibility of the offset roller compared to the stiff engraved roller [3].

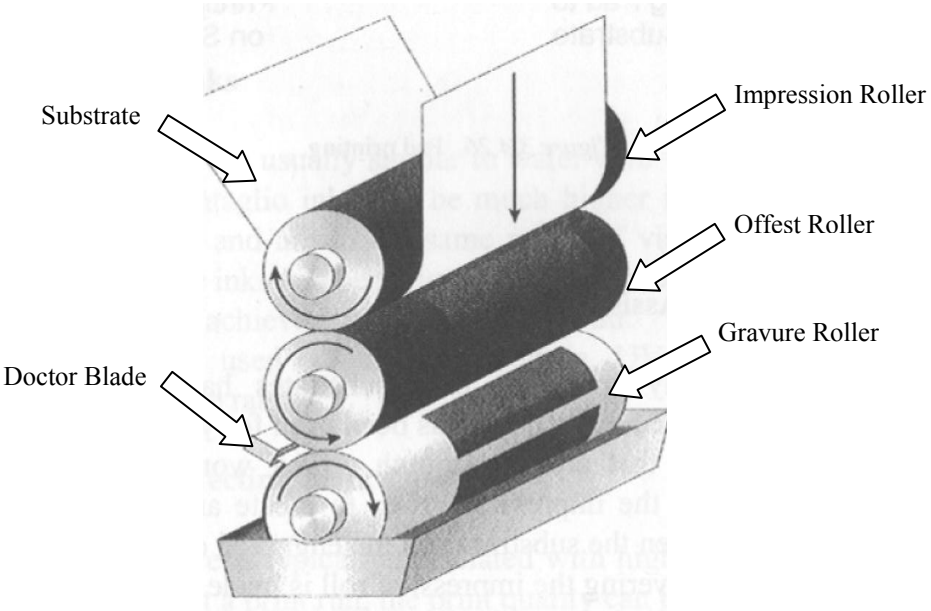

Figure 2.2: Gravure rotary offset printing [3].

Another variation of gravure printing is gravure coating. This process is used for applying thin, uniform layers of ink or other liquid onto a substrate using a gravure roller. The gravure roller has cells engraved uniformly over the entire surface, and the cells are filled as the roller passes through as reservoir, as in other forms of gravure printing. The ink is then transferred either to an intermediate rubber roller before transferring to the substrate (offset gravure coating), or transferred directly to the substrate (direct gravure coating) as illustrated in Figure 2.3. The substrate can move across the roller in either the reverse direction of the roller rotation or in the forward direction at a different speed than the roller. An impression roller is typically not used in this case.

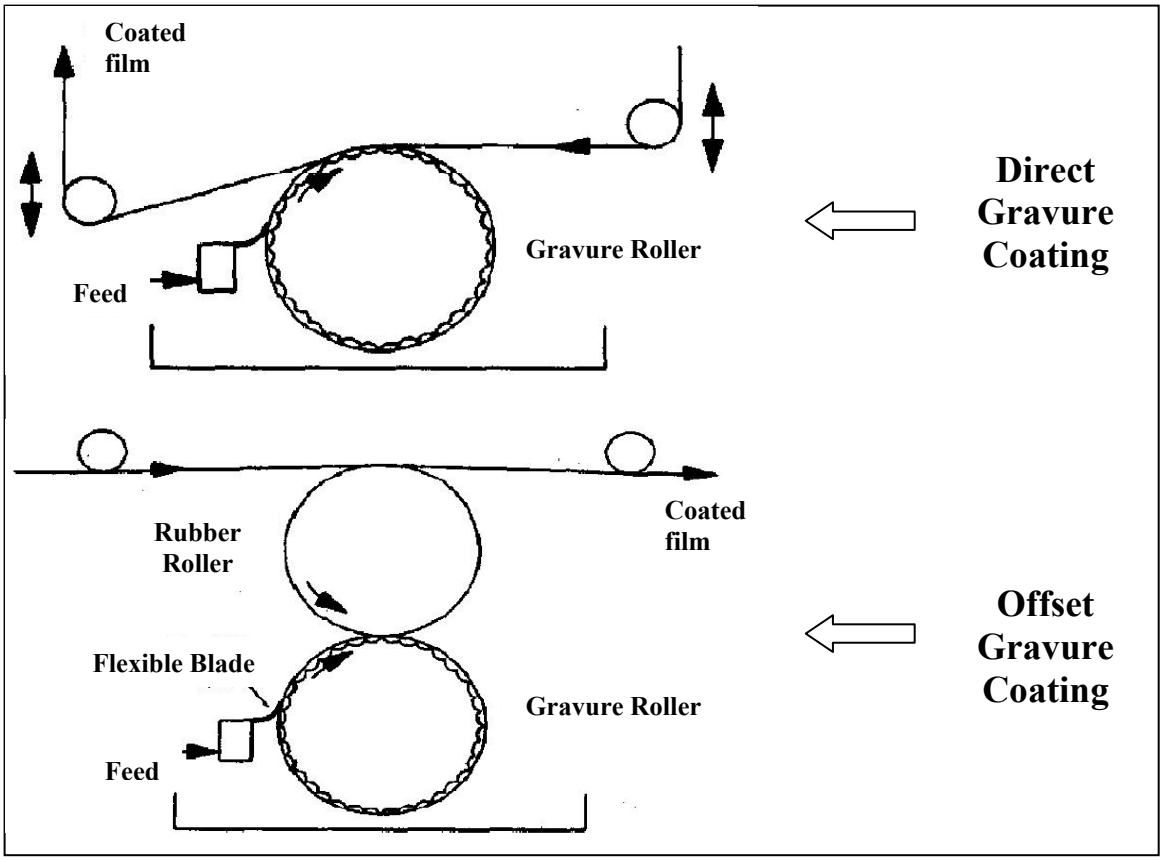

Figure 2.3: Direct and Offset Gravure Coating [4]

The ink is transferred by hydrodynamic forces resulting from the constant shearing of the ink at the point of contact as the substrate passes over the roller at differential speeds [4]. In this way, gravure coating is different than gravure printing in that there is an additional shearing action that acts to transfer ink. Because of the differential speeds of the roller and the substrate, gravure coating is only used to apply thin, uniform films, and has not been used to deposit graphics or complex patterns. However, it does offer several advantages characteristic of gravure printing, such as high speed and low cost, for the deposition of thin, uniform layers of material.

2.1.2 Gravure Cell Engraving and Parameters

The earliest gravure printing was performed in the 15th century. This process consisted of engraving an individual image by hand, and subsequently inking the image and placing paper in contact with the ink. The engraving was very difficult because certain features could not be reproduced accurately or consistently. The solid tones in the image were engraved deeper and wider to accommodate more ink, and there was often difficulty in controlling the transfer of ink from these engravings to ensure a good print. In the 19th century, the half-tone gravure was developed. This invention allowed the images in the engraving to be broken up into discrete cells of relatively uniform size. With half-tone gravure, the cells are arranged to reproduce different shades of a certain color ink, i.e. the cells can be packed closely together to form solid printed features or spread further apart to create a lighter-colored feature [1]. One of the main benefits of half-tone gravure is that the printing of ink can be controlled to give uniform feature size and location. Rather than relying on ink transfer from complex engraved geometries, the

discrete cells can offer more consistent and reliable results. Figure 2.4 shows a traditional gravure engraving, compared to a half-tone pattern.

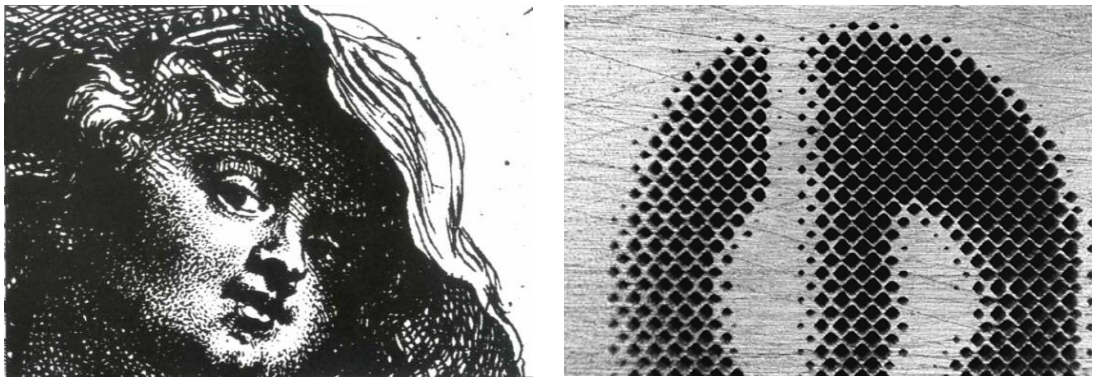

Figure 2.4: Comparison of etched and halftone gravure [1]

Another major benefit of halftone gravure is that the desired pattern can be converted into a digital image and then engraved using automated equipment, cell by cell. The engraving process is analogous to inkjet printing, in which a digital image is printed dot by dot, rather than all at once from a complex pattern. The immediate benefit is that the engraving process for halftone gravure is extremely fast and flexible. The automation of the engraving process makes the process more economical [1].

Gravure cell engraving can be accomplished using several different methods. Traditional engraving was done by hand by skilled craftsmen. Chemical etching was the next process to be developed, and is still in use today. Modern chemical engraving typically involves creating the pattern in a resist layer. The gravure cells are then etched as the resist protects the non-image areas of the metal surface. The resist is subsequently removed [1]. The chemical etching process is shown in Figure 2.5.

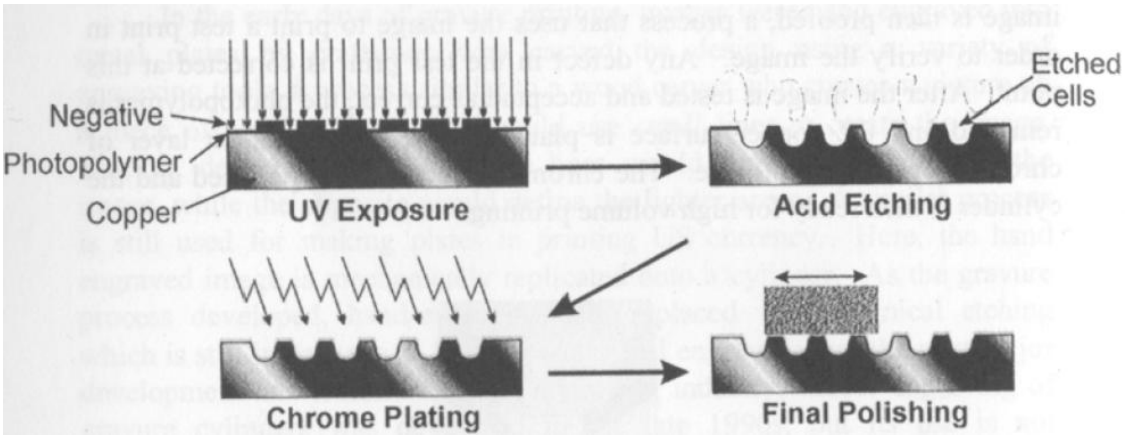

Figure 2.5: Chemical etching of gravure cells [3]

The next major advancement came with electromechanical etching. In this process an electromechanical head with a diamond stylus is vibrated against a rotating gravure roller, cutting individual cells into the surface. Modern methods allow for the control of the head to be linked to a digital image, allowing for quick reproduction of an image into an engraved pattern. Electromechanical engraving is currently the most widely used engraving process [3]. Direct laser ablation is another engraving method that has only recently been developed. In this process a laser is used to directly pattern the cells into the metal. Since most gravure cylinders are made of copper, which does not absorb the laser energy well, zinc is used on top of the copper to form an engraved layer. Due to its high cost, laser ablation is not yet widely used [3].

Since electromechanical engraving is the method used to engrave the pattern used in this study, a more detailed description of the engraving process will now be given. The cells are engraved using a diamond stylus, and assume an inverted pyramid shape below the surface (see Figure 2.6).

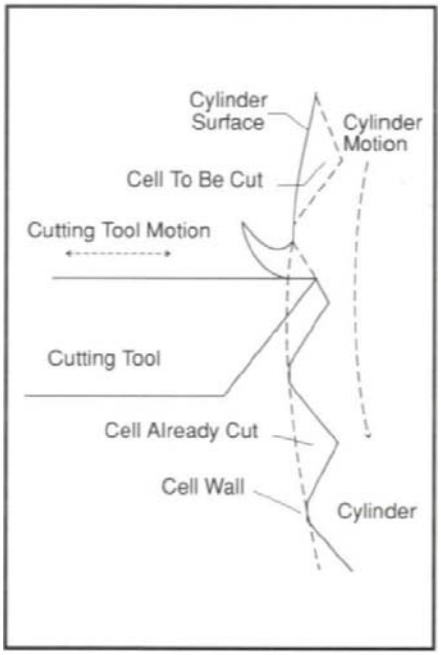

Figure 2.6: Electromechanical gravure cell engraving [1].

The cells are engraved in rows, with larger cells often being connected by small channels due to the stylus not being brought out of contact with the surface (see Figure 2.7). Adjacent rows are advanced by half a cell, so that the cells in adjacent rows can be "nested" together. For non-image areas and light tone areas, the stylus either does not engrave or only engraves into the surface very lightly. The spacing between rows of cells is typically kept constant, so that the only way to change the tone or size of the cells is to control the cutting depth. The spacing of the rows is called the line screen, and is typically specified in lines/inch or lines/centimeter [1].

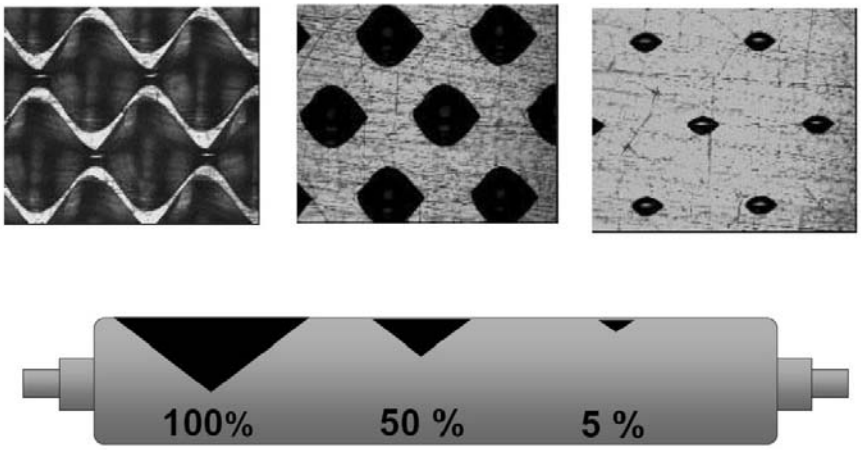

Figure 2.7: Electromechanically engraved gravure cells [5]

The tone is defined as the proportion of engraved area relative to the total surface area and ranges from 0 to 100%. In theory, cells at 100% tone would have no space between the edges of adjacent cells, while 0% tone would represent a smooth surface, with no cells engraved. In practice, cells specified at100% tone must have at least some area between cells in order to support the doctor blade during doctoring. It is also very difficult to control the spacing with such small cells, so even cells specified at 100% tone may have up to 20% of "bridge" area, i.e. non-engraved areas between cells (see Chapter 5 for details). This is also called the cell wall [1].

In a typical engraving setup, a diamond stylus is chosen with a specified geometry. The geometry is typically characterized by the stylus angle, which describes the sharpness of the stylus and the relative shape of the engraved cell. In general, the lower the stylus angle, the sharper the stylus, and therefore a deeper cell will be engraved. For a given line screen and tone, the size of the cell opening should be a constant, with different stylus angles changing the internal depth and size of the cell.

By specifying these three parameters, line screen, tone, and stylus, the size and shape of the cells can be controlled. For graphics patterns, a line screen and stylus may be specified, with the tone determined by the tone required by the image and color (CMYK) to be printed by the gravure engraving. Higher resolution images and features may call for a higher line screen (i.e. smaller cells), while some substrates or inks may require certain sizes or shapes of cells to optimize print quality, ink usage, and wear of the gravure image carrier [1].

2.1.3 Gravure Inks

Gravure inks are typically composed of four basic components: solvent, colorant, ink vehicle, and additives. The purpose of the colorant is to provide color. The ink vehicle disperses the colorant and provides printing and end-use properties of the ink. It contains resins and other materials that can be used to bind the colorant when the ink dries. The solvent dissolves the resins in the vehicle and can be used to alter the drying or printing characteristics of the ink. Additives can be used to achieve a specific performance of the ink and include materials such as wax, surfactants, and corrosion inhibitors [3]. A typical gravure ink composition is shown in Figure 2.8.

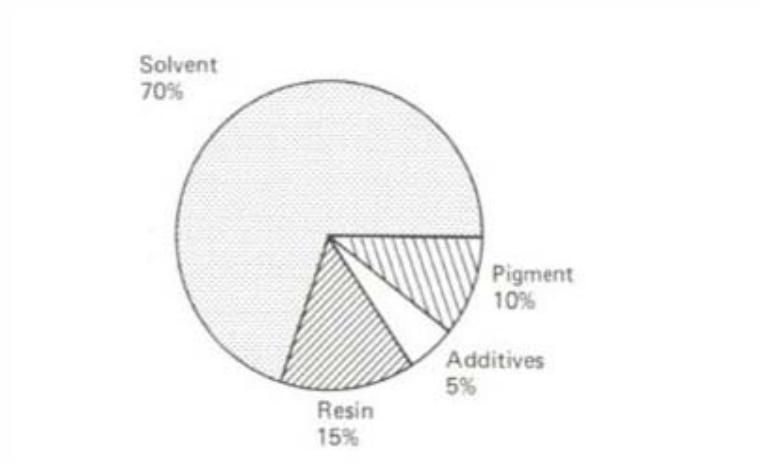

Figure 2.8: Typical press-ready ink composition [6]

Gravure inks typically have very low viscosity. This is in part due to the need for the ink to be able to quickly fill the gravure cells as the image carrier travels through an ink fountain at high speeds. In the gravure process, the ink typically dries very quickly after being deposited, so that the image can move to the next printing station without being altered. Additional drying systems are often used to increase drying speed [6].

Due to environmental concerns, gravure inks may be water-based, so as to avoid volatile organic compounds (VOCs) found in many industrial solvents. When VOCs are used, expensive environmental process controls are imposed. The use of radiation (UV, infrared, etc.) to cure inks containing photo-initiators can also help reduce environmental concerns. There are many different formulations for gravure ink. The formulation depends on the application, and because of the many different products that can be produced using gravure, there are many different considerations to be taken into account, from the substrate characteristics to the level of print quality desired [6].

2.1.4 Impression Roller

The primary function of the impression roller is to guarantee proper ink transfer from the gravure image carrier by ensuring the substrate comes into sufficient contact with the ink in the cells. The roller is typically a solid core covered in a rubber or other compliant material. As the pressure on the impression roller increases, the area of contact between the gravure roller, substrate, and impression roller also increases. This area of contact is often referred to as the printing nip. More pressure is typically required for stiffer substrates to ensure intimate contact between the ink and substrate. However, increasing the pressure can also increase the energy required to operate the press, as well as cause heat buildup in the press that can affect print quality. An increase in the contact area also affects the "dwell time", or the time for which it takes a point to completely pass through the printing nip. This time may affect the transfer of ink from the gravure cells, especially at high speeds [1].

2.1.5 Doctor Blade

The purpose of the doctor blade is to remove excess ink from the gravure image carrier. The blade is typically a thin, flexible blade made of steel or in some cases, plastic. There is a load applied to the blade to keep it in constant contact with the image carrier. Typically the blade oscillates back and forth across the length of a gravure roller as it rotates. This keeps contaminant particles from getting caught under the blade and gives a more uniform wear on the blade. If there is insufficient load on the blade, the hydrodynamic force of the ink may cause the blade to lift and separate from the image carrier, and allow a film of ink to penetrate under the blade. Therefore sufficient pressure

must be maintained on the blade to ensure proper doctoring, although the increased load will also cause the blade to wear more quickly [1].

2.1.6 The Gravure Press

A typical gravure press configuration is shown in Figure 2.9. The press consists of several printing stations arranged in series, with large ink drying systems on each. One of the challenges in a large press is keeping the ink properties constant. As time goes on, the solvent-based ink will evaporate some of its solvent and its temperature will rise. Both of these factors will tend to change the viscosity of the ink, which may affect print quality. Another issue in gravure printing is the issue of registration. As a single image is printed with a different color at each station, there is often a misalignment of images caused by differences in tension in the substrate or misalignment of rollers. Automated tensioning systems and other measures are used to combat this problem [1]. As with any piece of large industrial equipment, there are several issues with printing on a large scale, including the control and monitoring of ink properties, wear of components such as gravure image carriers and doctor blades, and a buildup of heat which may cause irregularities in the printing process.

Figure 2.9: Large rotogravure printing press [1]

2.2 Prior Research in Gravure Printing

Gravure printing has been used for many years for the production of graphics-based products, from publications to product packaging. As such the early research in gravure printing tended to focus on the problem of printing ink onto paper. This later expanded to include printing onto non-paper substrates and eventually onto virtually all other types of substrates. Many aspects of the process have been studied, from cell engraving technologies to ink chemistry and rheology. However, much of the prior research has been limited to industrial development and as such there is limited published literature available. There have, however, been several relevant studies to the current work presented in this thesis. These studies have been both theoretical and experimental in nature, and are presented here.

2.2.1 Theoretical Studies

Although gravure printing is a relatively simple process conceptually, there are many practical issues to be considered. Especially when gravure printing is performed on industrial scale presses, there are many factors relating to the process that can be analyzed. The handling of the substrate, or "web", within the press is critical to ensure accurate registration of printed images between different color printing stations. The drying of ink requires a careful optimization of ink formulation, press speed, and environmental control systems. There are many other factors to be addressed as well, depending on the product to be printed. However, many of these issues are common to all printing processes. In gravure printing, most theoretical work has addressed the issues unique to gravure printing. Specifically, the transfer of ink from the gravure cell to a substrate is among the least understood, yet most important problems in the process. It is a large problem involving complex ink flows at the microscopic level, moving contact lines and a continuously changing ink composition due to solvent evaporation.

Joyce and Fuchs [7] applied a previous model for ink transfer in letterpress printing to the gravure process. They found that the letterpress model could be reasonably applied to gravure. The model predicted ink transfer as a function of certain parameters, including substrate properties and ink viscosity. Their conclusions were that substrate type had an important influence on ink transfer, with paper substrates having greater ink transfer, most likely due to the absorption of ink. They also found that lower ink viscosity led to higher ink transfer on paper substrates, most likely also due to the absorption of ink and the resulting capillary flow of the ink during transfer. Their three-parameter equation and subsequent validation related gravure ink transfer to the area of ink in contact with

the substrate (controlled by the type of gravure etch), ink viscosity, and the nature of the substrate (i.e. absorbent paper vs. non-absorbing foil). Their analysis was limited to a series of special, slow-drying inks at constant roller pressure, speed, and doctor blade angle and speed. Their model was validated to within 4% of calculations, with some experimentally-determined fitting parameters.

Bery [8] developed a physical model of ink transfer on non-absorbing substrates. The model described the gravure process using fundamental physical parameters such as ink viscosity, solvent evaporation, and cell volume. His analysis showed that the amount of ink transferred from the cell was dependent on cell geometry, ink surface tension, density, and viscosity, and printing speed. The effects of these parameters were not straightforward. Depending on the stage of ink transfer (ink doctoring, touchdown of the substrate, ink pick-out, etc.), each physical parameter could either increase or decrease the amount of ink transferred. His analysis was performed for non-absorbing substrates, which made the analysis somewhat simplified (by ignoring the effect of substrate ink absorption, which is extremely substrate dependent). Of particular note in Bery's work is the discussion of the "flashing skin temperature" of the ink. This describes the temperature which the ink experiences at the surface of the gravure cell after the doctor blade passes over it. The pressure and friction from the blade, in theory, raise the surface to an extremely hot temperature, stimulating considerable solvent evaporation before the ink is transferred from the cell. This changes not only the volume of ink in the cell, but also changes the surface chemistry at the surface of the ink, creating a thin "skin" of ink with a different surface energy, which can affect ink transfer. An attempt to measure the temperature found that in some cases the temperatures reached nearly 200° C. The

temperature increased at higher speeds for a fixed load. Although the amount of time between inking the gravure cells and transferring the ink to the substrate is short, the extremely high temperatures are sufficient to appreciably change the volume and composition of ink in the cell.

Some theoretical work has also been done of ink transfer from gravure cells in gravure coating processes. The nature of the flow is somewhat different than typical printing in that the substrate and the gravure cell are moving at different speeds (and in some cases in opposite directions), thus creating a different boundary condition. However, several of the physical mechanisms of transfer are dependent on the same physical parameters. Schwartz et al. [9] constructed a 3-D mathematical model for gravure coating operations. They modeled a series of gravure cells coated in ink and passed under a meniscus formed between the cells and the substrate (see Figure 2.10).

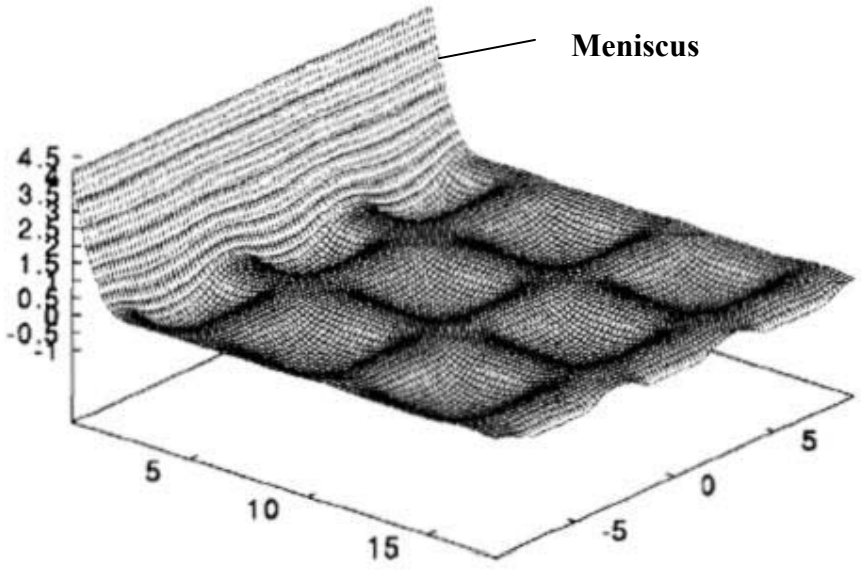

Figure 2.10: 3-D mathematical model of liquid flow in gravure coating [9]

The meniscus is formed because of the relative motion between the cells and substrate. The model assumed that ink transfer was governed by surface tension, viscosity, and gravity. The basic result of the model was that there was a size effect for the emptying of gravure cells, with smaller cells retaining a higher fraction of ink. The model predicted values ranging from 0.48 final liquid fraction after emptying for big cells (width=320 microns), to 0.92 for smaller cells (width = 80 microns). The model assumed typical industrial values for viscosity, surface tension, and speed, although the effects of different speeds were not investigated. The model also showed a strong dependence on the curvature of the meniscus, which is assumed to be constant in the analysis. In reality, the meniscus is highly dependent on speed, substrate tension, and other factors. Another limitation of their work was that they assumed a pinned, stress-free surface. In reality the surface of the ink will not be pinned in one position, but will continuously change as the cell is emptying. Thus the model cannot capture the effects of a complex boundary condition.

No mention was made whether the analysis for gravure coating could be applied to gravure printing, in which there is not a steady meniscus formed. However, the model does account for the phenomena of the ink surface being deformed due to surface tension forces pulling the ink out of the cells onto the “land” areas between cells. This effect would also be present in the inking of cells during gravure printing.

Powell et al [10] developed a 2-D mathematical model for gravure coating operations similar to the one proposed by Schwartz et al. Their model modeled a single, filled, rectangular cell, with a meniscus passing over. In their case, they considered the effect of the contact line formed between the ink and the cell continuously moving down

inside the vertical wall of the gravure cell as ink flows out of it. This was an improvement over Schwartz et al, who ignored this moving contact line and assumed a pinned ink surface. The effect of the moving contact line was found to be that it pushes the ink out of the cell. Powell et al used a finite element approach to model the ink behavior during cell emptying and found that the fraction of ink evacuated out of the cell was primarily dependent on Capillary number, with the amount of ink evacuated decreasing as Capillary number increases. The Capillary number describes the relative effect of viscous forces to surface tension forces. They also found that as cell aspect ratio increases, the amount of ink evacuated increases, and at large aspect ratios, the evacuation is independent on Capillary number. The finite element model also showed a re-circulation region at the bottom of the cell (see Figure 2.10) as the ink flowed out. Again, no mention was made of whether the analysis could be applied to gravure printing. However, the dependence of ink flow out of a small cell on Capillary number and cell aspect ratio may also hold for gravure printing, based on the similarities in the processes.

Ahn and Na [11] performed a finite difference method analysis of the flow of ink in the gravure cell. They also studied the effects of using a non-Newtonian fluid in the analysis. They concluded that the approach gave a realistic representation of the flow in gravure cells and validated their model with the work of Yin and Kumar [2].

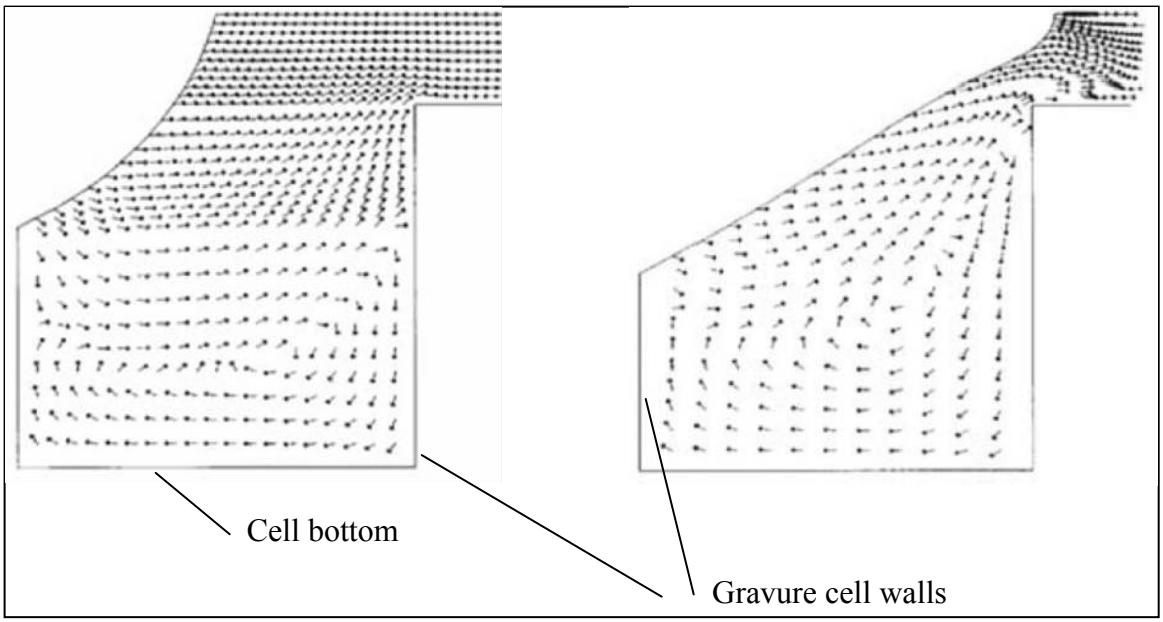

Figure 2.11: Simulated Flow of ink in gravure coating process [10]

Hennig et al. [5] also discussed the issue of cell aspect ratio and concluded that for cell aspect ratios <0.05 the ink would dry in the cells too quickly and not transfer to the substrate. For cells with aspect ratios >0.5, however, the cells would be too narrow and would not wet the ink, or would not release the ink due to Capillary forces. This concept is illustrated in Figure 2.12.

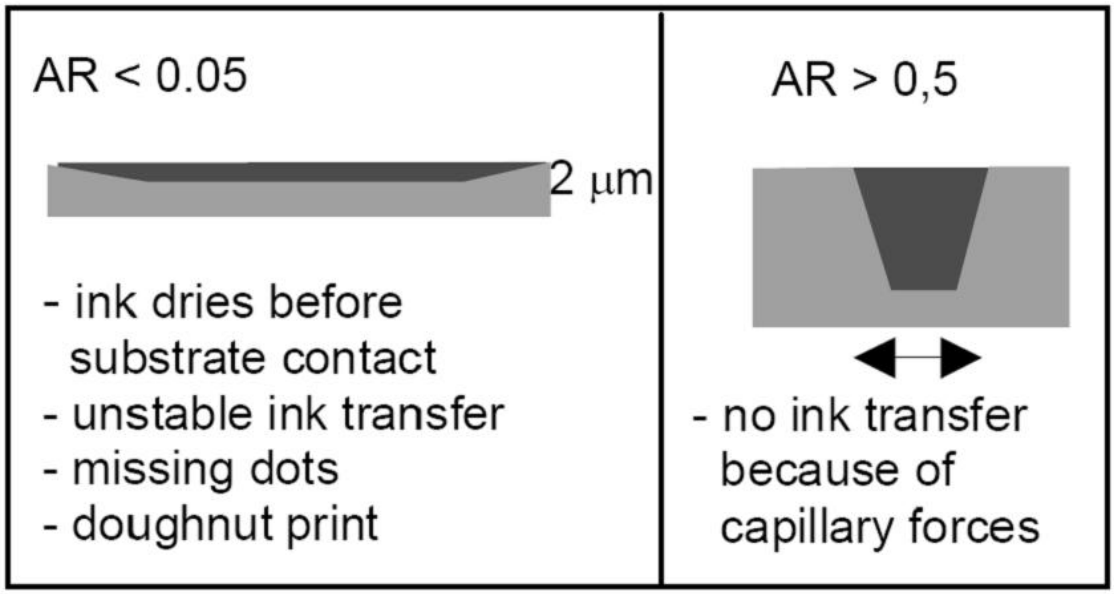

Figure 2.12: Aspect ratio and ink transfer [5]

2.2.2 Experimental Studies

There have been several important experimental studies of gravure printing. Bery [8] compiled some of the results of the earliest studies and developed a mechanistic description of the process based on both qualitative and quantitative analyses. Qualitative analyses included photographs and micrographs of different stages of gravure printing, as well as scaled-up physical models of gravure cells. Quantitative analyses included image analyses of prints, densitometry of prints, and ink transfer measurements on lab presses. Bery's study attempted to summarize the mechanisms governing the gravure process. Previous studies had given sometimes contradictory and incomplete pictures of different mechanisms within the process. Bery attempted to reconcile several of these previous studies with a global approach that resulted in a fairly complete mechanistic view. His conclusions will be discussed in more detail in Chapter 6.

Bohan et al [12-14] completed several experimental studies using production gravure presses. They investigated the effects of certain process parameters using orthogonal array techniques. The effects of impression roller pressure, ink viscosity, doctor blade angle and blade load were investigated. It was found that the ink viscosity and blade angle had a statistically significant effect on the amount of ink transferred, as measured by analyzing the color of the dried ink layer. Increasing viscosity tended to decrease color density, implying less ink transfer, while increasing doctor blade angle tended to increase color density. The effect of viscosity was also found to be nonlinear.

Benkreira and Patel [4], and Benkreira and Cohu [15] performed a parametric study of gravure roll coating and found that the coated film thickness was primarily dependent on gravure cell size, with larger volume cells giving a thicker coating. They also investigated forward gravure coating, in which the gravure roller and substrate are moving in the same direction, as in gravure printing, albeit at different speeds relative to each other. In forward gravure, they found that there were several operating parameters that could be used to control film thickness.

Yin and Kumar [2] performed a study in which they studied the flow of ink out of gravure cells using a scaled-up groove. This work helped to explain the fluid flow process in gravure cells, in particular how the ink empties out of the cells. Their experiments also validated some of the earlier computational results from Powell et al. They also correlated the residual ink volume directly to the Capillary number of the liquid, fitting a power-law relationship. Since this work was performed on scaled up grooves instead of cells, the effects of doctor blade angle and load, as well as any evaporative effects of the ink, were not studied.

2.3 Indium Tin Oxide

The use of Indium Tin Oxide for this study was based on several factors. First, in many organic electronic devices, ITO is used a transparent electrode, and is often the first layer deposited on the chosen substrate in such devices. Therefore the application of ITO directly onto a substrate material was very relevant. Another advantage to using ITO was its relative availability as a nanoparticle powder that could be mixed to form a basic "ink" with ITO taking the place of pigment. Since ITO is useful primarily for its transparency and conductivity, it therefore offered simple parameters for measuring its functionality. Although much of the motivation for this work came from purely organic materials, which typically have no solid content, the use of inorganic solids in particle form also presented a unique challenge. By using solid ITO particles, we were able to address some of the additional issues that arise when attempting to print inorganic materials.

2.3.1 Uses and Properties

Indium Tin Oxide (In_2O_3:Sn, ITO) is a transparent, conducting oxide material that is commonly used in thin film photovoltaic cells, as well as other devices which rely on a transparent conductor, e.g. thin film displays etc. It is most commonly used in ratios of 90% In_2O_3:10% Sn. It is most commonly deposited using processes such as sputtering and chemical vapor deposition [16, 17].

The resistivity of bulk ITO is as low as 10^{-4} Ω-cm, making it suitable for the above-mentioned applications. However, it is also very brittle, and is therefore limited in applications other than on glass or other rigid substrates. Chen et al [18] studied the fracture of commercially available ITO films on a compliant substrate and found that the

failure mechanism is buckling delamination followed by film cracking. The failure occurred under both tension and compression, at strain values between 0.9 and 1.7%. Leterrier et al [19] also studied ITO film failure on flexible substrates, and found that the loss of performance was caused by rapid crack propagation, rather than merely crack initiation.

2.3.2 ITO Nanoparticles

Although ITO is commonly used, it is typically restricted to applications in which it is deposited on a rigid substrate, or in which the strain experienced is extremely low. The use of ITO nanoparticles in place of a contiguous solid film has several advantages. First, it enables lower cost deposition in place of the often expensive processes previously mentioned for solid films. Using nanoparticles may also create functional films that are less rigid and therefore have more desirable mechanical properties for applications on flexible substrates, for example. The primary drawback, however, is that creating a film out of nanoparticles will inherently cause a loss of performance compared to a solid film that may not satisfy device requirements. However, if the tradeoffs between mechanical properties and functional performance can be optimized, using nanoparticles may be an attractive option.

Ederth et al [20-23] studied the properties of thin nanoparticulate ITO films. The films were prepared by spin coating and subsequent annealing. They found that the sintering of nanoparticles could be used to produce films that had excellent electrical conductivity and optical transparency, although the performance was not as good as a typical solid ITO film. They also applied several theoretical models based on effective

medium theory for the optical and electrical properties with good agreement with their measurements. Ogi et al [24] also studied ITO nanoparticle films prepared using a dip coating process. They measured the optical and electrical properties, and also documented a nanoparticle size effect, with smaller nanoparticles giving better electrical and optical properties. They also studied the effects of sintering at various conditions.

2.4 Flexible Printed Electronics

The term "flexible electronics" in the context of this thesis refers to the production of electronic components or complete devices by depositing electronic materials onto flexible substrates using printing processes. Implicit in this definition is the assumption that there is a large potential for making low cost electronic products at high volume using such processes. It also assumes that there is added value to electronic devices that are flexible, and that there will be future market demand for such products. This section summarizes some of the products, processes, and issues relevant to flexible, printed electronics.

2.4.1 Products and Potential Applications

There are many potential applications for printed electronics. Among the most significant are those products for which the cost structure of manufacturing can be significantly transformed through the use of printing, and for which current manufacturing technologies are not currently competitive. As previously mentioned, much of the motivation for this work comes from the need for cost-effective manufacturing of solar cells based on organic or other thin film technologies. Traditional

silicon-based solar cells are not currently competitive on a wide scale with other forms of power, and there are few gains to be made, due to the extremely high cost of materials. A reduction in cost of an order of magnitude, however, could revolutionize the solar industry, making it competitive in all markets, even with the inherent limitations of lower efficiencies and shorter lifetimes currently shown by non-silicon based PV. Such a reduction in cost is potentially possible using low cost printing processes. Although some current crystalline silicon-based PV has solar conversion efficiencies >20%, the current cost of around $4/W installed is still much too high to be feasible. The United States Department of Energy (DOE) has a current cost goal of $0.33/peak watt ($W_p$) installed, or $0.05-$0.06/kWh for utility scale production. However, some current projections suggest that in the next 10 years crystalline silicon PV will only reach $1-$1.50/W_p, still much higher than the current goal. Therefore there is a lot of incentive to find alternative PV technologies that have the potential to meet the $0.33/$W_p$ goal. Even though the best reported OPV solar conversion efficiencies are just above 5%, due to the low cost of the materials and the potential processes there is the possibility that they may reach the cost/W_p goal [25].

Other technologies frequently mentioned are flexible, large-area displays based on organic light-emitting diode (OLED) technology, as well as radio frequency identification (RFID) tags for supply-chain engineering, and low cost logic devices for intelligent packaging. One figure commonly mentioned is a target of $0.01/tag for RFID using printing processes [26]. In theory, any electronic device could potentially be manufactured solely using printing processes if its corresponding component devices (resistors, transistors, capacitors, etc.) can be formed using the thin layers inherent to

printing. Because of this, there are potentially endless possibilities leading to transformation of existing markets and the creation of new markets based on printed electronics [27-29].

2.4.2 Printing Technologies

There are many different printing processes that have been widely discussed as a potential for manufacturing electronic devices. The choice of which process to use is driven by many factors, including cost, quality, and complexity. Some processes are more suited to certain materials than others. Some materials can be printed using one of several different processes with comparable results. Therefore the choice becomes very complex with a number of potential solutions for every printed product. With printed electronics, where there is most likely a need to print different materials for different functions (conductor, transistor, etc.), there will also likely be a need to use several different printing processes for one product.

Among the printing processes that have been explored for printed electronics include screen printing, inkjet printing [30-33], flexographic printing [34], and gravure printing [35-39]. Screen printing has been used for many years in the production of printed circuit boards. It has also been investigated as a platform for other devices, including polymer solar cells [40]. Several more printing and coating processes are addressed by Krebs [41].

One of the main limitations of all the work on gravure printing for flexible electronics is that there are very few investigations that address the parameters governing the gravure process. Although gravure cell geometry and ink variables are often

mentioned as potentially important parameters, there are no efforts to understand the effect of those parameters on the printed product. There are many attempts to demonstrate the feasibility of using roll-to-roll techniques for producing flexible electronics, but relatively few attempts to understand or develop the process for flexible electronics.

2.4.3 Challenges of Printed Electronics

There are many unresolved challenges for printed electronics. To a certain degree, In general, the performance requirements of electronic devices can only be achieved by optimizing the materials formulation to a desired performance. However, this invariably affects the printability of the material. For example, a bulk material suspended in an electronic ink will most likely have the best performance at high concentrations, but as the concentration increases, the ink will typically get more and more viscous until it can no longer be printed using traditional printing processes. Organic materials have a similar problem. The performance and lifetime of these materials is strongly dependent on the formulation of the material, and any additives or changes in that formulation to improve printability can dramatically reduce the materials functionality.

Another challenge of printed electronics is quality and reliability. One of the most attractive characteristics of printing processes is the potential to process materials under atmospheric conditions at high speeds. Traditional printing operations that operate under these conditions are subject to contamination that is harmless for graphics printing but could be very harmful to functional products. Any attempt to bring the process into "clean room" like conditions would inevitably lead to much higher costs. Furthermore,

many organic materials have inherently short lifetimes, and are affected by thermal, electrical, and atmospheric degradation.

Sheats [42] and Schmidt et al. [43] have documented several of the challenges facing flexible, printed electronics. Sheats mentions issues such as feature size control, registration, and defect elimination as issues that can be resolved only with considerable engineering effort, which raises the cost of production. He also notes that the idea of printed electronics is attractive in part because it implies low cost, even though in reality it may not achieve low cost for certain electronic devices and markets. Schmidt et al. also notes that printing electronic structures is not straightforward, based primarily on the differences in material properties in electronic materials that make them more difficult to process. They suggest that both the materials and processes need modification.

2.6 Summary

Gravure printing is a well-established printing process that has the potential to be used in the production of many flexible electronic devices. Prior work has covered both theoretical and experimental aspects of the process, but there is not yet a complete understanding of the process for the wide range of materials and substrates that can be used in the process. Gravure is one of several printing processes that have been investigated for printing flexible electronic devices. The number of potential applications is quite large and continually growing as new technologies and markets are developed.

ITO is a unique material that has found wide application in organic electronic devices, typically as a transparent conducting electrode in a photovoltaic device or electronic display. The use of ITO nanoparticles in place of a bulk ITO layer has the

potential to reduce processing cost for such devices and has been studied in depth. The use of gravure printing to deposit ITO nanoparticles has been investigated, with promising results.

Flexible, printed electronics have the potential to overcome prohibitively high manufacturing costs through the use of printing processes. However, there remain many challenges that need to be overcome. These challenges include materials processing limitations, performance limits, and short device lifetimes. These challenges will likely be addressed in a variety of ways, with improvements to be made in both processing technologies, device design, and materials technologies.

CHAPTER 3

SCREENING EXPERIMENT

In order to become familiarized with how the gravure printing process would work with an ITO nanoparticle based ink, a screening experiment was designed and carried out. The goal of this experiment was to look at a large number of process parameters to gain an understanding of how the process would work and what affect the process parameters had on different responses. The precise responses were not known at the outset of the experiment. Although the general approach was to try to understand the effect of process parameters on "print quality", the method of characterizing quality was not defined. However, after the experiment was performed, two quantitative responses were chosen in order to compare the quality of the print. These responses are discussed later in this chapter. The design of the experiment was a 2^{8-1} fractional factorial design that included eight process parameters at two levels. The selection of the eight parameters was based on the capabilities of the lab scale gravure printer used, the specific requirements of the intended application of the printed layer, and a review of previous work. This chapter explains the choice of experimental factors for the screening experiment, as well as the results and some discussion of the experiment.

3.1: Parameter Selection

Although the gravure process is fairly simple in principle, there are a large number of factors that can potentially influence the print. For example, Figure 3.1 gives a fairly comprehensive list of process factors in a conventional gravure process. This list

includes several factors that are specific to graphics printing, as well as some factors that are only important on a large-scale production press. Since the screening experiment was performed on a lab scale gravure printer, several factors could not be studied, e.g. color sequence, web handling etc. In this section, the parameters associated with the gravure printer, gravure printing plate, and ink formulation are discussed, as well as the selection of the parameters for the screening experiment.

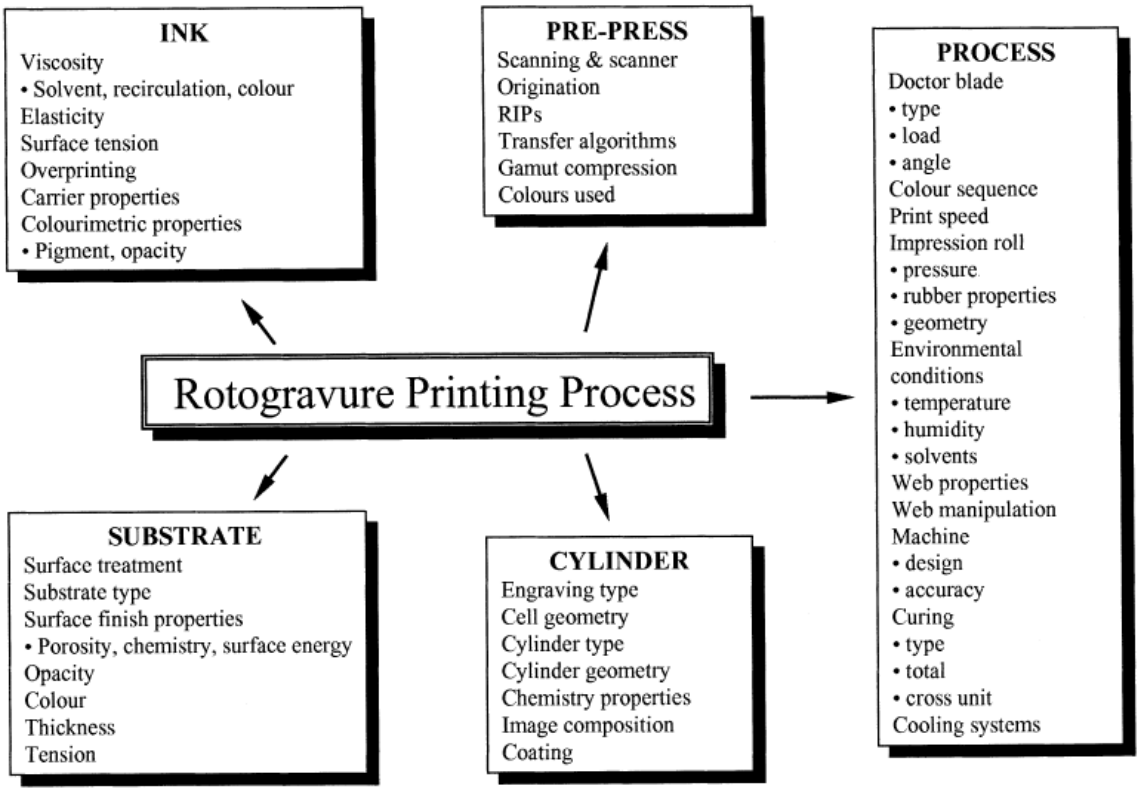

Figure 3.1: Potential factors governing a rotogravure printing process [12]

3.1.1: Gravure Printer

The lab scale gravure printer used to perform the experiment was the K Printing Proofer from RK Print Coat Instruments (Hertfordshire, UK). The proofer is different from a typical gravure press in several ways. One of the most significant differences is

that it is not a roll-to-roll press. Sheets of paper or other substrates are attached to the pressure roller and then rolled over a gravure plate, instead of a gravure roller. The fundamental mechanics of the process are the same, but the lab scale press cannot print continuously and does not have an ink well. Instead, ink is manually placed in front of a doctor blade and then fills the cells as the blade translates across the plate. The difference in the configurations of the presses is given in Figure 3.2.

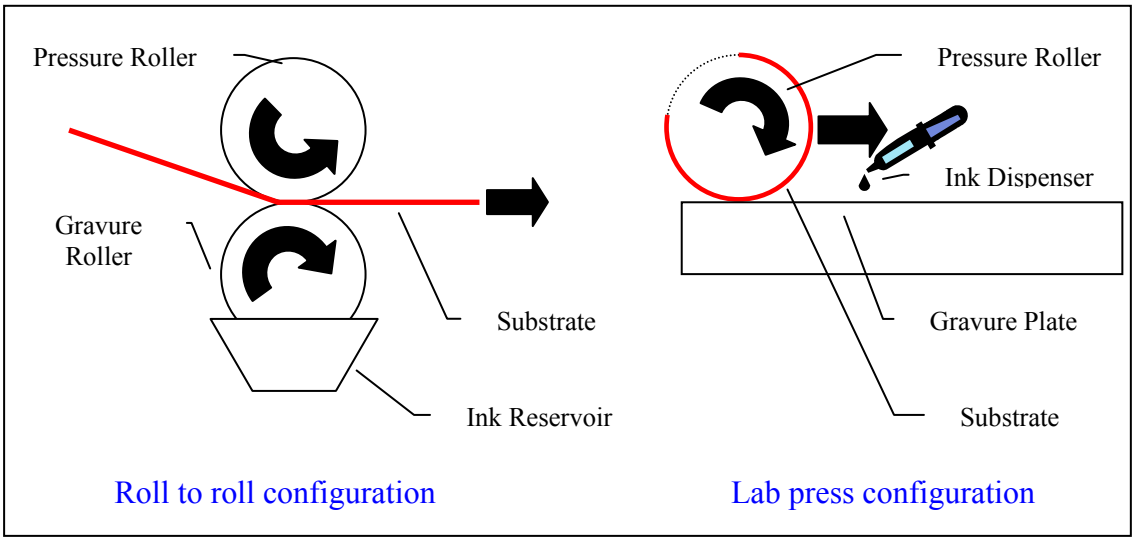

Figure 3.2: Comparison of roll-to-roll and lab scale gravure presses

The K Printing Proofer is shown in Figure 3.3. It has an engraved gravure plate, an adjustable doctor blade, an adjustable pressure roller, a speed dial, and a control switch. The operation of the press is quite simple. First, a pre-cut substrate is attached to the pressure roller using pressure sensitive tape. The roller is then lowered into position onto the plate and clamped down, with the pressure roller applying pressure to the substrate. The pressure of the roller can be adjusted via the micrometers controlling the position of the roller. The doctor blade also comes into contact with the plate, and a light

pressure is applied to it as well. The doctor blade itself is also adjustable, with micrometer adjustments on each side, and an angle adjustment screw.

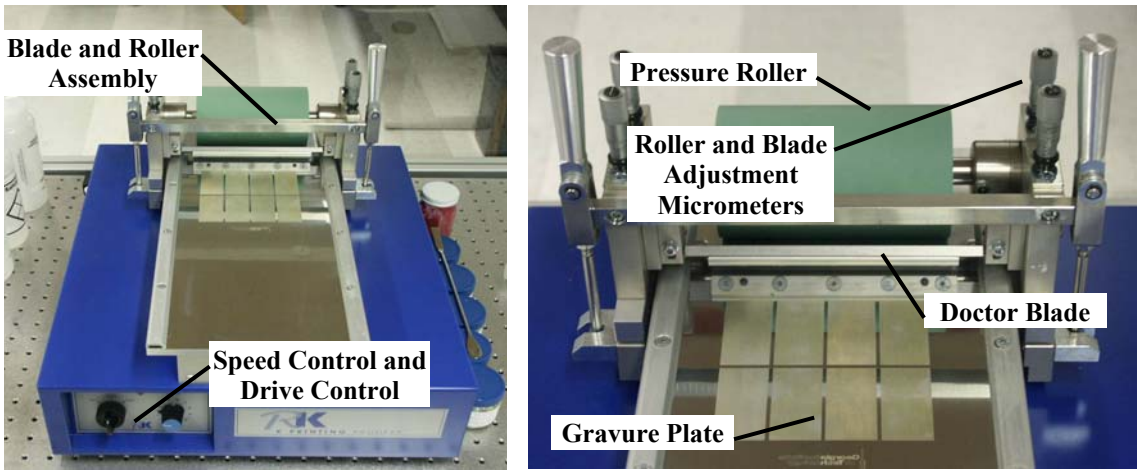

Figure 3.3: K Printing Proofer (RK Print Technologies, UK)

Once the substrate is loaded and the machine set, a small amount of ink is placed in a line in front of the doctor blade. The switch is then turned on, and the entire blade/roller assembly translates across the plate, simultaneously inking, doctoring, and printing the ink. The printed substrate is then carefully removed and allowed to dry at ambient conditions.

3.1.2: Gravure Plate

The gravure plate for the K Printing Proofer was engraved electromechanically, with a diamond stylus. The thin metal plate was wrapped around a cylinder and rotated at high speed as the stylus moved in and out, engraving one cell at a time and thousands of cells per minute. The plate was made of aluminum, which was then coated with copper before engraving. After engraving, the plate was chrome-plated. The chrome plating adds

abrasion resistance and a protective coating. The engraved cell geometry was controlled by varying the three different cell parameters of line screen, stylus, and tone (see Chapter 2). The plate was engraved with eight sections, each with an area of approximately 25x50 mm (1x2 in.), and each with different cell geometry. These geometries corresponded to the 2^3=8 combinations of the three cell parameters at two levels each. A layout of the plate is shown, in Figure 3.4, with the areas labeled for line screen, stylus, and tone. The cell geometry parameters were chosen to enable printing of a thin, solid, continuous film of ITO ink, as would be used in printing a transparent, conducting electrode in a solar cell or display device. Relatively high line screen values (i.e. more cells/inch, and thus smaller cells) were chosen to ensure a thin film. High tone values were chosen to give a continuous film. Stylus angles were chosen that covered the typical range of values used in gravure printing (typical angles range from about 90 degrees to 150 degrees), and which represented large variations in cell geometry and would thus allow a comparison of not only cell size, but also geometry. As the experimental runs were performed, the ink would dry almost immediately, leaving dried ink in the cells. A special gravure ink cleaner and ultra-fine brass bristled brush were used to clean the plate after each run.

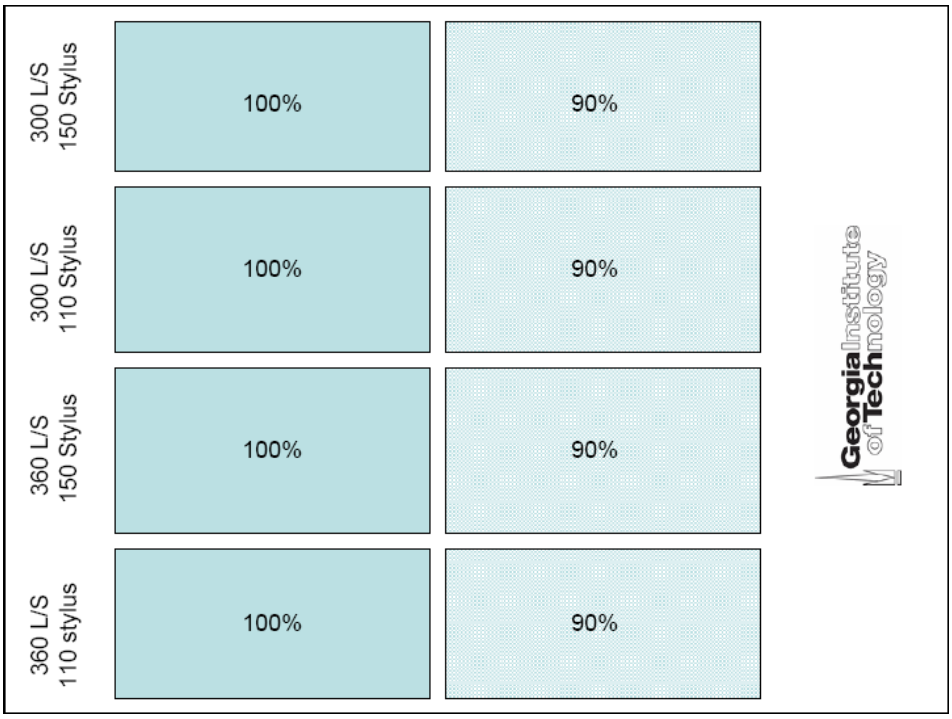

Figure 3.4: Layout of gravure printing plate

3.1.3: Ink formulation

A typical gravure ink is made by mixing together an ink vehicle, pigment, and additional solvent. The ink vehicle consists of a binder material, typically a polymer, additives such as wax or diluents for printability, and solvent. The ink vehicle is often a pre-formulated product sold by the ink manufacturer. The pigment is typically a solid and is milled until the particles are several microns or less in size. Additional solvent can be added into the ink to optimize the ink properties. If more pigment is needed to reach a desired color, it may increase the viscosity of the ink and therefore more solvent can be added to reduce the viscosity. The ink is mixed and used to print a test sample, or *proof* on a gravure proofer, which is used to ensure the correct color and quality before beginning a printing run. In the case of the current experiment, two different

commercially available ink vehicles were combined with ITO nanoparticles and solvent in varying quantities. An SEM photo of the ITO nanoparticles is shown in Figure 3.5.

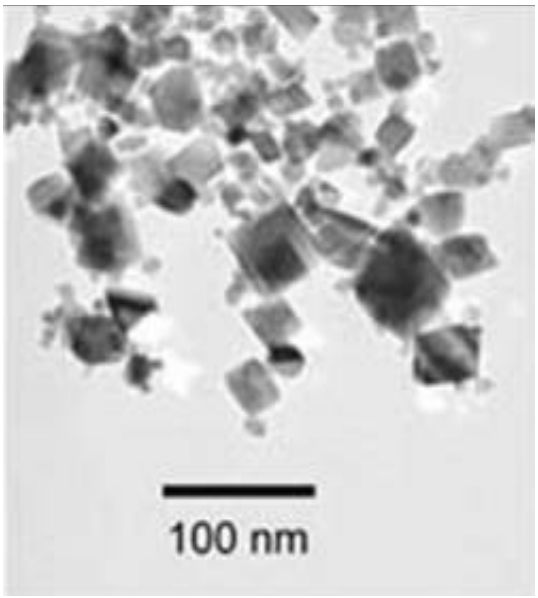

Figure 3.5: SEM photo of ITO nanoparticles (Nanophase Technologies) [44]

The ink vehicle type then became one of the experimental factors, as well as the amount of ITO and amount of additional solvent. The two ink vehicles were Flexomax (Sun Chemical), which contained a urethane-based binder, and Sunester (Sun Chemical), which contains a polyester-based binder. The solvent used was a 90% ethanol/10% acetone blend (Sun Chemical).

In this screening experiment, the primary interest was in determining the general process requirements for gravure printing. Since ITO nanoparticles were used in place of the pigment, it was expected that the properties of the ink to be quite different from the properties of a typical gravure printing ink. Table 3.1 shows the typical composition of a gravure printing ink, and a comparison of the composition of our inks.

Table 3.1: Comparison of typical gravure ink to ITO inks.

Typical gravure ink	% by weight	ITO inks in this study	% by weight
Solvent	70	Ink vehicle	30-60
Resin	15	Additional solvent	0-20
Additives	5	ITO nanoparticles	40-50
Pigment	10		
Total	**100**	**Total**	**100**

As shown in Table 3.1, the relative solid content of pigment is quite low, usually less than 10%, in a typical gravure ink. However, due to the need to increase the functional performance of the ITO ink by increasing the loading of ITO nanoparticles, an ink that had a significantly different composition was created. Therefore, it was of interest to determine whether or not the ITO inks behaved similarly to typical gravure inks, despite the much higher solid content, and the use of nanoparticles instead of regular, microscopic pigments. It should be noted that the ITO inks used in the screening experiments were relatively viscous, with the most viscous behaving more like a paste than a liquid ink. In contrast, most gravure inks have a viscosity more comparable to water. All of the inks were blended using a stirring rod, and further mixing was achieved by the use of ultrasonic vibration. The inks were held in an ultrasonic bath (Bransonic model 5510) for 60 minutes before being printed (see Figure 3.6)

Figure 3.6: Ultrasonic mixing of gravure inks

3.1.4: Summary of Experimental Factors

The eight experimental parameters that were chosen were parameters governing the ink formulation, gravure cell geometry, and process conditions. A complete list of the experimental factors and their two levels is given in Table 3.2. It should be noted that one potential factor that was not addressed was the doctor blade. The lab scale printer had the capability of changing both the load and angle of the blade. Furthermore, it has been found in previous work that the doctor blade may have an influence on the print quality in gravure printing. However, this factor was excluded from the experimental design in favor of a more economical and simpler model. The doctor blade was set at a 45 degree angle, with the load being adjusted by micrometer setting. The recommended load for the doctor blade, according to the machine specifications, was to adjust the micrometers on each side down one full turn, equal to 0.64 mm (25 mils), after the blade came into contact with the plate. This load was set and the angle and load were not modified during the experiment. It was assumed that the recommended load would ensure adequate wiping of the ink without losing any ink under the blade due to hydrodynamic forces.

Table 3.2: Screening experiment factors and levels

Factor	Low Level (-1)	High Level (+1)
Roller Pressure	20 lb/in	80 lb/in
Solvent Weight %	none added	add 20%
Speed	5 m/min	25 m/min
Tone	90%	100%
Binder	Flexomax	Sunester
Stylus Angle	150	110
ITO Weight %	40%	50%
Line Screen	300 cells/inch	360 cell/inch

3.2: Experimental Procedure

For a full listing of the experimental design, including the factor level settings for each treatment, see Appendix A. The experiments were performed at ambient conditions. The inks were all prepared at once. The PET substrates were cleaned with ethanol and inspected for creases and scratches. If there were excessive creases or scratching, the substrate was not used. The gravure plate was also cleaned with solvent before each experimental run. A small amount of ink was placed on the printing plate in front of the doctor blade, but not directly onto the cells. The control switch was then used to start the print. The doctor blade simultaneously spread and doctored the ink. The pressure roller with the substrate attached then rolled directly onto the plate and the ink was transferred. The printed substrate was then removed and allowed to air dry at ambient conditions for several hours.

3.3: Results and Discussion

The ITO inks did, in fact, print successfully, in that a thin layer of ITO ink was transferred to the substrate from the printing plate. There were differences in the appearance of the different films, with some being thicker or having more variations than

the others. From the outset it was not clear how to compare the "quality" of the printed films. Typical measures in the printing industry focus on the color, reflectivity, and associated measures. In this experiment the primary purpose was to determine the ability of the process to produce thin, uniform films. After the experiment was performed, two metrics were devised based on the results. These metrics and the experimental results are discussed in this section. In the analysis of this and other results, the significance of the factors was judged by the p-value given in a regression analysis. Those factors with a p-value of less than 0.05 were judged to be statistically significant with 95% confidence. In comparing the factors, it was often more convenient to compare the t-value, which gave a relative measure of the magnitude of the significance of each factor. The statistical analysis was performed using MINITAB statistical software.

3.3.1: Response: Void Area

There was a lot of variation in the thickness of the printed layer, and there were many cases in which there were voids in the printed layer, in which no ink was transferred. These voids were manifested as blank spots in the printed film, and ranged in size from a few mm to a few tens of mm. Figure 4.6 shows several examples of the printed samples. The samples were converted into grayscale digital images using an image scanner. It should be noted that the images shown were scanned against a black background. Since the ITO film was a pale yellow color, the thicker films appear lighter in color in Figure 3.7. All of the samples shown are 25x50 mm (1x2 in.). The samples exhibit not only the void areas, but also the relative variation in thickness of the films. This represents groups of tens to hundreds of adjacent cells from which the ink was not

transferred. In no case was the total void area greater about 1% of the total printed area. However, it did represent a general "failure" to print. Because of the void areas observed, it was decided to analyze the effects of the experimental factors on the total unprinted area, in mm^2.

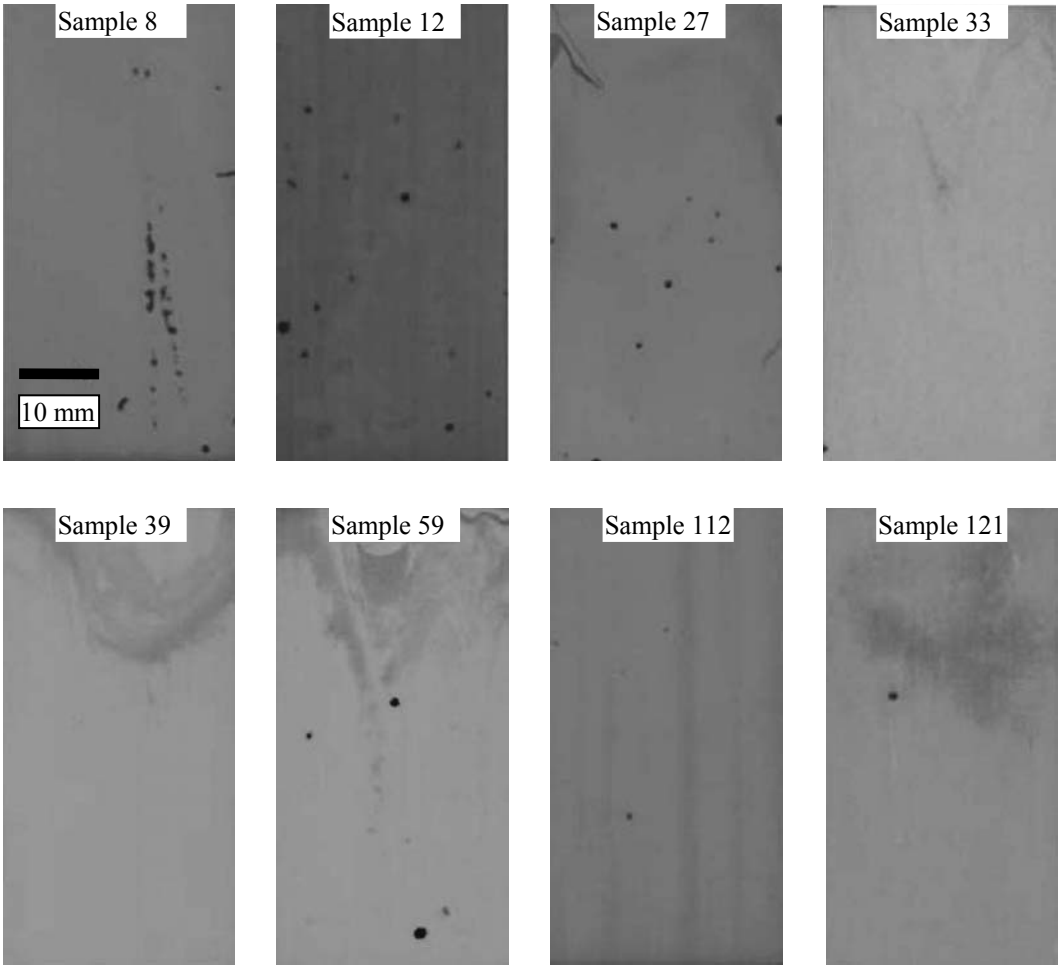

Figure 3.7: Various samples of the printed ITO films

The films were digitally scanned, converted to grayscale, and then filtered using an image processing routine in MATLAB to convert the grayscale images into a binary image, i.e. black and white. The total unprinted area was then calculated by counting

pixels. Figure 3.8 shows a digital image of the ITO film and the corresponding binary image.

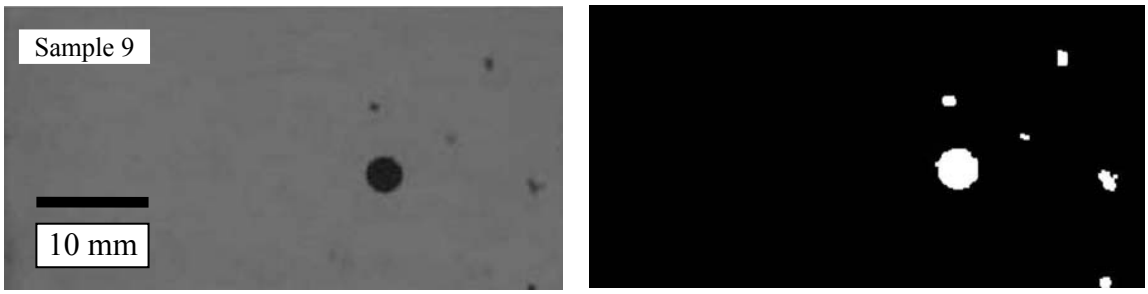

Figure 3.8: Digital image of ITO film and corresponding binary image

The full MINITAB results are shown in Appendix B. The main effects plots for the eight experimental factors are shown in Figure 3.9. A summary of the statistically significant effects, i.e. those effects significant with at least 95% statistical confidence, are shown in Table 3.3, along with the ANOVA output from MINITAB. The main effects plot shows the relative effect of each individual factor on the void area, expressed in mm^2. Therefore the larger the slope of the line in the plot, the more significant the effect is.

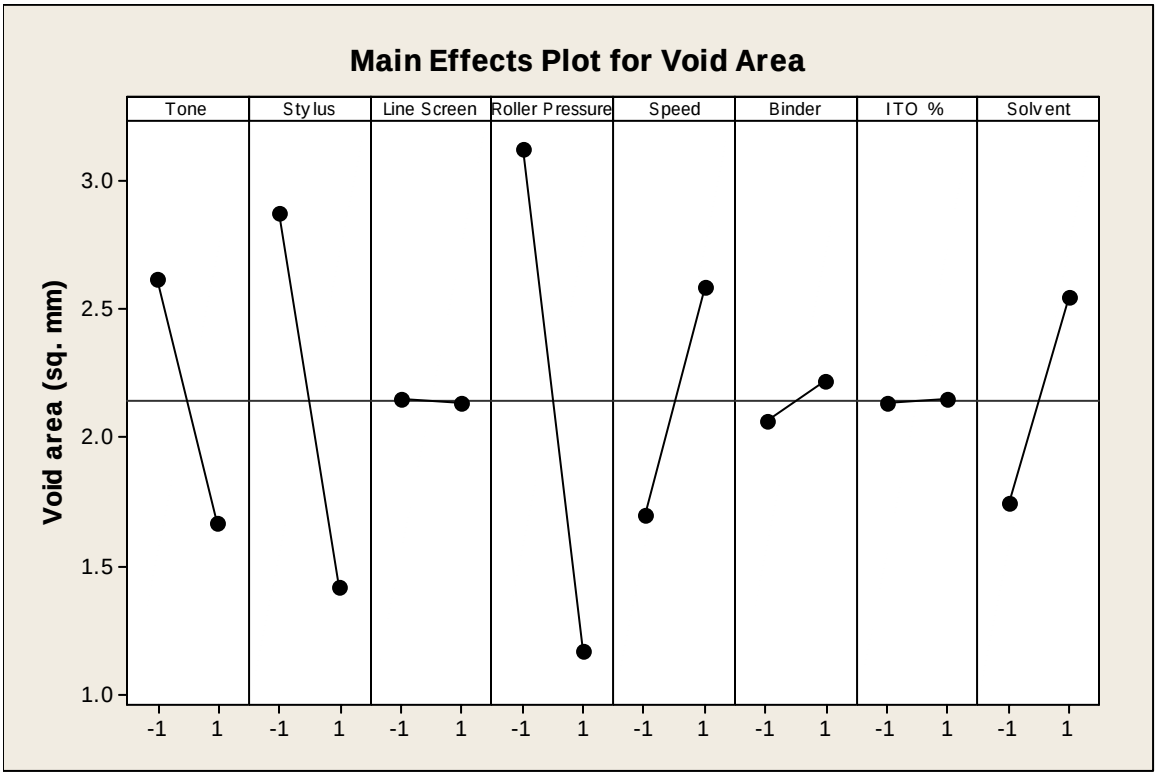

Figure 3.9: Main effect plots for void area

As can be seen from the main effects plot, the most significant effect appears to be the roller pressure, with higher pressure resulting in lower void area. The tone, stylus, speed, and solvent also appear to be important. The line screen, binder, and ITO concentration seem to be either less important or insignificant altogether.

Table 3.3: Selected ANOVA results for void area

Term	Effect	Coef	SE Coef	T	P
Tone	-0.9505	-0.4753	0.2229	-2.13	0.036
Stylus	-1.4529	-0.7265	0.2229	-3.26	0.002
Roller Pressure	**-1.9463**	**-0.9731**	**0.2229**	**-4.37**	**0.000**
Speed	0.8861	0.4431	0.2229	1.99	0.050
Tone*Solvent	-1.0885	-0.5443	0.2229	-2.44	0.017
Stylus*Line Screen	0.8970	0.4485	0.2229	2.01	0.047
Stylus*Solvent	-1.0197	-0.5099	0.2229	-2.29	0.024
Line Screen*Solvent	-0.9178	-0.4589	0.2229	-2.06	0.042

S = 2.52141 PRESS = 1144.63
R-Sq = 47.13% R-Sq(pred) = 0.00% R-Sq(adj) = 26.21%

Analysis of Variance for Void Area (coded units)

Source	DF	Seq SS	Adj SS	Adj MS	F	P
Main Effects	8	264.1	264.1	33.010	5.19	0.000
2-Way Interactions	28	251.6	251.6	8.984	1.41	0.113
Residual Error	91	578.5	578.5	6.358		
Total	127	1094.2				

Based on a comparison of the p- and t-values, the roller pressure was found to be the most significant effect, with higher pressure resulting in lower void area. The speed was also found to be significant, with higher speed resulting in higher void area. The cell geometry also seems to be a factor, with an increase in tone and stylus angle both decreasing the void area. The increase in tone and stylus correspond to an increase in cell size, as well, suggesting that larger cells may have result in less void area in the printed film. However, the line screen was found to be insignificant, even though the line screen also changes the overall size of the cells. This suggests that not only cell size, but also cell geometry is important. There were also several two factor interaction effects that are significant at the 95% confidence level. An interaction plot comparing those factors is shown in Figure 3.10.

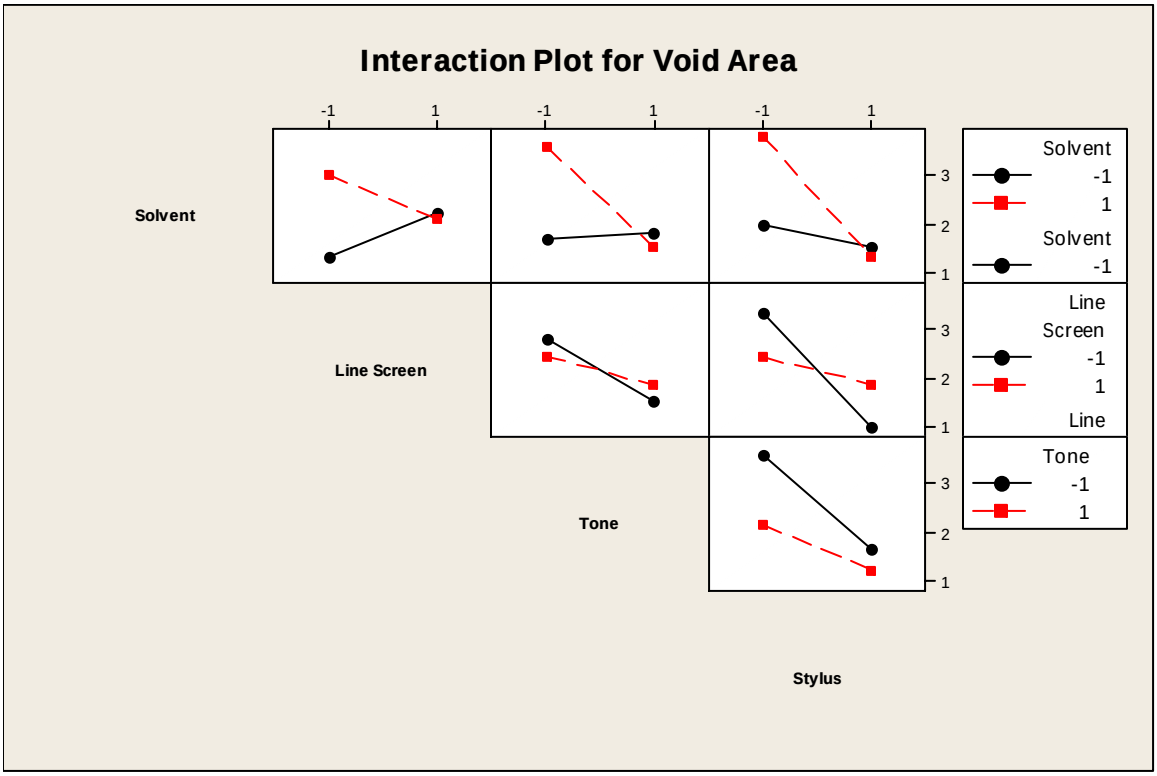

Figure 3.10: Interaction plot for void area

The interaction effects as described in Figure 3.10 give more insight into the effect of the process variables on the void area. The interactions between solvent and the three cell geometry factors are interesting. The solvent was not significant at the 95% level as a main effect, but all three interactions between solvent and cell geometry factors are significant, as shown in Table 3.3. From Figure 3.10 it appears that an increase in solvent actually increases void area at low line screen, tone, and stylus values, but actually decreases void area at higher levels of these factors. This suggests that as the cells get more shallow and have more bridge area between cells, i.e. have lower tone and stylus values, the solvent has a detrimental effect. As the cells get larger, i.e. have lower line screen, the solvent also has a detrimental effect. The addition of solvent tended to

decrease the viscosity of the inks, and may also have affected the surface tension and drying behavior of the inks. Some of these effects will be discussed in later sections.

The other significant interaction effect was that between the stylus and line screen, with the stylus angle having a more significant effect on void area at lower line screen values. This suggests that the smaller cells, i.e. those with lower line screen, are more sensitive to the stylus angle. The sharper stylus (deeper, narrower cells) gave lower void area at both levels of line screen. But the importance of stylus is more apparent at lower line screen. These results give insight into some of the practical aspects of gravure printing, as well as the physical phenomena behind the transfer of ink from a cell to the substrate. the process could possibly be used to print high solid content inks simply by increasing roller pressure, for example, or optimizing the cell geometry.

3.3.2 Response: Pinhole Area

In addition to looking at void area, the ITO films were also analyzed under a light microscope to observe the general physical characteristics of the printed layer. It should again be noted that even in cases where the films had unprinted voids, the voids took up less than 3% of the film area in all cases. Therefore a void-free printed area was chosen on each ITO film and photographed under a light microscope at two different magnifications. The microscope images allow a view of the physical characteristics of the films on a microscopic scale. There are several features present in some or all of the films that are worth noting. The first is pinholes, or holes in the films corresponding to an individual gravure cell. Most of the films had regular, repeating pinholes corresponding to most, if not all of the individual gravure cells. Most of the pinholes were circular and

had only one pinhole per cell. Other films had pinholes that were larger and irregularly shaped. Figure 3.11 shows several films with different sizes, shapes and number of pinholes.

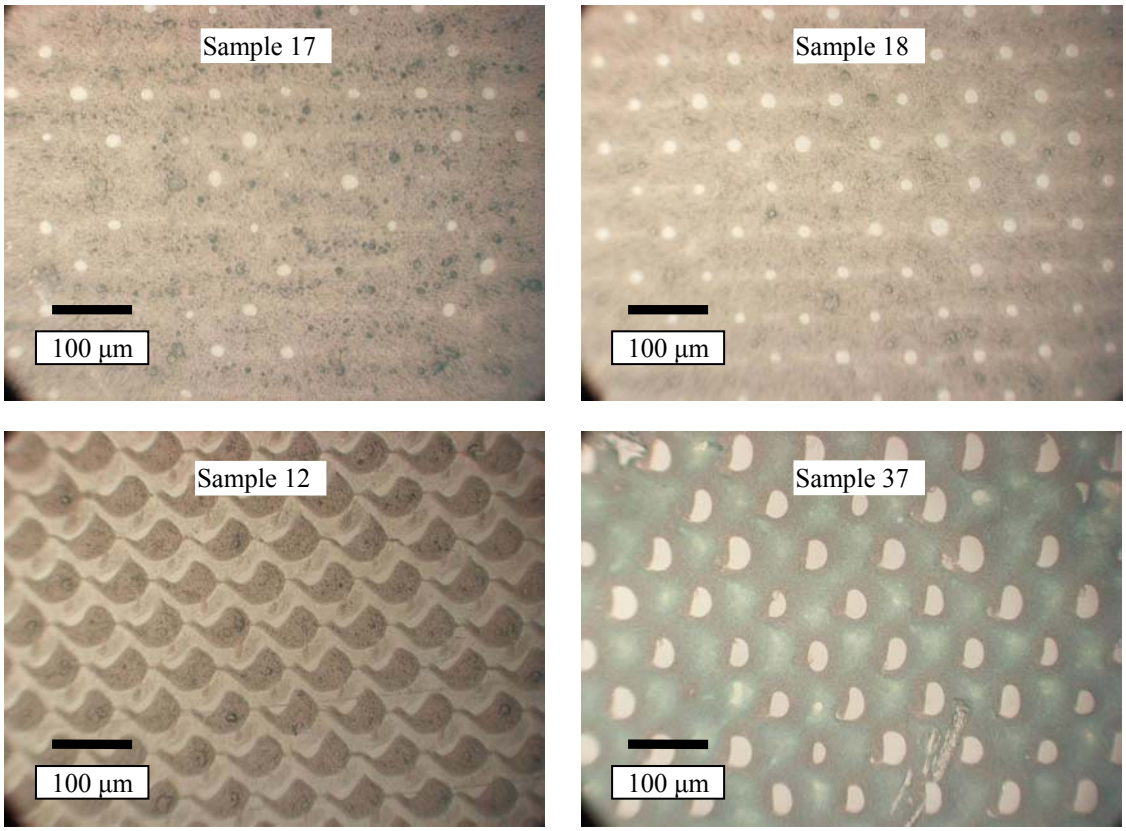

Figure 3.11: Various shapes and sizes of pinholes in printed ITO films

The pinhole area is a defect that is in general detrimental to the function of the ITO layer. Pinholes would interrupt the conductive pathways necessary to conduct electricity, driving up the sheet resistance value. Therefore it is desirable to have pinhole-free ITO layers. Since this metric was so important, the pinhole area was used as a second response variable for the experimental design. The pinhole area was calculated in the same manner as the void area calculated above, using image processing routines in

MATLAB. A sample micrograph and its corresponding binary, processed image are shown in Figure 3.12.

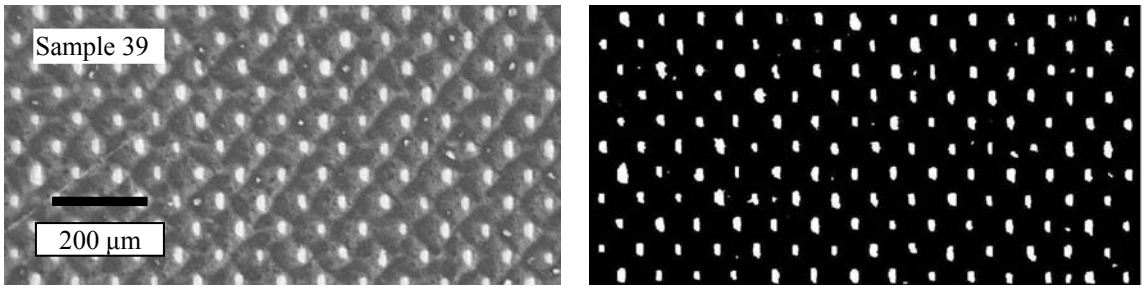

Figure 3.12: Grayscale micrograph of pinholes and corresponding image

In this case the pinhole area gives an indication of two related physical responses. The pinhole area first gives an idea of how much ink was transferred form the cell to the substrate. More ink transfer should reduce the pinhole area since there is more material to cover the substrate. However, if the ink forms pinholes at the moment of contact and solidifies before it can spread, it may contain a lot of ink and yet still retain those pinholes when dried. Therefore the pinhole area also gives an idea of how the ink spreads due to wetting forces once it is transferred to the substrate. Again, the most desirable result is that a uniform layer is deposited without pinholes or variations in thickness, so measuring the pinhole area helps define those experimental factors that will give the best printed ITO layers. The full MINITAB output for analysis of the unprinted pinhole area and effect of the experimental factors is given in Appendix B. A main effects plot summarizing the most significant main effects is given in Figure 3.13, with the response measured in numbers of pixels per image of pinhole area.

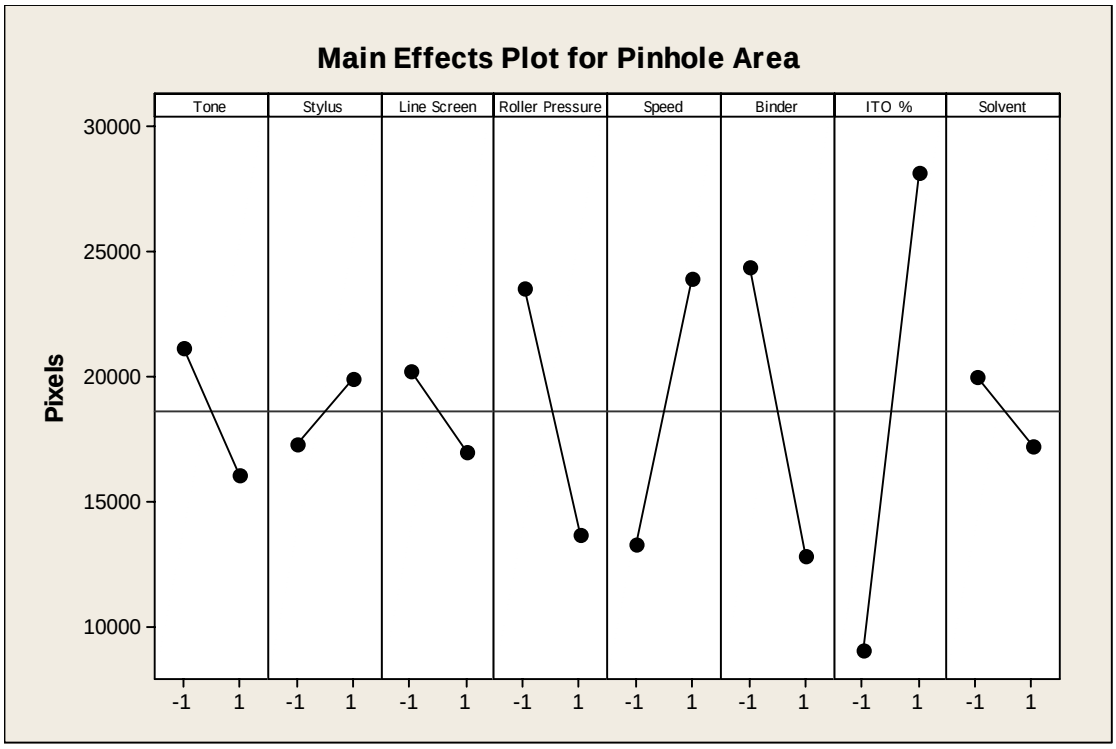

Figure 3.13: Main effects plot for pinhole area MINITAB

In this case almost all the experimental factors seem to have a significant effect on the pinhole area, with the ITO concentration being the most significant main effect. This was interesting since the ITO concentration had little effect on the void area, but was the most important factor for pinhole area. As ITO concentration increased, the inks became more viscous. This suggests that the pinholes are larger when the ink fails to spread and coalesce on the substrate after being transferred form the cells. This failure to spread could be caused by high ink viscosity or low ink surface tension. It could also be caused by premature evaporation of solvent in the ink before the ink has a chance to spread.

The binder also became an important factor for pinhole area, where it was not at all important for void area. The solvent and stylus factors seemed to reverse their effects from those on void area. In general these results were surprising, since both responses

were quantitative measures of print “quality”, and it was not expected that the experimental factors would have such divergent effects. A summary of the main and interaction effects that were found to be significant is given in Table 3.4, along with the ANOVA output from MINITAB.

Table 3.4: Summary of ANOVA results for pinhole area

Term	Effect	Coef	SE Coef	T	P
Constant		18602	789.1	23.58	0.000
Tone	-5115	-2558	789.1	-3.24	0.002
Line Screen	-3166	-1583	789.1	-2.01	0.048
Roller Pressure	-9923	-4961	789.1	-6.29	0.000
Speed	10646	5323	789.1	6.75	0.000
Binder	-11484	-5742	789.1	-7.28	0.000
ITO %	19122	9561	789.1	12.12	0.000
Tone*Stylus	3170	1585	789.1	2.01	0.048
Tone*Roller Pressure	3393	1696	789.1	2.15	0.034
Tone*Speed	-4702	-2351	789.1	-2.98	0.004
Tone*ITO %	-5336	-2668	789.1	-3.38	0.001
Stylus*Line Screen	-5624	-2812	789.1	-3.56	0.001
Stylus*Speed	-4959	-2479	789.1	-3.14	0.002
Stylus*Solvent	3983	1991	789.1	2.52	0.013
Roller Pressure*ITO %	-3585	-1792	789.1	-2.27	0.025
Speed*ITO %	5481	2741	789.1	3.47	0.001
Speed*Solvent	-7604	-3802	789.1	-4.82	0.000
Binder*ITO %	-4253	-2126	789.1	-2.69	0.008

S = 8927.28 PRESS = 14348857443
R-Sq = 82.58% R-Sq(pred) = 65.53% R-Sq(adj) = 75.68%

Analysis of Variance for Pinhole Area (pixels) (coded units)

Source	DF	Seq SS	Adj SS	Adj MS	F	P
Main Effects	8	24330463789	24330463789	3041307974	38.16	0.000
2-Way Interactions	28	10038482870	10038482870	358517245	4.50	0.000
Residual Error	91	7252373565	7252373565	79696413		
Total	127	41621320224				

For the response of pinhole area, there were many more significant effects than for void area, including interaction effects. Most significant was the influence of ITO content on pinhole area, with a higher ITO content resulting in a higher pinhole area. From the mechanistic view of gravure printing, pinholes are created when the printed ink from the gravure cells fails to spread and coalesce due to wetting forces. If the ink is too

viscous to flow under the influence of the wetting force, or if there is insufficient wetting energy for the ink to wet the surface and spread, pinholes that are present at the instant of transfer may not be filled. Additionally, if the amount of ink is very small and the internal surface tension is high enough that it counteracts the wetting force of the ink on the substrate, a pinhole may also remain. In addition to the effect of ITO content, the effects of speed, binder type, roller pressure, and several cell geometry factors were found to be significant. Higher speed resulted in higher pinhole area, while increasing roller pressure decreased the pinhole area. The Sunester polyester-based ink vehicle was found to be better for lower pinhole area, suggesting better wetting characteristics or decreased viscosity for the Sunester.

For cell geometry, a higher tone and higher line screen (more cells/inch, therefore smaller cells) gave lower pinhole area, while a higher stylus angle (sharper, deeper cells) increased pinhole area, although the stylus was not significant at the 95% level. The influence of the cell geometry suggests that smaller cells with lower bridge area between cells gives the best combination for reducing pinholes. One explanation for this is the likelihood that the ink will be transferred to the substrate in a pattern of densely spaced "pockets" of ink from the densely spaced cell pattern, and therefore will have less area to spread over to eliminate pinholes. Figure 3.14 also illustrates some of the interaction effects for pinhole area.

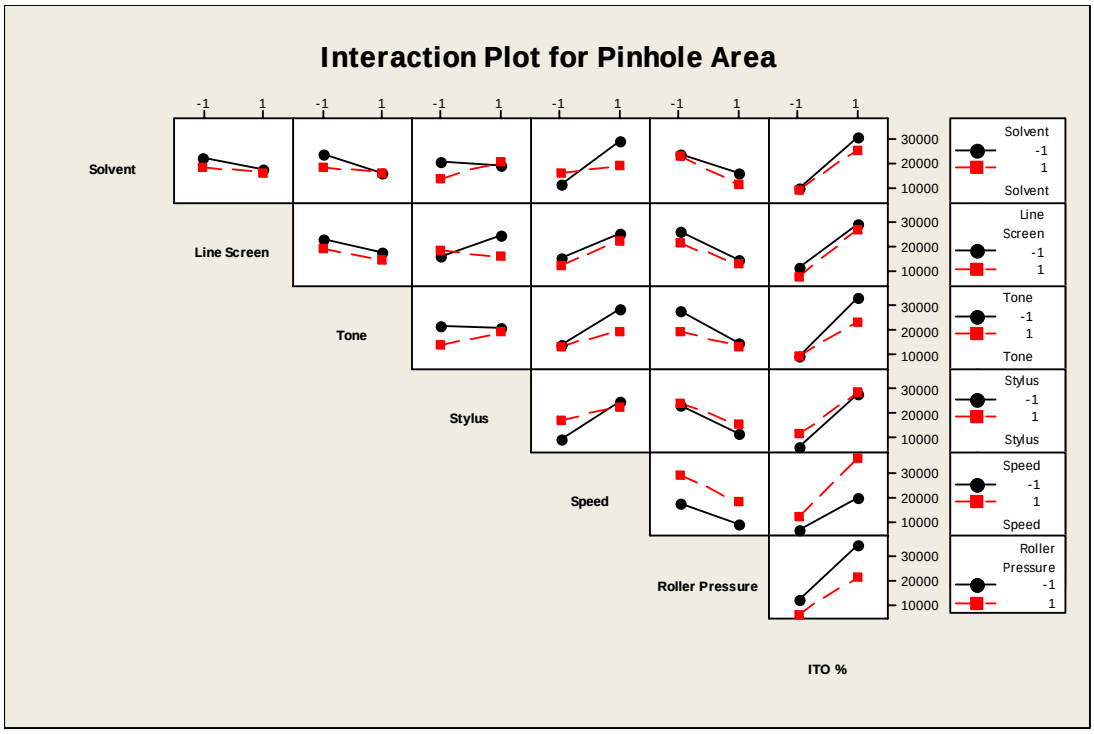

Figure 3.14: Interaction plots for pinhole area

Due to the number of interaction effects, not all of the statistically significant interactions will be discussed here. However, there were a few interactions worth noting. The interactions between speed and solvent and between speed and stylus seem to suggest that although higher printing speeds correlate with increased pinhole area, the effect of speed is less significant if there is an increase of solvent or an increase in the stylus sharpness. Therefore the solvent seems to mitigate the effects of speed, while a deeper cell is less affected by speed than a shallow one. Speed also has an interaction with tone, with a higher tone value also resulting in a less important effect of speed. In general this suggests that although speed is generally bad for pinhole area, its effects may be "tempered" by adjusting other parameters.

Some of the effects dealing with cell geometry were also interesting, such as the interaction between stylus and line screen. For higher line screen (smaller cells), the

pinhole area is reduced for an increase in stylus (sharper, deeper stylus), while there is little effect of stylus on cells at lower line screen (larger cells). This suggests that the shape of the cells, i.e. the stylus angle, has a different effect on small cells than larger ones. The sharper cell angle creates more cell volume, and therefore may contribute to increasing the amount of ink transferred for larger line screen cells.

It is interesting to note that the stylus angle has several interactions with other factors that are inconsistent, e.g. when stylus is interacted with solvent, as seen in Figure 3.14 there is an inconsistent effect on pinhole area. At higher solvent content, the sharper stylus correlates with increased pinhole area, while at lower solvent content the sharper stylus correlates with lower pinhole area. Therefore the effect of stylus angle could be better or worse for pinholes, depending on the other process parameters. For most of the other parameters, the interaction effects are at least consistent, i.e. for a given factor level the effect of another factor will wither increase or decrease. The effect of stylus geometry is unique and has a complex effect on pinhole area. Since the stylus angle has the most effect on the shape of the gravure cell, this suggests that different cell geometry may significantly affect the way ink is transferred to the substrate. It should be noted, however, that the different stylus angles used produced considerably different cell shapes, with the sharper stylus giving a more jagged bridge area than the other (see Appendix E).

It should also be noted that the coefficient of correlation, R^2, is much higher for the pinhole area response than for the void area response. For the response of void area, the R^2 is only 48.88%. This suggests that the creation of voids is at least partially influenced by factors not taken into account during the experiment. For the response of

pinhole area, the R^2 value is 82.58%, suggesting that there is much better relationship between the experimental factors and that response.

3.4 Other Observations

There were also several phenomena observed in the screening experiments that give insight into the ink transfer process. In the case of pinholes, it was found that the location of the pinholes corresponded to the center of the individual gravure cells. That is, when the substrate comes into contact with a gravure plate, a pinhole can occurs where individual cell comes into contact with the substrate, the ink appears to wet the outside edges of the cell, but not in the center. This is illustrated in Figure 3.15. The micrograph shows several different inking patterns, with one portion having no ink transferred from the land area between cells, and other areas with ink filling the area corresponding to the land area, and yet still having pinholes in the center of the cell.

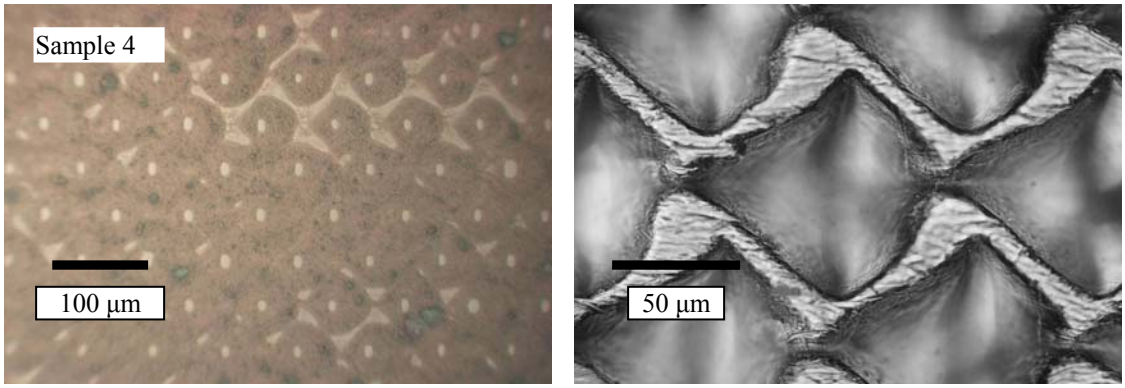

Figure 3.15: Pinholes and corresponding cell geometry

In fact, it appears that the pinhole occurs not at the very center of the cell, but offset slightly from the center in the direction of print. In Figure 3.15, the film was

printed from right to left, which means that the small pinholes occur near the rear of the cell as it is printing. In addition to the pinhole in the rear-center of the cell, it also appears that in the same micrograph there are locations in which the ink was not transferred from the bridge locations, suggesting that the ink did not wet the bridge area and flow out of the cell under the wetting force. From this we can conclude that the ink does in fact print from the bridges and edges of the cells, most likely due to concavity in the center of the cells created by the wetting force pulling ink out of the cells at the edges, as well as reduction in ink volume due to the evaporation of solvent.

The ink also formed interesting topology when examined under the microscope. In many of the films, when viewed at a lower magnification, distinctive patterns could be observed, with a clear pattern in the variation of thickness across the film. The thickness seemed to vary according to rows of cells, with greater film thickness corresponding to the area between rows and columns of cells. Figure 3.16 shows this variation in some of the various patterns observed.

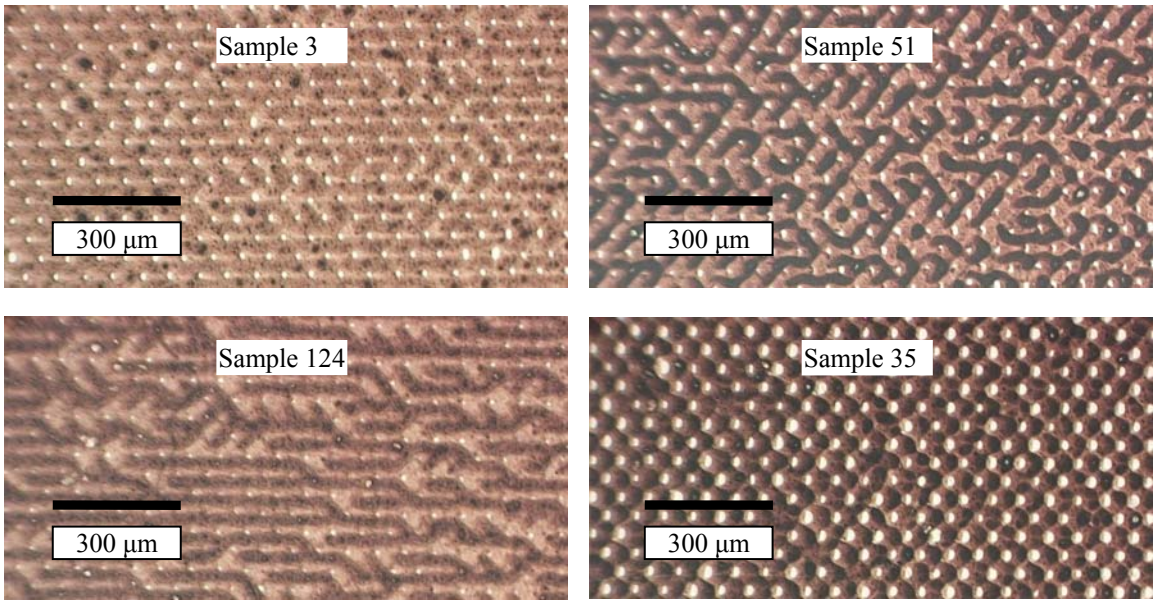

Figure 3.16: Varied thickness profiles in printed ITO films

The patterns shown above give insight into how the ink transfers from the cells to the substrate. In appears certain that the ink does not stay level, but is pulled away from the centers of the cells, most likely due to the wetting force. Depending on the characteristics of the ink and the process parameters, the ink may deform in regular patterns before coming into contact with the substrate. The ink may also continue spreading and forming such patterns before finally solidifying due to evaporation of the solvent in the ink.

Another phenomenon that was observed was the occurrence of clumps of in the printed films. These clumps were randomly occurring, with variation in size and location. In general the clumps were a few microns to a few tens of microns in diameter. Since these clumps were a source of non-uniformity, they had the potential to reduce the functional performance of the printed ITO layer. Figure 3.17 shows an ITO film with relatively uniform thickness, except for pinholes and the presence of clumps (dark spots).

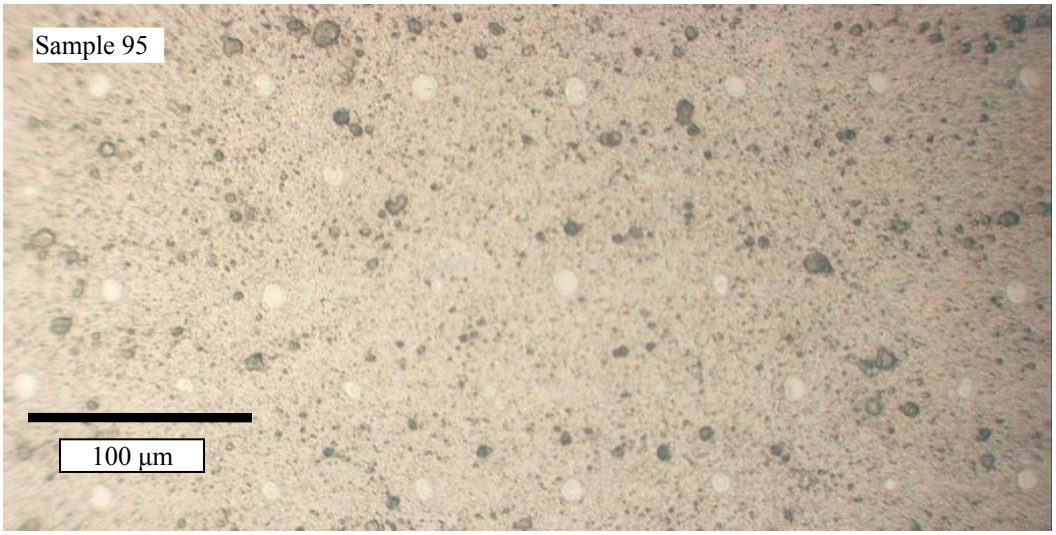

Figure 3.17: Pinholes and clumps in printed ITO film

It was assumed that the clumps were primarily composed of ITO nanoparticles. However, it was not clear whether the ITO had formed into clumps due to the agglomeration of individual particles prior to printing, or whether the clumps were simply due to the drying behavior of the ink on the substrate as the solvent rapidly evaporated. Although the inks were mixed ultrasonically, there was no analysis of whether or not the nanoparticles were uniformly dispersed within the ink. An analysis of this problem, including scanning electron microscope (SEM) image analysis, is described in Chapter 6.

3.5 Summary

The screening experiments were valuable in understanding the gravure process and under what conditions ITO nanoparticle-containing inks can be printed. The conclusions drawn from this set of experiments are summarized below.

Analysis of the effects of process parameters on the void area lead to several important conclusions. In general, ink can successfully be transferred from a gravure cell as long as it wets the cell initially and is able to wet the substrate after doctoring. The ink properties, such as ITO content, have little influence on whether or not the ink will wet the substrate, even though ITO content can greatly affect ink properties. Increasing roller pressure can reduce the occurrence of any void areas, most likely by ensuring intimate contact between the cell and substrate. The cell geometry is also an important factor, with void area deceasing as tone increases and as stylus angle decreases. The exact cause of this is unknown, although it likely has to do with the interaction between the wetting forces between the ink and the edge of the cell, and how the ink deforms due to the wetting force prior to coming into contact with the substrate. Interaction effects between cell geometry variables (stylus, tone, and line screen) were significant, as well as interactions between these variables and the amount of solvent. These interactions suggest the shape of the cells, the amount of bridge area between cells, and the behavior of the ink in the cells and on the bridge area before ink transfer all affect the ability of the ink to transfer from the cells to the substrate.

Analysis of the effects of the process parameters on the pinhole area also led to some very important conclusions. The most interesting finding was that the ITO content was the most significant factor, with higher ITO content corresponding to higher pinhole area. This is interesting when contrasted with the results for void area, since ITO had little effect on void area. This shows that even though ink with high ITO content can be printed, it does not necessarily print high quality films. There was also a difference between the two different ink vehicles, with the polyester resin-based Sunester ink

vehicle correlating with lower pinhole area than the urethane resin-based Flexomax vehicle. The addition of solvent also decreased pinhole area. This was also interesting because the addition of solvent had an adverse effect on void area, with more solvent corresponding to an increase in void area. In general more parameters were significant to this response than to void area, suggesting that the control of surface morphology of a dried ink film is a very complex and must take into account many different factors. However, the ANOVA results also showed a better correlation as measured by the R^2 value of process parameters on pinhole area. The R^2 value for void area was quite low, suggesting that the response is significantly affected by random factors not taken into account in the experiment. Pinhole area also seemed to be influenced by interaction effects between several different variables, suggesting complex interactions of cell geometry, speed, and ink formulation.

In addition to the effects of the process parameters on our chosen responses, the physical characteristics of the printed films, e.g. pinhole location, film thickness variation, and clumping in the films give an insight into how the ink behaves during the process and on the substrate as it dries. These characteristics of the printed film are important as they relate directly to the functional characteristics of the ITO. In general for a conductive film it is important to have a continuous film with consistent thickness and consistent physical properties throughout the film.

CHAPTER 4

MAIN EXPERIMENT

The main experiment was designed to give a more complete description of the gravure process and the deposition of functional ITO films. From the screening experiment there appeared to be several effects that were significant, including several interaction effects. However, the screening experiment was designed primarily to explore the process and determine suitable factor levels for achieving thin, uniform films. Once the suitable factor levels for the ink and gravure press were identified, the main experiment was then designed to investigate the process under these improved conditions, and at different levels. A central composite design was chosen in order to allow estimation of quadratic effects. For this main experiment the choice of response variables was based on the need to characterize the ITO films in terms of physical characteristics, which in turn could be related to the functional characteristics of the film. This chapter describes the experimental approach taken and the results of the experiment.

4.1: Experimental Design and Selection of Factors and Levels

From the screening experiments, it was observed that ITO and solvent content significantly affected the characteristics of the printed film, specifically the pinhole area. Since pinholes are generally undesirable for functional films, an effort was made to reduce the pinhole occurrence by changing the ITO and solvent composition in the inks. Therefore ITO content was reduced somewhat and solvent was kept approximately the same levels. Since a central composite design was chosen, five levels of each factor were

chosen. The factor levels for speed and pressure were kept at approximately the same range, with additional factor levels chosen in between the two extremes. Table 4.1 gives the factor levels chosen for this experiment. It should be noted that the cell geometry factors were set at only two levels, as the same plate used in the screening experiment was used in this experiment.

Table 4.1: Factor level settings for printing experiment

	Cube Points for Central Composite Design				
Factor	**-2**	**-1**	**0**	**1**	**2**
Roller Pressure (lb/inch)	30	35	40	45	50
Solvent Weight %	10%	15%	20%	25%	30%
Speed (m/min.)	5	10	15	20	25
ITO Weight%	25%	30%	35%	40%	45%
Stylus Angle	N/A	150	N/A	110	N/A
Tone	N/A	90%	N/A	100%	N/A
Line Screen (cells/in.)	N/A	300	N/A	360	N/A

It was originally anticipated that the screening experiment would identify factors that were unimportant and could be eliminated. However, only the ink vehicle type was dropped for the main experiment. The ink vehicle had no effect on void area, and the effect on pinhole area was clear, with the Sunester vehicle giving lower pinhole area. Therefore the Sunester was chosen as the ink vehicle for the main experiment. The cell geometry variables remained the same, since the same gravure plate was used and could not be changed. All of the other factors were found to be significant on the screening experiment and were therefore included in the main experiment, for a total of 7 experimental factors. MINITAB statistical software was used to generate a mixed central composite design, with 4 of the variables at 5 levels, and the cell geometry variables at two levels. MINITAB was also used to perform the analysis of the data after the

experiment was performed. The experiment was performed using the same procedures for operating the printing press as described in Chapter 3, and the run order was again randomized.

4.2: Results and Discussion

The printed ITO films were very much improved from those obtained from the screening experiments. The void areas observed in the screening experiments all but disappeared, with the films showing much improvement in thickness uniformity. Additionally, the pinholes visible under microscope were also reduced, and in most cases disappeared altogether. Thus the choice of factor levels based on the results of the screening experiments was very successful in reducing both voids and pinholes. However, there was still a lot of variation in the thickness and there were also very many clumps again visible in the films. Since there were virtually no voids or pinholes, a new set of responses was chosen to characterize the films. The average thickness is important because many functional characteristics, e.g. transparency and sheet resistance, are thickness dependent for ITO. Thus the effect of process parameters on the average thickness was analyzed. In addition to the thickness, a measure of the non-uniformity in thickness of the films was also desired. There are many ways of measuring this, but it was decided that a simple average roughness, R_a, value could give a general characterization of all the irregularities, clumping, and thickness variation.

4.2.1: General results

In addition to the physical characteristics, the functional performance of the ITO was measured. The films were all conductive to some degree, however the sheet resistance was very high. A typical sputter-deposited ITO-on-glass film has a sheet resistance of a few tens of ohms/square, while the lowest sheet resistance of the printed ITO films was several hundred of *kilo*-ohms/square (kΩ/□), with some films measuring a sheet resistance into the many *mega*-ohms/square (MΩ/□) The films were also transparent to a certain degree, but certainly not as transparent as a typical ITO-on-glass film, which typically has over 95% transparency in the visible spectrum. The % transparency at 550 nm light wavelength ranged from around 30-65%. Thus the performance was very poor compared to a typical ITO film. This was not surprising because the ITO ink was not completely optimized for functional performance and was composed of nanoparticles in a polymer matrix instead of a solid film. However, the variations in performance did allow for analyzing the relative effects of the various process parameters on performance, specifically the sheet resistance and transparency of the ITO. Because of difficulties and time involved in measuring the sheet resistance and transparency, only a subset of the samples, or about 1/3 of the total number, was measured. Because of this, a full analysis of the effects of all the process factors on sheet resistance and transparency was not available.

The performance of the ITO films was dependent on many factors. Some of these factors are materials issues which cannot be properly addressed here. However, because of the wide range in performance, it is clear that different process factors can contribute to how well the ITO performs. It is unclear, however, whether those factors contribute

directly to the performance, or whether other parameters are responsible. In an effort to understand some of the underlying mechanisms and causes for variation in performance, the sheet resistance and transparency were studied not only in terms of the effects of the process parameters, but also the correlation with other fundamental variables. These variables include measured values such as viscosity and surface tension of the ink, as well as measured values of the cell, such as measured cell volume, bridge area, and cell aspect ratio. These variables give insight into the mechanism of the process beyond the effects of the experimental factors. The effects of these variables will be discussed in Chapter 5.

4.2.2 Average Film Thickness

The analysis of the effects of the experimental factors on average film thickness was completed using MINITAB. Full results from MINITAB are available in Appendix B. A summary of the statistically significant effects is given in Table 4.2. The film thickness was obtained by scanning the edge of the film sample using a stylus profilometer and measuring the step height. A sample graph of the profile data is shown in Figure 4.2. Each sample was measured five times in different locations to calculate an average value for analysis. It was assumed that this average value represented the true thickness of the sample.

The determination of a thickness measure for the printed ITO films was challenging in a number of ways. The first challenge was to measure a layer that was under a micron thick, but was relatively rough, with R_a values of several hundred nm in some cases. There was also a need for a nondestructive method since the films needed to

be analyzed for sheet resistance, etc. at a later time. A stylus profilometer (KLA Tencor Alpha-Step IQ) was chosen as the measurement tool. Several trial measurements were taken to verify that the samples were not damaged by the profilometer, and to verify that the thickness could be detected. The films were printed on polyester films which were extremely smooth, and it was therefore easy to detect a step height change in the profilometer scan.

There was, however, an issue with the waviness in the flexible substrate. Since the films were under a micron thick, and the substrate was not rigid, it was difficult to determine the thickness away from the edge. This was due to the lack of a reliable reference to measure from away from the edge of the film, since the substrate itself was taken as the reference, and could only be detected at the edge of the samples. This is illustrated in Figure 4.1. Since the estimate of the thickness was less reliable away from the edge, it was impractical to take profilometer scans over long distances. An attempt to filter the data so the waviness of the substrate was eliminated also resulted in an undesired adjustment of the reference line, which also gave inaccurate measurements. Therefore the thickness measurement was only taken on very short profilometer scans at the edges of the films. It was assumed that the thickness at the edges of the films were representative of the entire film.

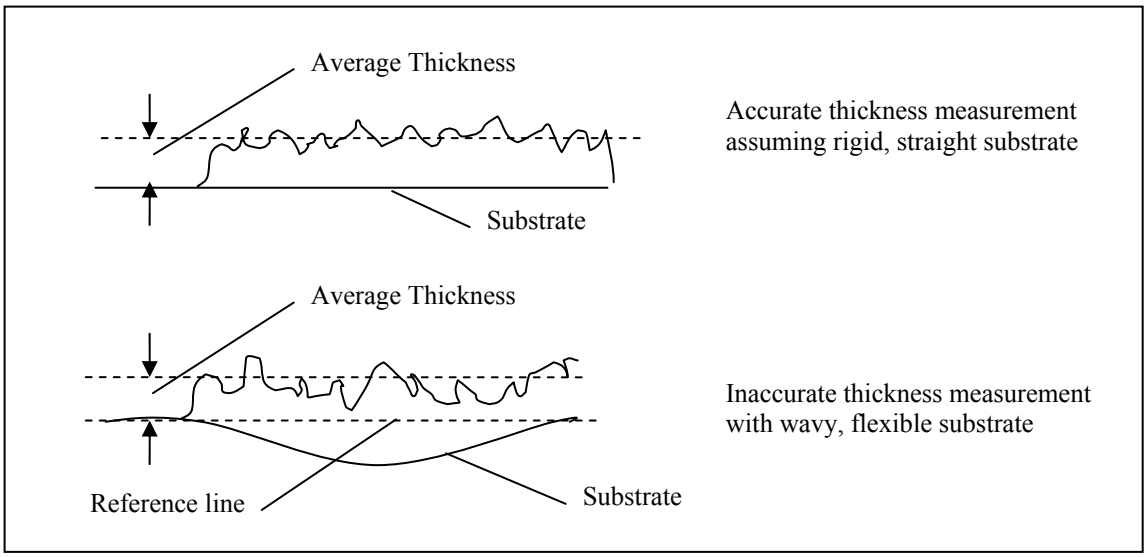

Figure 4.1: Illustration of waviness effect on thickness measurement

The thickness was measured over a scan length of 1000 μm. The profilometer stylus was located just off of the film on the substrate to start the scan. The scanned profile included about 70% film thickness and 30% substrate, i.e. on a 1000 μm scan 200 μm would scan the substrate, at which point the stylus would reach the film edge and then scan over the film thickness for 700 μm. It was assumed that the thickness was approximately constant from the edge of the film to the end of the scan on the interior of the film area. It was also assumed that the waviness of the substrate was not significant over the length of the scan. A sample scan is shown in Figure 4.2.

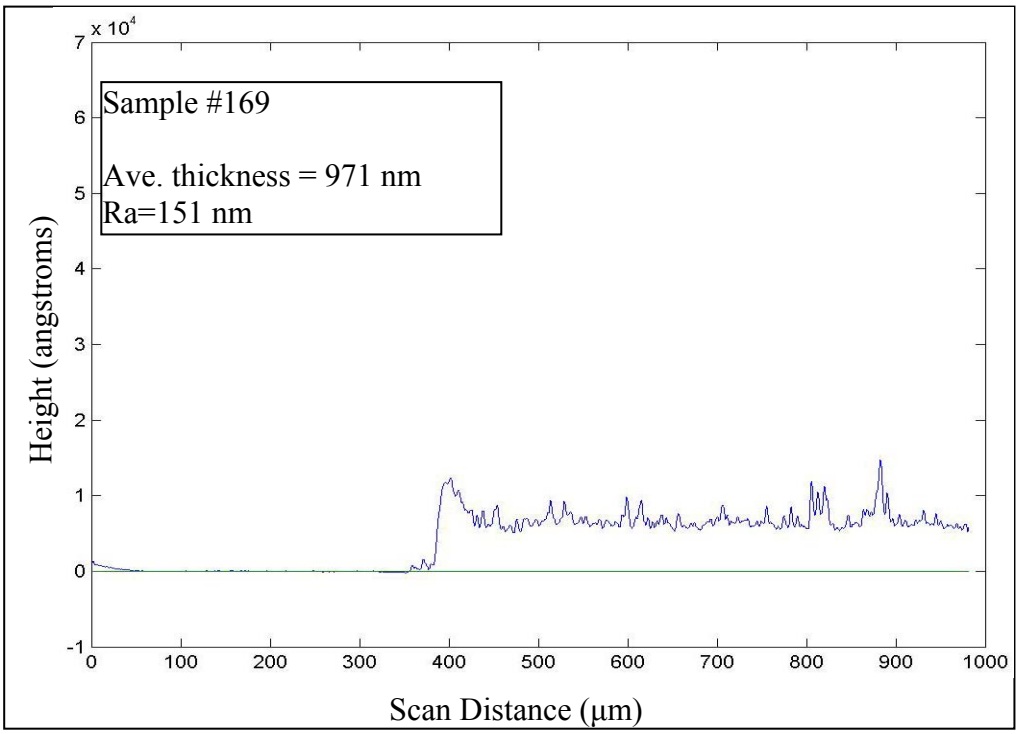

Figure 4.2: Profilomer scan for thickness measurement

Table 4.2: Regression coefficients for average thickness

Estimated Regression Coefficients for Average Thickness

Term	Coef	SE Coef	T	P
Constant	621.971	10.623	58.547	0.000
Speed	-34.867	8.559	-4.074	0.000
ITO%	122.124	8.559	14.268	0.000
Solvent	-21.708	8.559	-2.536	0.012
Line Screen	-54.102	3.955	-13.679	0.000
Stylus	56.181	3.955	14.204	0.000
Tone	65.816	3.955	16.640	0.000
Speed*Speed	-42.919	17.334	-2.476	0.014
ITO%*ITO%	72.252	17.334	4.168	0.000
Solvent*Solvent	-60.872	17.334	-3.512	0.001
Pressure*Speed	79.695	20.823	3.827	0.000
Pressure*Solvent	-43.101	20.823	-2.070	0.040
Pressure*Tone	-18.010	8.522	-2.113	0.036
Speed*Line Screen	19.172	8.522	2.250	0.026
Speed*Stylus	-31.955	8.522	-3.750	0.000
ITO%*Solvent	51.926	20.823	2.494	0.013
ITO%*Line Screen	-22.679	8.522	-2.661	0.008
ITO%*Tone	28.533	8.522	3.348	0.001
Solvent*Stylus	18.140	8.522	2.128	0.035
Solvent*Tone	-18.339	8.522	-2.152	0.033
Line Screen*Stylus	-8.258	3.945	-2.093	0.038
Stylus*Tone	8.066	3.945	2.044	0.042

S = 60.0954 PRESS = 988655
R-Sq = 83.88% R-Sq(pred) = 77.82% R-Sq(adj) = 81.29%

It can be seen that the largest effects are the ITO content and the cell geometry variables. Nearly every main effect was found to be significant, along with several interactions and quadratic effects. However, the model did have an R^2 value of over 80%, suggesting that the process parameters have a relatively high correlation on the average thickness, but that there is still a lot of variability that cannot be explained by the experimental factors.

The cell geometry factors all had a large influence on the average layer thickness. The levels of the geometry factors corresponding to larger cell volumes, i.e. lower line screen, higher tone, and higher stylus, corresponded to higher thickness values. So in general larger cells produced thicker films, which is not surprising given the increased volume of ink that they contained. The ITO content also had a major influence on the thickness. Higher ITO content led to higher thickness values. Part of this effect could be explained by the fact that as ITO content increased, the amount of ink vehicle decreased. Since the dried ink film consists only of the ITO non-evaporative components of the ink vehicle, an ink with higher ITO content would contain less overall solvent concentration, and therefore retain more mass after solvent evaporation. Therefore a dry ink film with high ITO content would be expected to be thicker than a film with low ITO content, even if the transferred volume of the ink was the same. This effect also partially explains the effect of solvent content, which in this experiment had the effect of reducing thickness as solvent content increases. Again, since the solvent in the ink evaporates, then more solvent would invariably lead to lower thickness.

The effect of speed was also significant. A higher speed resulted in a lower average film thickness. There is no clear explanation for this, although from our mechanistic view of the ink transfer process, it would seem that the inertia of the ink in the cell may prevent the ink from flowing out of the cells as quickly at higher speeds. The ink would tend to stay in the cell due to its inertia if the substrate was removed too quickly, and therefore less ink transfer would occur.

A main effects plot for the experimental factors is shown in Figure 4.3. This figure shows the relative effects of the individual factors on the average ITO layer thickness. The main effects plot shows not only the trends of the thickness as process parameters change, but also shows the nonlinear nature of the effects. From Table 4.2, it appears that some second order effects (e.g. speed*speed) are also statistically significant. This is especially interesting in the case of the factors speed and solvent content.

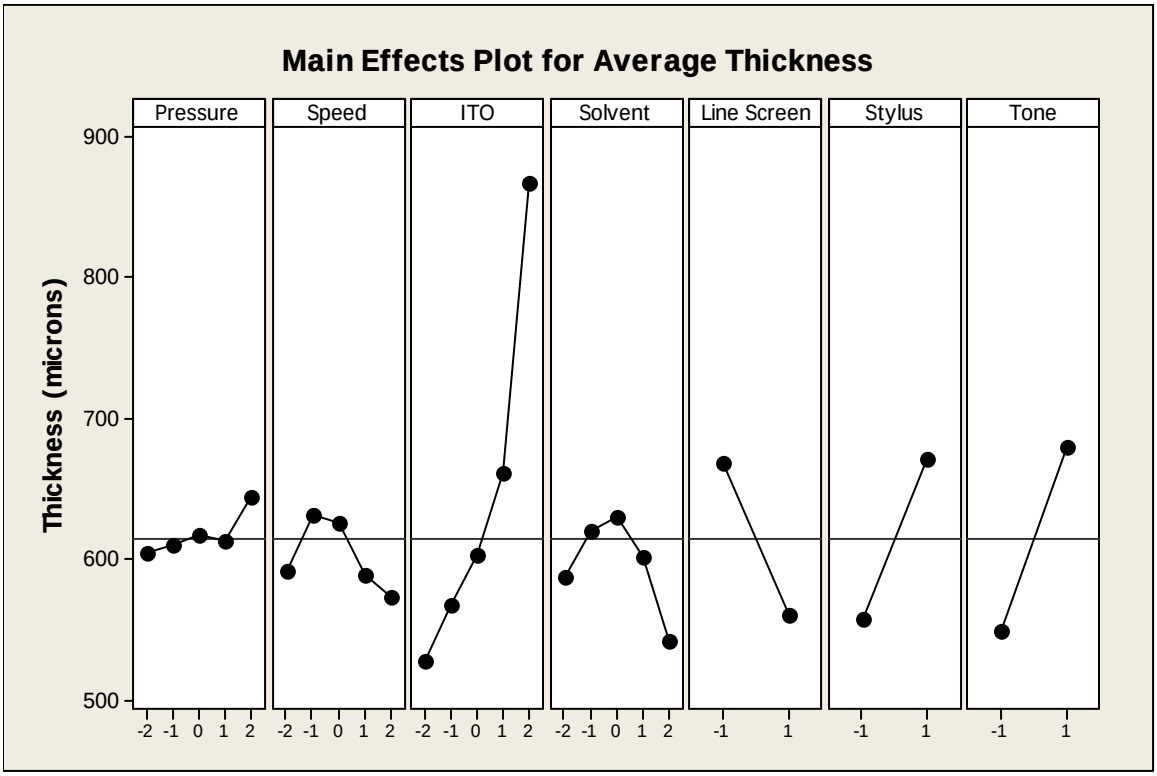

Figure 4.3: Main effects plot for average ITO thickness

The main effects plot illustrates several important effects observed in the experiment. The pressure was found to be insignificant at the 95% level, but in general the main effects plot suggests that an increase in pressure may slightly increase the thickness, although any effect appears to be small. One explanation for this is that an increase in pressure on the roller increases the size of the contact area of the roller, thereby increasing the amount of time the substrate is in contact with the gravure plate. This could give better ink adhesion and therefore more ink transfer.

The speed factor seems to have a nonlinear effect, with an increase in speed corresponding to an increase in thickness at low speeds, and then a decrease in thickness at higher speeds. This may be due to solvent evaporates immediately after the plate is doctored, reducing the amount of ink in the cell. If the speed increases, it will reduce the

amount if time the solvent has to evaporate and therefore have more ink in the cell to transfer. Therefore printing at higher speed will allow the ink transfer to happen when there is more ink in the cell, thereby increasing the amount of ink transferred. However, at even higher speeds, the ink may not wet the substrate as well, or may tend to stay in the cell due to the inertia of the ink if the substrate separates from the cell at too high of a speed. With the solvent, it appears that although an increase in solvent will cause a decrease in thickness due to the decrease in non-evaporating volume, as discussed above, at lower solvent levels the increase in solvent also has the opposite effect. This may be due to the effect of ink viscosity or surface tension, which would be affected by the solvent content.

As the amount of ITO increased, the thickness also increased. This is most likely due to the increase in relative solid content (ITO and binder) as ITO increases, as discussed previously. However, it may also be in part due to the change in ink properties as the composition changes. An increase in ITO will generally increase the viscosity of the ink, and may affect the internal cohesive forces of the ink. Therefore the increase in ITO may lead to higher film thickness due to better ink transfer properties of a more viscous or cohesive fluid. The effect of adding solvent is also related to the effects of the ITO. At lower levels of solvent, the addition of solvent actually increases film thickness. Although the addition of solvent tends to reduce the viscosity of the ink, it may actually help the ink to wet the substrate and therefore enhance the transfer of ink. However, at higher solvent concentrations, the solvent will dilute the ink so there is less total solid left after the solvent evaporates, thereby reducing the thickness.

There were also many statistically significant interaction effects among the experimental factors. Because of the number of interactions, it would be very difficult to understand all of these interactions and why they occur. A full interaction plot is found in Appendix B. Some of the interactions, however, may be of particular interest. Figures 4.4 and 4.5 illustrate some of the more interesting interactions.

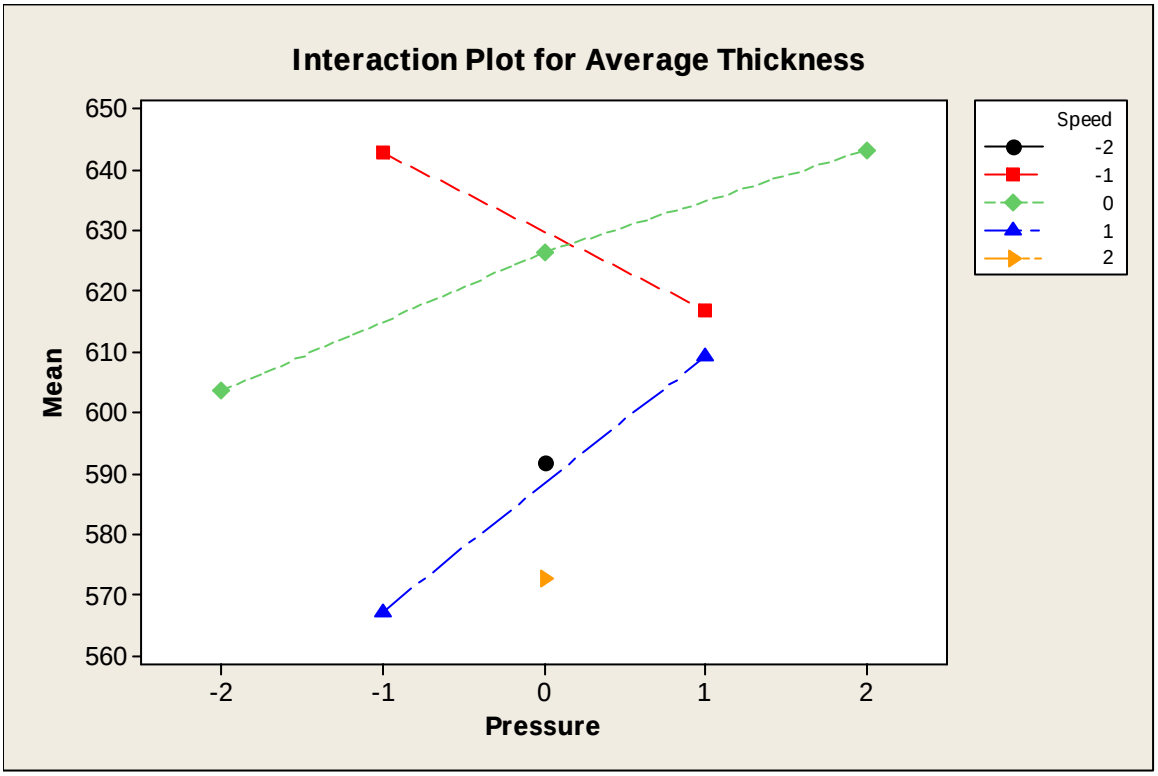

Figure 4.4: Interaction effect plot of pressure and speed

The interaction between pressure and speed is interesting because pressure and speed both affect the time that the substrate is in contact with the cell. The pressure affects this indirectly by increasing the width of the contact area. In Figure 4.2 it appears that in general increasing the pressure corresponds with higher thickness. One exception, however is apparent at a speed at the "-1" level (shown in red). At this level the increase

in pressure corresponds to a decrease in thickness. This again may be due to the evaporation of solvent form the cell. At lower speed there is more time for the solvent to evaporate, resulting in less ink available to transfer.

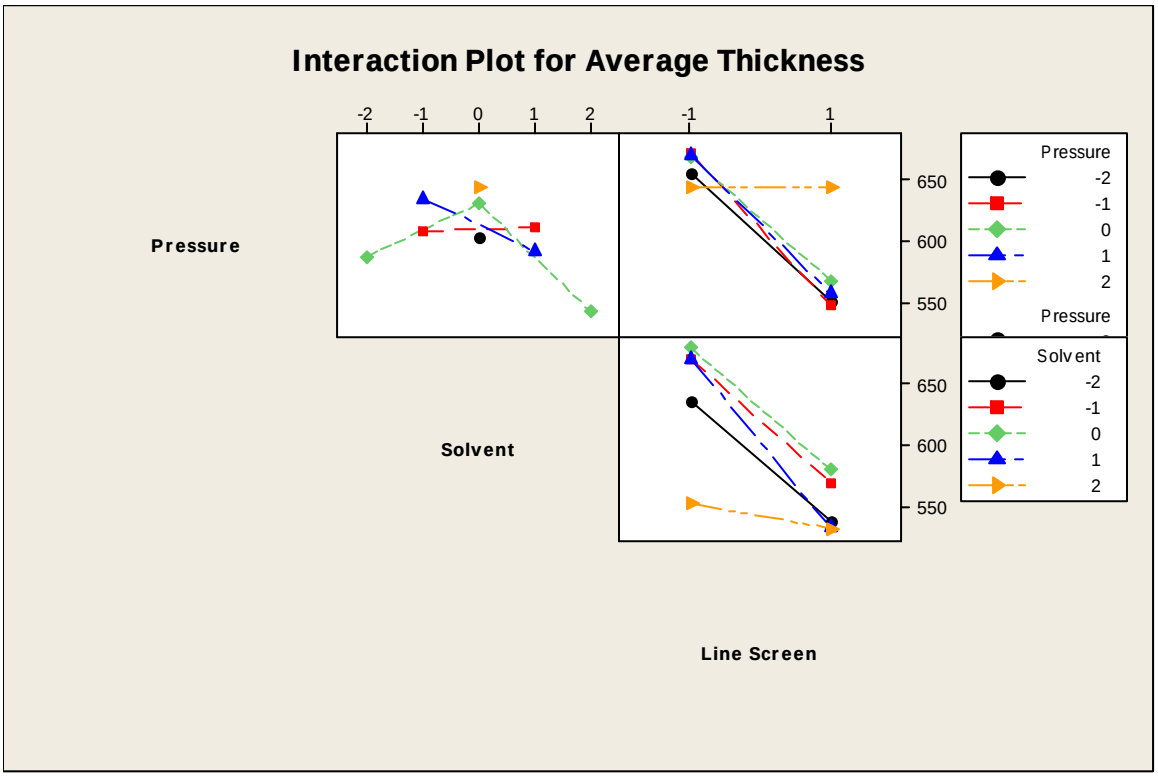

Figure 4.5: Interaction plot for average thickness

Figure 4.5 illustrates several more interesting interactions. The interaction of line screen and solvent shows that at the highest level of solvent, the effect of line screen is less significant. Although an increase in line screen (decrease in cell size) corresponds to a lower thickness value, as the solvent increases, there is a drastic decrease in the thickness at lower line screen. This suggests that an increase in solvent may decrease the amount of ink transferred in larger cells. This may be due to changes in the viscous or

cohesive properties of the ink, or may be related to how the solvent evaporates from larger cells.

The other interaction effect illustrated in Figure 4.5 worth noting is the interaction between pressure and line screen. At high levels of pressure, there is a drastic increase in thickness corresponding to the higher line screen. In fact, at all other levels the higher line screen corresponded to lower thickness. At the highest pressure, however, there was no effect of line screen on the thickness. It therefore appears that an increase in pressure may somehow contribute to a higher proportion of ink being transferred from the cell to the substrate. The reason for this is not clear, and it only appears as an effect at the highest level of pressure, as can be seen in Figure 4.5. It may be related to the increase in time that the substrate is in contact with the cell, caused by increased contact width at higher pressures, as mentioned previously. It may also be related to a difference in boundary conditions between the cell and substrate, including differences in pressure, contact area, or even sliding of the substrate over the cell.

4.2.3 Roughness

The effects of process parameters on the roughness, R_a, will now be discussed. The roughness of the ITO films is a measure of the relative variation in thickness. Although several different roughness parameters were available and could be easily calculated with the profilometer analysis software, the R_a value was easily able to characterize differences in surface texture (see Figure 4.6). The roughness was measured using a stylus profilometer, the same instrument used to take the thickness measurements. However, in this case the profilometer scans were not taken at the edges of the films, and

were taken in random locations and in different lay directions. The scan settings used to characterize the roughness are shown in Table 4.3.

Table 4.3: Roughness measurement settings

Scan length (μm)	5000	Measurements taken on a KLA Tencor Alpha-Step IQ surface profilometer
Scan Speed (μm/s)	200	
Vertical Resolution (μm)	0.2	
Filter type	Gaussian	
Filter Cutoff (μm)	250	

The roughness measurements were taken on the same KLA Tencor profilometer as were the thickness measurements. In order to characterize the average roughness over the entire sample, five measurements were taken. Through a trial and error approach, a filter cutoff of 250 μm was chosen. A scan length of 5000 μm was chosen and the five separate scans were taken at approximately evenly spaced intervals across the samples. The response was defined as the average R_a value of the five measurements. Three measurements were taken in the lateral direction across the samples, while two measurements were taken in the longitudinal direction. The variation in thickness of the films can be seen clearly in the micrographs in Figure 4.6. These pictures show the different patterns observed on the ITO films. All the films were characterized by the formation of clumps from a few to several tens of microns in diameter across the film. The roughness value seems to correlate well to the differences in texture of the films.

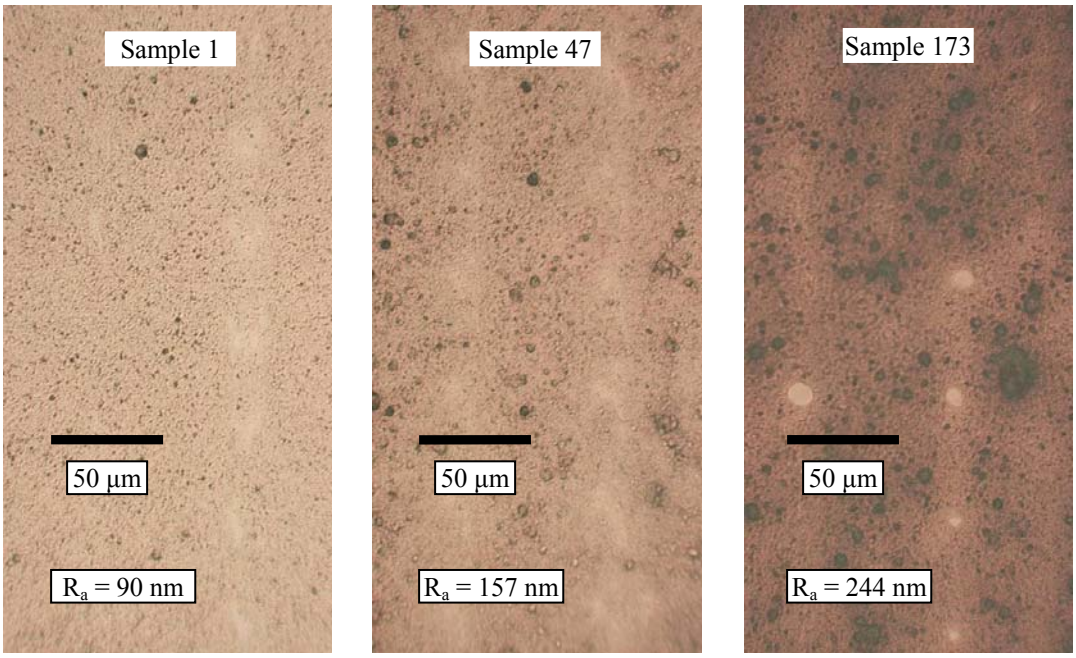

Figure 4.6: Printed ITO films of varying roughness values

The effect of the process parameters on the average roughness as calculated in MINITAB is given in Appendix B. A summary of the most significant effects, i.e. p-value is less than 0.05, is shown in Table 4.4. A main effects plot is shown in Figure 4.7.

Table 4.4: MINITAB regression results for average R_a value

Estimated Regression Coefficients for Average R_a

Term	Coef	SE Coef	T	P
Constant	122.276	3.907	31.295	0.000
Speed	-11.617	3.148	-3.690	0.000
ITO%	46.678	3.148	14.828	0.000
Solvent	-7.287	3.148	-2.315	0.022
Line Screen	-8.138	1.455	-5.595	0.000
Stylus	6.961	1.455	4.786	0.000
Tone	9.738	1.455	6.695	0.000
Speed*Speed	-37.143	6.375	-5.826	0.000
Solvent*Solvent	-41.560	6.375	-6.519	0.000
Pressure*Speed	29.684	7.659	3.876	0.000
Pressure*ITO%	-19.129	7.659	-2.498	0.013
Speed*ITO%	-36.931	7.659	-4.822	0.000
ITO%*Solvent	16.184	7.659	2.113	0.036
ITO%*Line Screen	-13.617	3.134	-4.344	0.000
ITO%*Tone	11.043	3.134	3.523	0.001

S = 22.1022 PRESS = 128353
R-Sq = 72.10% R-Sq(pred) = 63.16% R-Sq(adj) = 67.61%

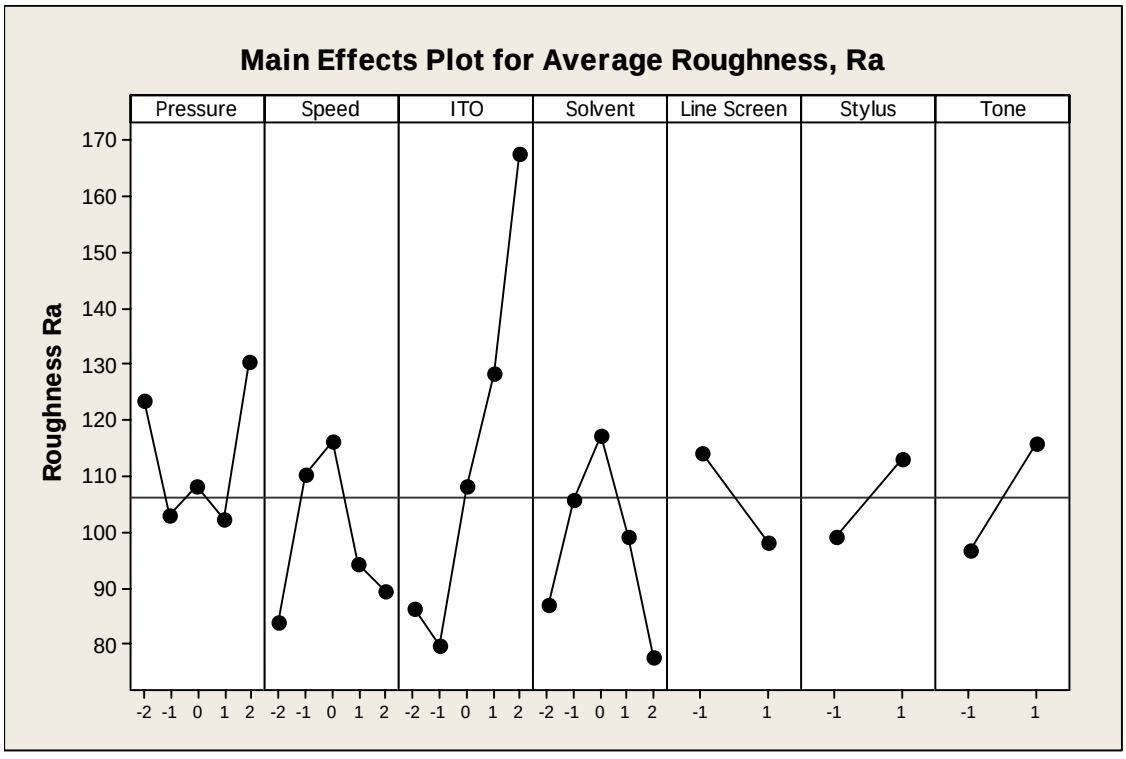

Figure 4.7: Main effects plot for roughness, R_a

The effects of the process parameters on the roughness had a coefficient of correlation, R^2, of only 72.1%, which was not as high as the R^2 value for thickness. It is quite interesting that from the main effects plot the effects are very similar to those for average thickness, suggesting very strongly that the thickness and roughness are largely dependent on the same factors, with similar relationships for both responses. ITO content again was the most significant effect. This is not surprising, since the texture of the films is characterized by the "clumps" of ITO discussed previously. As discussed in Chapter 3, it is unclear whether the ITO nanoparticles agglomerate within the ink and never disperse into the solvent and binder matrix, or whether the clumps that occur on the films are formed by the drying behavior of the ink, with the nanoparticles well-dispersed within the clump. Section 6.5 describes a scanning electron microscope (SEM) analysis that gives further insight into this question.

Among the other main effects that have a significant effect on roughness, it appears that the cell geometry factors are relatively important. As line screen increases, roughness decreases, and as tone and stylus increase, the roughness increases. This suggests that the size and shape of the cells can affect the surface morphology of the dried ink film. This may be due to the fact that in an evaporative solvent based ink, the ink has limited mobility as it dries. Therefore the ink may be transferred to the substrate and have a certain "starting morphology" From there the ink will be under the influence of surface tension and wetting forces that will tend to cause the ink to coalesce and form a more level surface. However, as the solvent evaporates, the movement of the ink under these wetting forces is interrupted, and the ink "freezes" in whatever position it was in when it reached a critical level of solvent evaporation. The effect of cell geometry on

roughness is likely due to the different "starting morphologies" created by different cell shapes and sizes. The effects of speed and pressure would also likely contribute to this effect.

The effect of speed increased the roughness at lower speeds but reduced the roughness at higher speeds. The effect at lower speeds makes sense because an increase in speed may give the ink a rougher "starting morphology" as previously discussed. However, the opposite effect at higher speeds is not as clear. One explanation is that as speed increases the amount of time between ink doctoring and transfer to the substrate decreases, leaving more solvent in the ink (due to decreased evaporation time). The ink would then have more solvent to evaporate after transfer, causing it to coalesce and level for a slightly longer period before "freezing" in place on the substrate, and therefore having a smoother surface. The effect of solvent as seen in Figure 4.6 also suggests that an increase of solvent above a certain level can contribute to lower roughness, which gives further support for this theory. The effects of speed and solvent also have quadratic terms that were found to be significant, further emphasizing their nonlinear effect.

It should be noted that the main effects plot for both thickness and roughness look very similar, with the variables having the same main effects on the responses. This suggests a very strong correlation between film thickness and roughness. Indeed, it can be observed in Figure 4.4 that the thicker films (darker in color) had higher roughness values. There were also several interaction effects listed as significant in Table 4.4 that were of interest. Some of these effects are shown in Figure 4.8.

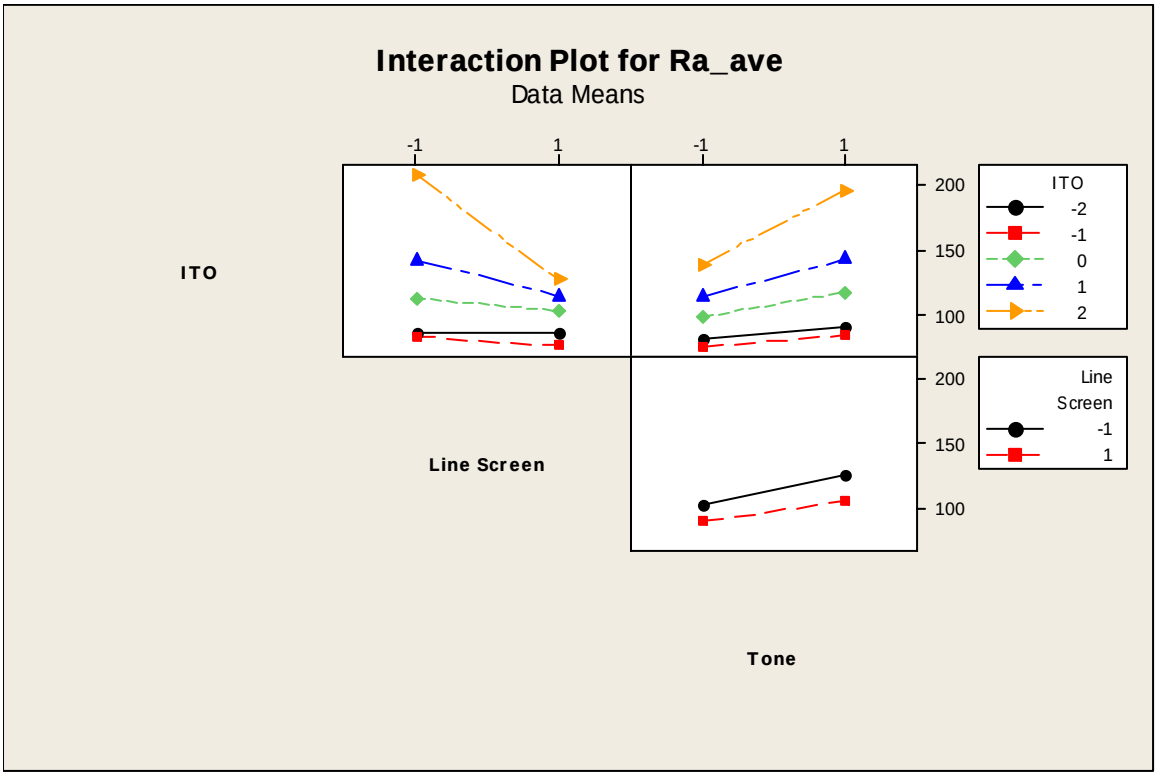

Figure 4.8: Interaction plots for average roughness

The interaction between ITO and line screen is interesting because it shows that the effect of line screen is more significant as ITO increases. The roughness decreases for an increase in line screen (decrease in cell size) in all cases, but at lower ITO concentrations the effect is relatively small. For each level of increase of ITO, however, the effect of line screen becomes larger. The same is true of tone. Roughness increases as tone increases at all levels of ITO. But as ITO increases, the effect of tone also increases. Since an increase in ITO results in a more viscous ink, it is likely that these interactions are due to more significant differences between the "starting morphology" of the transferred ink as the ITO increases. As ITO increases, the ink will not spread and coalesce as readily on the substrate, therefore the morphology of the ink when it is first

transferred is more critical. If the ink is transferred in a very uneven layer, it will be more significant if the ink is very viscous and cannot flow easily.

There were other interactions that were also found to be statistically significant. The interaction plots for all of the interactions are shown in Appendix B. Most of the other significant interactions did not offer easy explanations, and it was unclear what the effects were, so they will not be discussed.

4.3 Summary

The main experiment was designed to investigate the influence of the process factors on average film thickness roughness. The films were very much improved from the screening experiment, with no void areas and almost no pinhole areas. The films were relatively uniform but had varying surface morphologies that corresponded to differences in roughness and thickness.

The thickness was most influenced by the amount of ITO in the ink, with higher ITO giving higher thickness. There were two potential causes identified that controlled the thickness. The first was the amount of ink transferred from the cells to the substrate, while the other was the composition of the ink that was transferred. The first cause is influenced by the properties of the ink as well as the other process factors, such as speed and cell geometry. The amount of ink transferred seems to be higher with larger cell geometry. Several other main effects and interactions were found to be significant, most likely because of their effect on how and when the ink contacts the substrate and flows out of the cells.

The second main cause is due to the varying amounts of solvent, ITO and binder in the ink after it transfers to the substrate. Since the solvent evaporates out of the ink after being transferred to the substrate, ink with more solvent relative to ITO and ink vehicle will tend to have lower thickness. However, this is not completely straightforward, since solvent is continuously evaporating out of the ink, even before ink transfer. The amount of solvent evaporation before ink transfer can be influenced by speed, cell geometry, as well as initial solvent content.

The effects of the experimental factors on average roughness, R_a, were also investigated. The main effects were highly correlated to those of thickness, with ITO again being the predominant effect. ITO increases corresponded with higher roughness values. Larger cell volumes and higher speed also corresponded to higher roughness values. Most of the main effects and interactions suggested that roughness is dependent on the amount of ink transferred to the substrate, as well as the "starting morphology" of the ink and its ability to spread and level out before the solvent evaporated and "froze" it in place in its final rough state.

This experiment gave further insight into the transfer of ink in the gravure process. Several important factors were identified that can potentially be used to control and optimize the thickness and surface morphology of thin nanoparticle based films.

CHAPTER 5

ANALYSIS OF FUNDAMENTAL PARAMETERS

In the previous chapters, the effects of certain experimental parameters on the characteristics of the printed film were discussed. However, based on the analysis of the experimental results, very few precise conclusions could be drawn. It is known, for example, that cell geometry influences both the thickness and roughness of the printed film. However, it is unknown whether this is simply a size effect, or if the shape of the cell also plays a role in the influence. The relative effects on thickness and roughness by changing the ITO concentration in the ink is also known. That this composition changes the fundamental properties of the ink is also known. However, it is not known which fundamental property, e.g. viscosity or surface tension, is most significant to the process. Therefore an analysis was performed that looked at the experimental data based on not only experimental factors, but also the fundamental parameters of the process.

The approach taken to deal with this type of analysis was to list all the potential fundamental variables that may be important to the process, and then perform a best subsets regression analyses on the data from the main experiment to determine which factors best explain the effect of the process parameters on the measured responses. The best subsets regression approach is an established method that is suitable for identifying an experimental model that best fits the data, without including factors that may not be significant [39]. The method is useful for identifying experimental models in cases where some of the factors may be highly correlated and would therefore be found to be statistically significant even if they did not improve the model significantly. This chapter

describes this analysis, including the choice of potential variables and the results of the best subsets regression routine performed using MINITAB statistical software.

5.1: Fundamental Factors

The choice of fundamental parameters was based on the results of the previous screening and main experiments. From these experiments several experimental factors and interaction effects were identified for the different responses. However, some of the effects were insufficient to give a complete explanation of the data. Several potential factors were identified that were closely related to the experimental factors, but were more fundamental and could be measured independently of the process factors. The selection of these fundamental parameters is described in this section. In general parameters were chosen that either were known to have an effect on the responses, or that were assumed to have an effect based on the results of the experiments.

5.1.1: Process Factors

The factors of speed and roller pressure were two factors used in the experiments that were experimental as well as fundamental factors. That is, they represent a fundamental measure based on a calibrated setting on the printing press. The speed was calibrated using high-speed photography and the pressure was calibrated using thin-film pressure sensors. The speed and pressure have already been shown to be significant to the gravure process in the previous analyses. Therefore pressure and speed were included in the list of potential fundamental factors. Another factor related to the speed and pressure is “dwell time”. The dwell time is the time that the substrate is in contact with the cell.

Since the pressure roller flattens and pushes more of the substrate into contact with the gravure plate with increasing pressure, the area of contact increases for increasing pressure. Thus the substrate will be in contact for a longer period of time at a given speed. The change of speed, likewise, will change the dwell time. The dwell time was calculated by measuring the area of contact at each pressure setting and then using that measure with the process speed to calculate the dwell time.

5.1.1.1 Speed

The printing speed on the K Printing Proofer used in the experiments is controlled by an analog dial with settings from 1 to 10. The machine specifications state that the machine has printing speed capabilities up to 40 m/min, however it does not have any built-in measurement capabilities. The printing speed refers to the speed at which the pressure roller assembly translates across the gravure plate. In order to calibrate the machine for testing, a high speed camera was used to capture the movement of the roller head assembly against a fixed length reference (see Figure 5.1). The press was operated at each dial setting, and the speed was calculated by obtaining the time elapsed between two fixed reference points, three inches apart, from the high speed camera software. The calibrated speed chart is shown in Figure 5.2.

Figure 5.1: Gravure press with scale for measuring speed

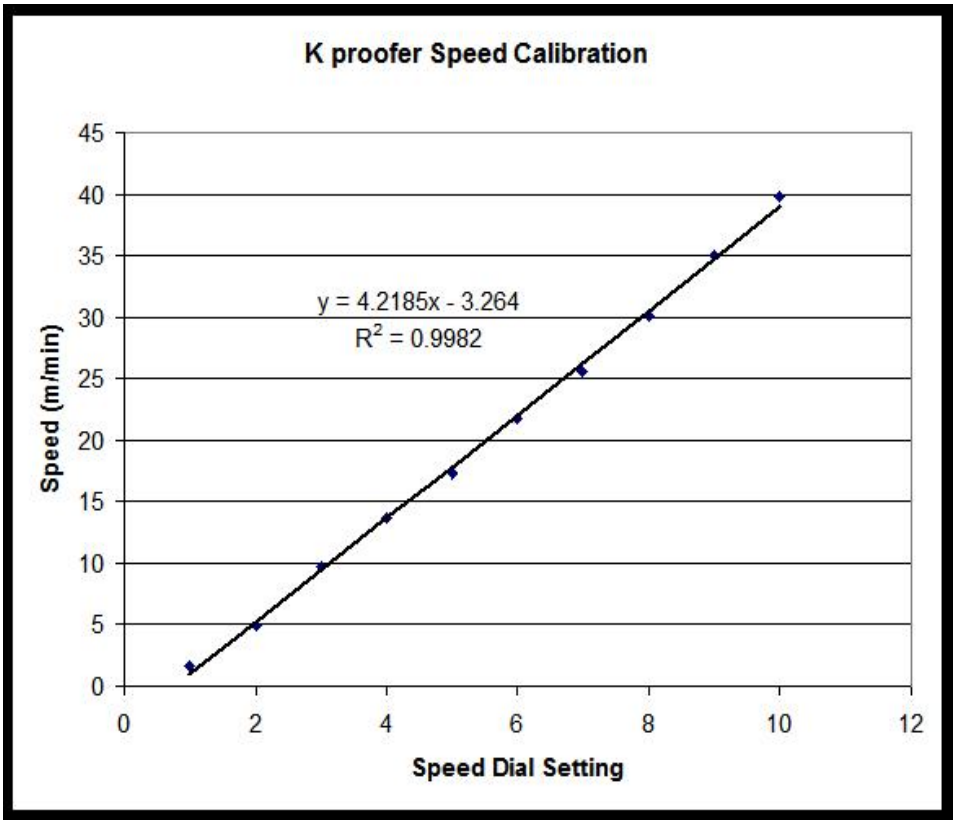

Figure 5.2: Speed Calibration Chart for gravure printer

5.1.1.2: Pressure

The pressure of the impression roller was measured by using Flexiforce thin film pressure sensors. There is no direct control of pressure on the K printing proofer. However, the location of the roller relative to the gravure plate can be controlled using built-in micrometers. Therefore the pressure can be controlled indirectly by calibrating the micrometer setting to pressure. The actual contact pressure between the roller and gravure plate is a complex problem involving to the geometry of the pressure roller, the friction between the roller and the substrate, as well as between the substrate and gravure plate, and the dynamic conditions under which it operates, Furthermore, the roller is covered in a viscoelastic rubber that was observed to relax under pressure. As pressure on the roller increases, the rubber flattens and the area of contact increases. Therefore in practice it is more practical to express the pressure in force per unit length of roller, or lbs/inch. This can be obtained by measuring the force exerted by the micrometers on the ends of the roller as it is adjusted. Two Flexiforce piezoresistive force sensors were used to measure the force. Two small steel discs were used on the top and bottom of the force sensors to give a uniform loading over the sensing area of the sensors. The change in force gave a change in resistance form the sensors, and the resistance was used to calibrate the pressure settings on the machine. The calibration charts for the two sensors used are given in Figure 5.3.

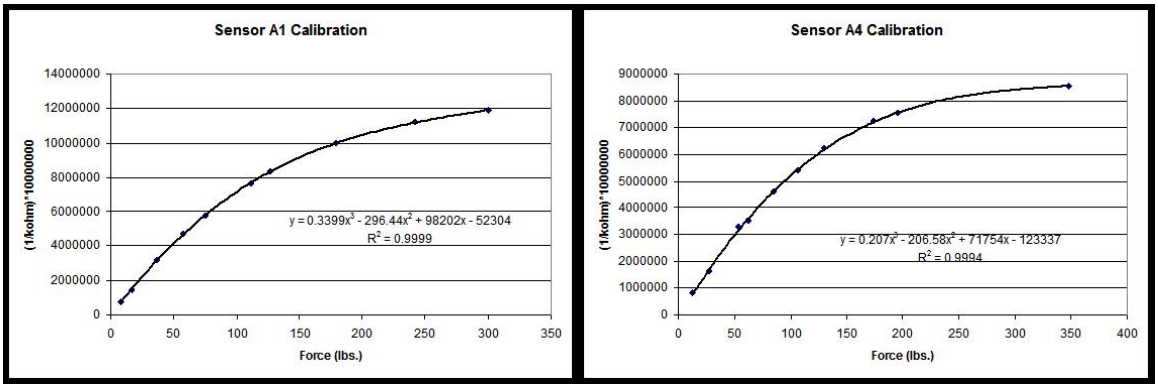

Figure 5.3: Flexiforce sensor calibration curves

5.1.1.3: Dwell Time

The dwell time is defined as the time for which a point on the substrate is in intimate contact with the gravure surface. This is easily calculated by measuring the length of contact for a given impression roller pressure and then dividing by the speed of the roller. The contact length of the rubber roller for each pressure setting used is given shown in Table 5.1.

Table 5.1: Pressure, Speed, and dwell time for factor level combinations

Linear Pressure (lbs/in)	Speed (m/min)	Roller Contact Length (mm)	Dwell Time (s)
35	10	15.0	0.090
45	10	17.0	0.102
35	20	15.0	0.045
45	20	17.0	0.051
30	15	13.5	0.054
50	15	17.5	0.070
40	5	16.5	0.198
40	25	16.5	0.040

5.1.2 Cell Geometry Factors

The cell geometry for the experiments was controlled by altering the cell spacing, angle of the stylus used to engrave the cells, and the relative area (tone) that the cells covered. The tone was indirectly controlled by changing the depth of cut of the stylus for a given cell spacing and stylus. However, these parameters do not directly give us the shape or size of the cell. The cells were analyzed using a Zygo white light interferometer to measure the dimensions of the individual cells, and to estimate the volume from these measurements. Additionally, the rows of cells were counted by hand using a light microscope to verify the line spacing. It was found that the actual tone and cell spacing values were quite different from what was specified. The parameters of cell depth, cell volume, cell aspect ratio (depth:width), and nominal cell width were chosen to describe more clearly the shape and size of the cells.

The gravure cells were engraved with a diamond stylus, giving the cells an approximately pyramidal shape. The cells are engraved at high speed while the gravure plate is spinning. The plate is thin and is affixed to a large base roller to perform this procedure. The engraving was performed by Gravure, Inc. in Lyman, SC according to the specified layout in Figure 5.4 The plate is made of aluminum and electro-coated in copper. After engraving, the plate is then chrome-plated for abrasion resistance. As a result, the geometry of the cells is affected by the cutting conditions including engraving machine settings, stylus sharpness, and specified cell size. For a given plate, there is not expected to be a difference in uniformity of the cell volume. A study of gravure cylinder characterization found that an electro-mechanically engraved gravure roller had variation in cell volume to be less than 5% [45]. However, as the diamond stylus wears and

machine parameters evolve over time, there may be considerable variation in gravure cell geometry from engraving to engraving.

In order to characterize the gravure cells, a Zygo white light interferometer and a Nikon light microscope were employed. In order to measure the actual tone value for each of the eight different cell areas, an image of a group of several cells was captured using the interferometer. The images were then processed in MATLAB in order to separate the solid area from the engraved cells. The images and corresponding MATLAB images are shown in Figure 5.5. Surprisingly, the measured tone values were quite different from the specified values. Although the cells specified at 100% were not expected to have 100% tone because of the necessity of having a bridge between cells, the measured values were still significantly different. The tones specified at 90% and 100% were measured at ~60% and 80% "tone", respectively. The specified values are summarized in Table 5.2.

Table 5.2: Cell geometry nominal values

Cell	Nominal Line Screen (cell/inch)	Nominal Stylus (° angle)	Nominal Tone (%)
1	360	110	100
2	360	110	90
3	360	150	100
4	360	150	90
5	300	110	100
6	300	110	90
7	300	150	100
8	300	150	90

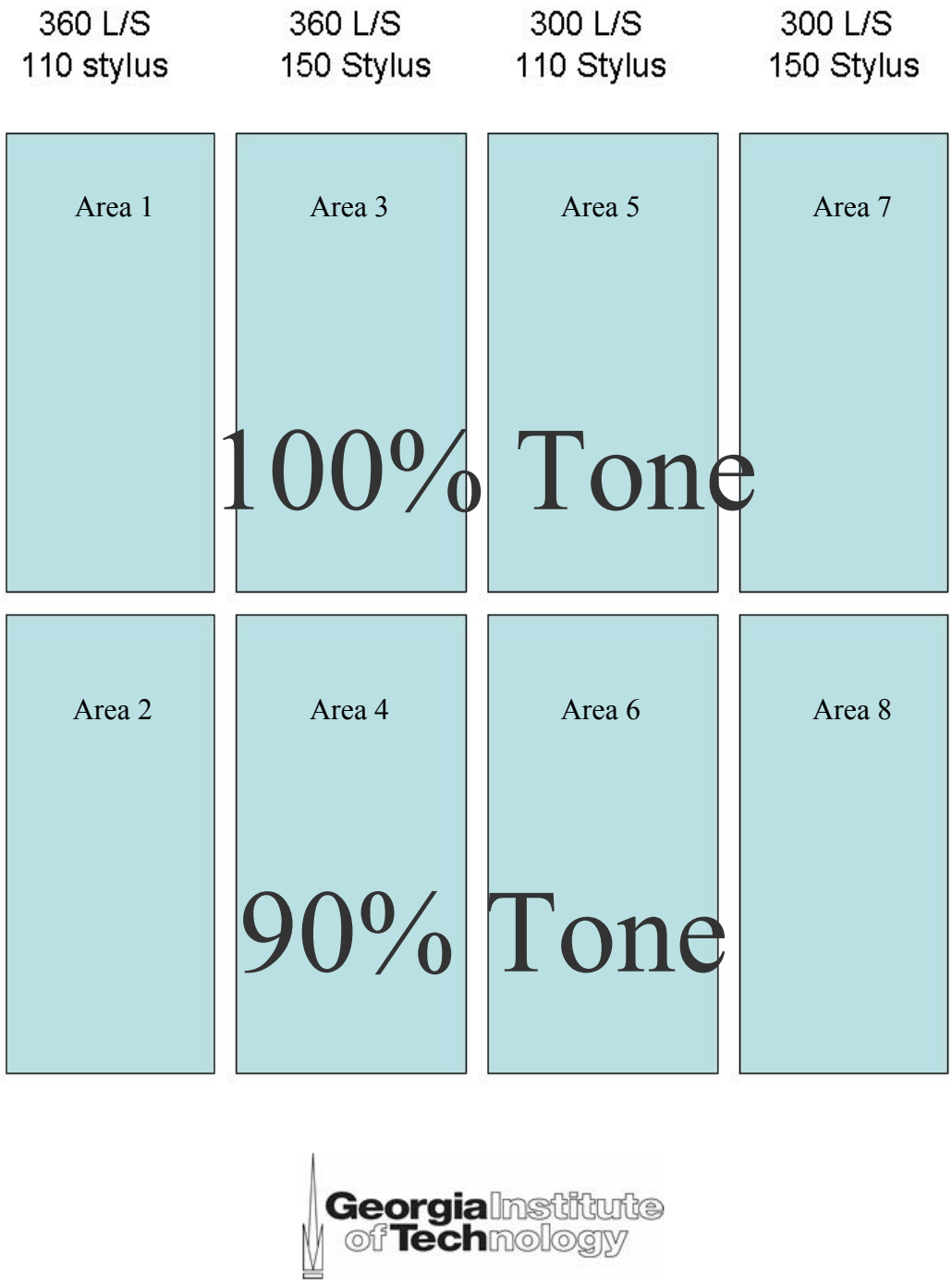

Figure 5.4: Gravure printing plate layout

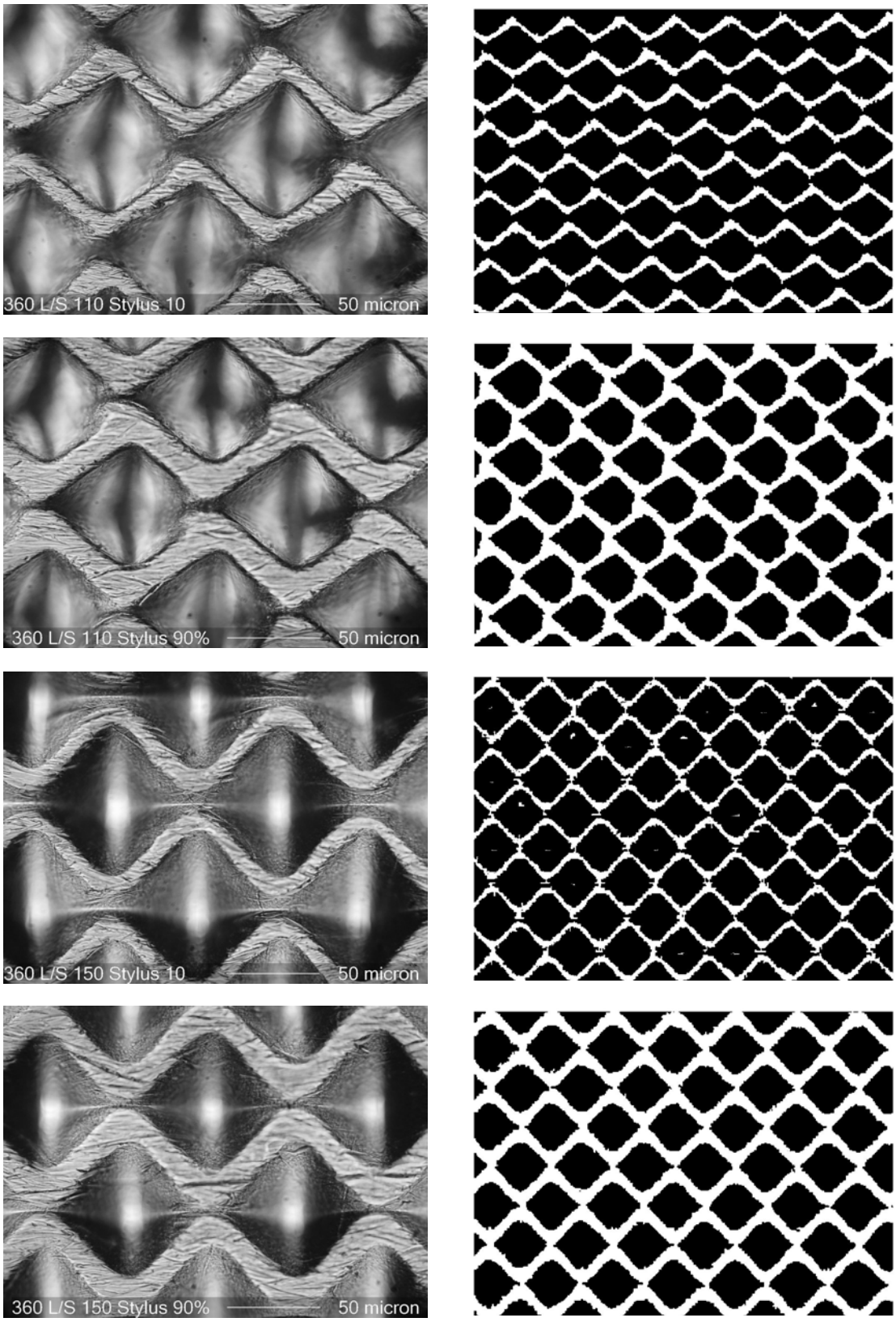

Figure 5.5: Gravure cell micrographs and bridge area measurement

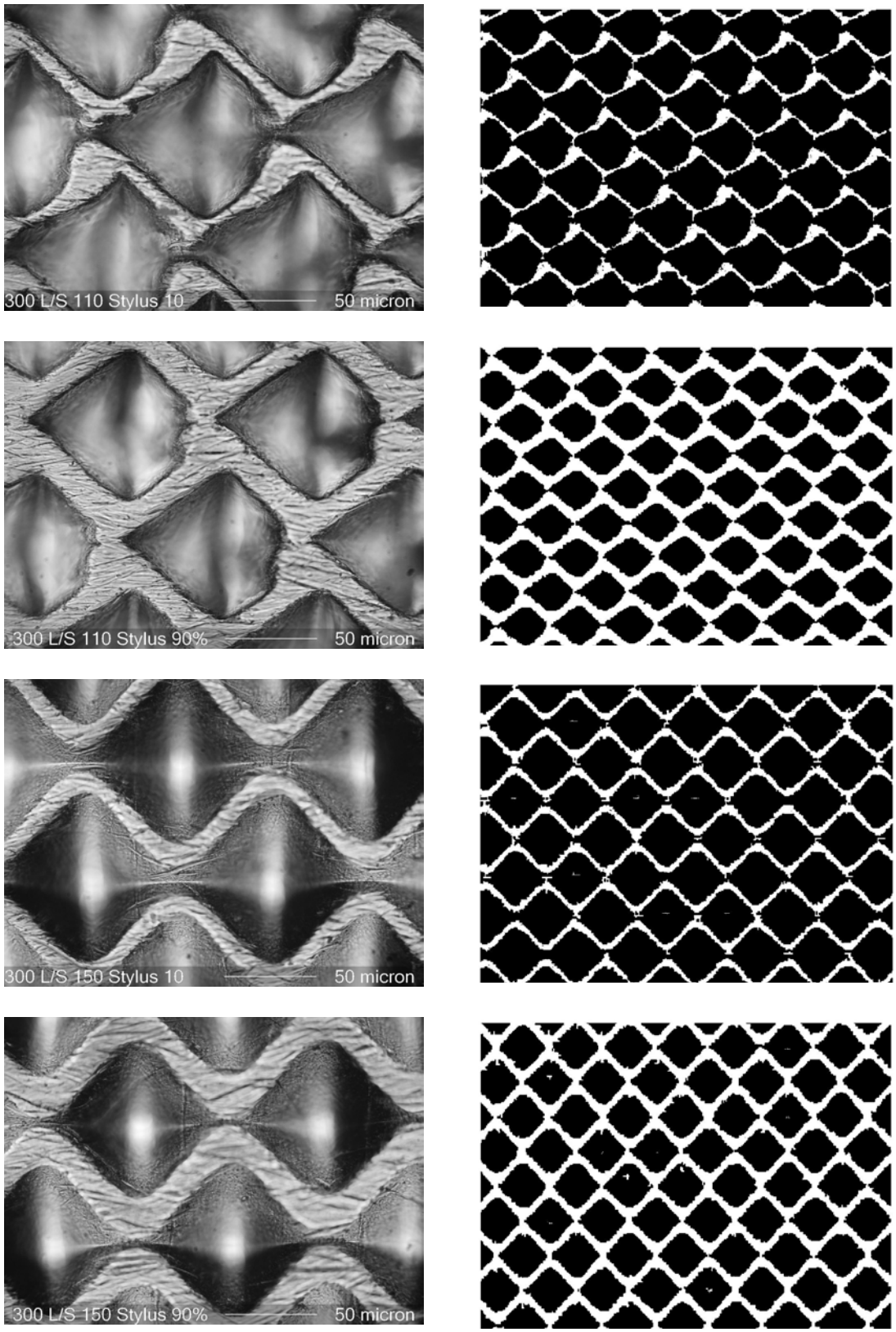

Figure 5.5 Cont'd

The depth of the cells was also measured on the Zygo interferometer. A sample Zygo plot showing the profile measurement that was used to get the cell depth is shown in Figure 5.6.

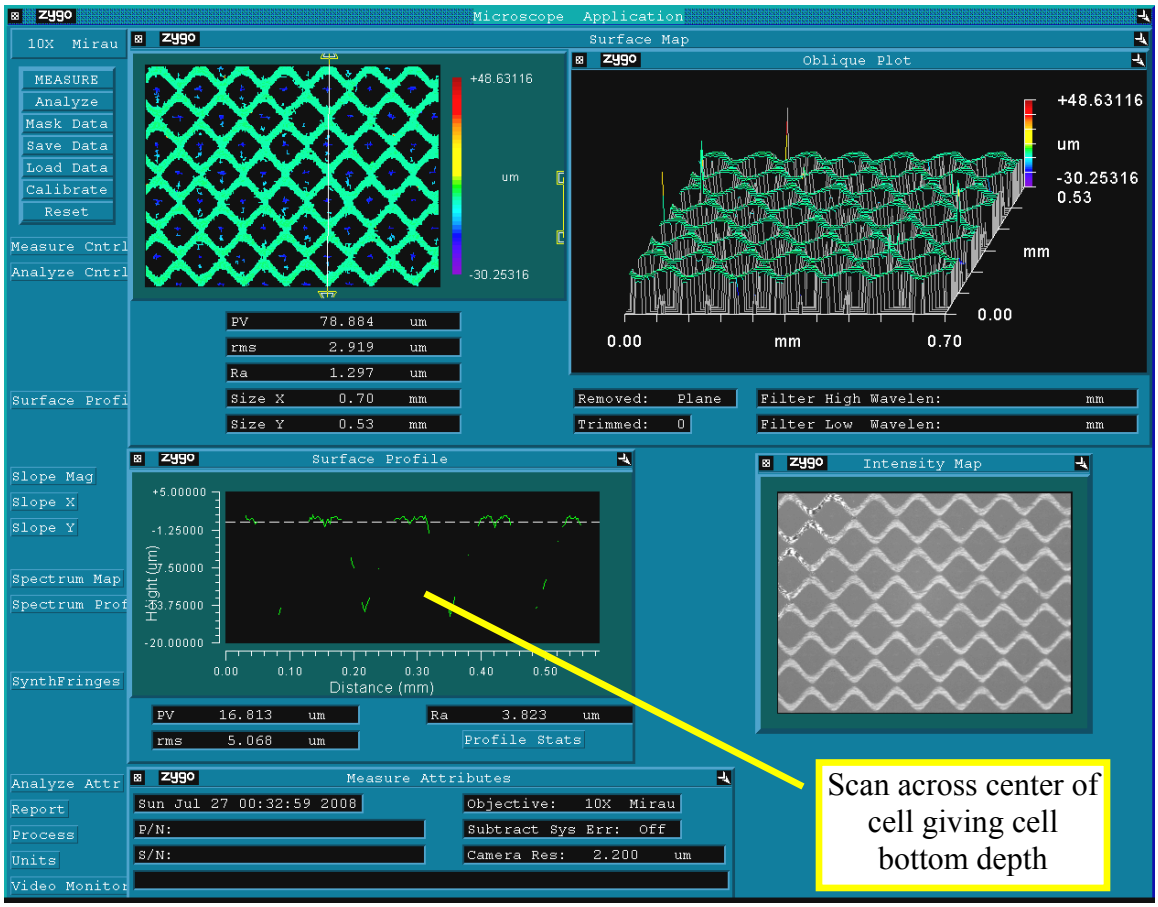

Figure 5.6: Zygo snapshot showing cell depth measurement

From the counting of the total number of cells, and from the measurement of the "bridge area" via the MATLAB analysis, the area per unit cell was calculated. This area was then used to find the dimensional width each cell for each of the 8 cell patterns. The measured depth and calculated width were then used to compute cell aspect ratio. Table 5.3 list all of the relevant cell geometry parameters for the 8 different cell geometries.

Table 5.3: Gravure cell actual values

Cell	Actual Line Screen longitudinal (cell/inch)	Actual Line Screen lateral (cell/inch)	Cell Surface Area	Cell Depth (µm)	Cell Width (µm)	Cell Volume (μm^3)	Cell Aspect Ratio
1	220	300	79.46	25.5	72.9	16427	0.35
2	220	300	80.33	25.0	100.4	13139	0.25
3	220	300	66.56	15.5	57.0	10026	0.27
4	220	300	79.79	15.0	26.0	8311	0.58
5	190	250	68.34	36.0	65.3	33044	0.55
6	190	250	79.46	30.0	85.8	22815	0.35
7	190	250	64.82	17.5	54.3	16070	0.32
8	190	250	80.33	16.0	64.3	12111	0.25

5.1.3 Ink Formulation Factors

The fluid properties of the ITO inks of varying composition were of primary interest in this analysis. Based on prior work, the fluid properties of the ink are seen to be very important in the gravure process. The viscosity, density, and surface tension of the inks are known to affect print quality in traditional printing and are very likely to affect significantly the properties of the final ITO film. Since the ratios of solvent, binder and solid were varied in the experiments described in this work, the fluid properties of these inks were also changed. These fundamental factors were measured for each of the inks (i.e. compositions of ITO, ink vehicle, and solvent) used in the experiment.

In addition to these fundamental measures, two dimensionless ratios were calculated. The first was the weight ratio of ITO to binder material. Since the conductivity of a composite material is dependent on both the content of conductive particles, and also the presence of non-conductive material, this ratio was calculated to give a relative measure of the concentration of ITO in the dried films. In general, a higher ITO/binder ratio would be expected to give a lower sheet resistance, because of the

increase in conductive pathways present when the concentration of ITO is increased. The second ratio was the ratio of solid material to solvent in the ink. Since the drying behavior of the inks is dependent on the solvent content, and because the ink vehicle is composed of mostly solvent, a relative measure of the solvent content was desired. Therefore the ratio of the total solids in the ink, i.e. ITO and binder material in the ink vehicle, to the total amount of solvent, i.e. the solvent in the ink vehicle plus the additional solvent added, was calculated.

The inks used in this study were composed of three primary components: ITO nanoparticles, a solvent of 90% ethyl alcohol and 10% acetone, and an ink vehicle. The ink vehicle, in turn, was composed of the polymer binder, solvents similar to the alcohol/acetone mix, and a variety of other additives designed to improve the properties of the final ink product. After the ink has been printed, it was assumed that the dried ink was composed only of the nanoparticles and the polymer binder and select additives from the ink vehicle. The mixture ratios of all these ingredients affected the fluid and later solid properties of the ink. The viscosity, surface tension, and certain material ratios were measured for each of the different inks and the methods are described here.

5.1.3.1: Viscosity

In the printing industry, the viscosity of gravure inks is measured using an efflux cup or similar methods. The cup is a standardized tool consisting of a cup with a rounded base and a hole in the bottom. The cup is filled with ink and the amount of time for the ink to flow out is recorded. Although very simple and easy to operate, this method is subject to errors of up to 20%, depending on the method used [5]. Additionally, the

measurement cannot easily be converted into standard units, and thus only provides only a relative measurement. For this reason a more precise measurement was desired. There were a total of nine different inks formulations measured corresponding to nine different combinations of levels of ink parameters occurring in the main experiment design (see Appendix A). The viscosity of the Sunester ink vehicle was measured as a reference. Additionally, three different mixtures of Sunester vehicle and solvent were measured.

Figure 5.7: Efflux cup for measuring viscosity [1]

The viscosity measurements were made on an ARES series rheometer (TA Instruments). A schematic of the machine is shown in Figure 5.8. The principle of operation of the rheometer is that a material is placed in between two parallel plates. The bottom plate is rotated at a given speed, while the top plate measures the torque generated. From this torque and the known torque and speed of the bottom plate the viscosity can be calculated. The parallel plates used had a diameter of 25 mm. Through a

trial and error approach, the gap between plates was set to 0.5 mm. This gap is material dependent, and must be chosen so as to give an accurate measurement. A larger gap will transmit less torque, and therefore provide a less sensitive measurement, while a smaller gap will require higher torque, and may exceed the limits of the machine. Typically the largest gap that will give a good measurement is desired. Typical gap values for viscous materials range from 0.5 mm to over 1.5 mm, with less viscous materials requiring a smaller gap.

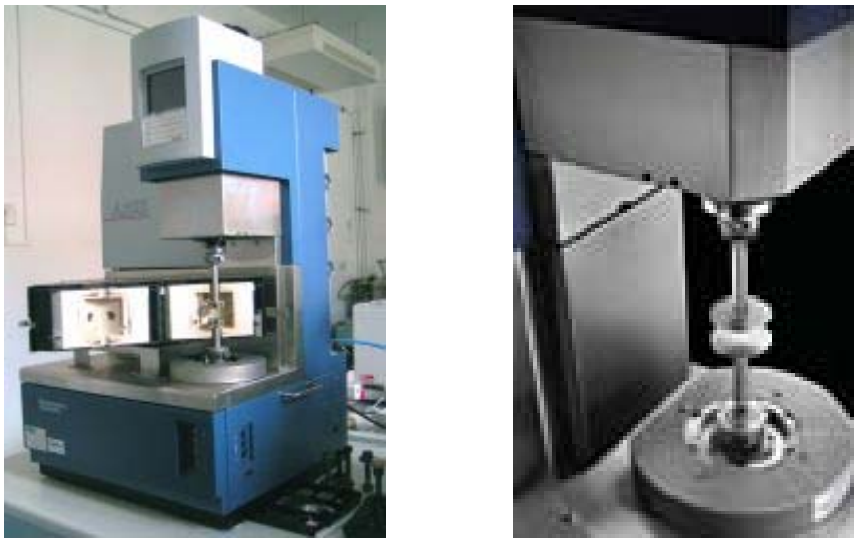

Figure 5.8: ARES Rheometer and parallel plate measuring tool (TA Instruments)

The viscosity can be measured at different strain rates, frequencies, and temperatures on the ARES rheometer. For characterization of the gravure inks, a strain rate sweep was performed. This sweep measured the viscosity at different strain rates from 1 to 1000 Hz, taking a measurement at five points per decade, allowing the characterization of the strain rate dependency of the inks. At low strain rates, however, the ARES did not have the sensitivity to measure low viscosity fluids with the parallel

plate geometry available. However, at higher strain rates, the measured viscosity values dropped to more reasonable values in the expected viscosity range, and remained steady over several measurements. At a strain rate of 400 Hz, the rheometer measured consistent values for all of the inks. To standardize the measurements, the viscosity was taken to be the average viscosity measured at a strain rate of 400 Hz. Three samples of each ink were measured, with the ink being removed and a fresh sample loaded for each measurement. At even higher strain rates, the viscosity measurement began to drop rapidly as the centrifugal force from the plates caused the ink to leak out of the region between the two plates. Therefore the rheometer failed to characterize accurately the viscosity at both high (~1000 Hz) and low (~1 Hz) strain rates. As a check of the accuracy of the viscosity measurements, water was measured as a controlled sample. As was the case for the inks, the ARES did not accurately characterize the inks at very low or very high strain rates. However, at the intermediate values, from about 100 to 400 Hz, the viscosity of the water was measured to be between 793 and 890 mPa-s, compared to a reference value of 894 mPa-s [46]. Thus the accuracy of the rheometer was judged to be quite good at the intermediate strain rates.

5.1.3.2: Ink Surface Tension

The surface tension of the different ink mixtures was measured using a needle of known geometry. The camera takes a picture of the drop and a software program analyzes the image, giving the size and shape of the drop. The drop can be placed on a substrate using the *sessile drop* method to measure the contact angle, which can then be used to find the surface energy of the substrate, The surface tension of the ink can be

found using the *pendant drop* method, in which a drop of liquid is suspended from the dispenser and the surface tension is calculated using the shape and size of the drop. Figure 5.9 shows pendant drops of the solvent, water, and ink #8, and the related measurement lines overlaid by the software.

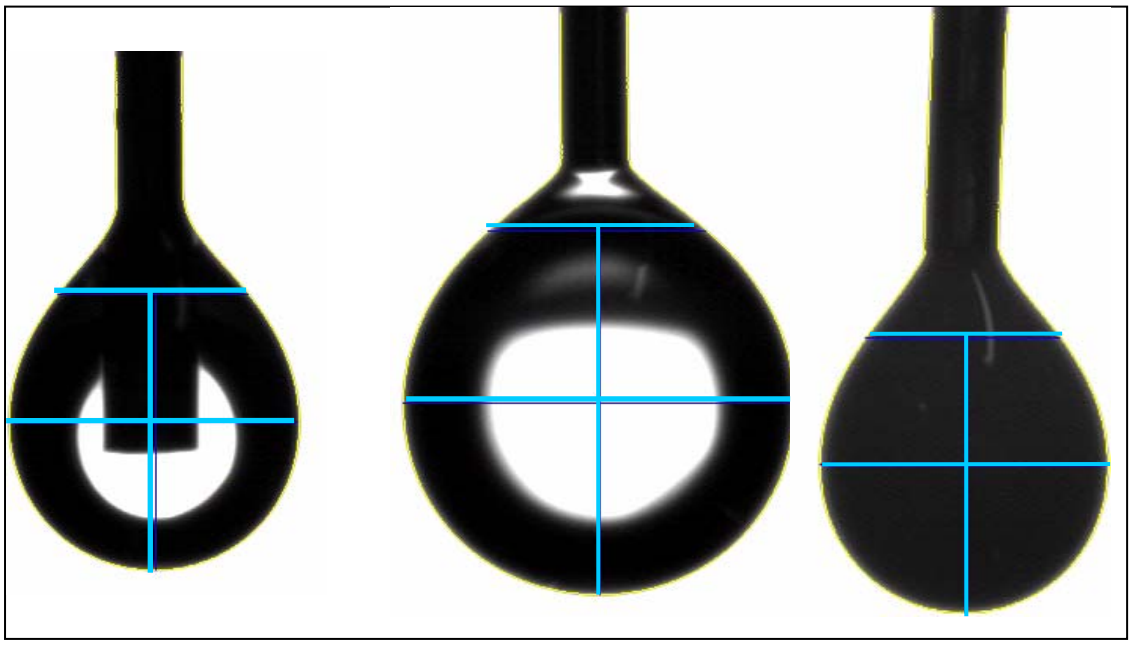

Figure 5.9: Sessile drops for ethyl alcohol, water, and ink #8

The surface tension of an evaporative ink is a complex problem due to the fact that the solvent begins to evaporate immediately after being exposed to the atmosphere. Therefore a quick measurement is desired, although due to the limitations of the goniometer and the related software this can be difficult. However this is one of the simplest measurement approaches and requires only a very small amount of liquid to make a measurement. Other methods, such as the Du Noüy ring method or the Wilhelmy plate, require a larger amount of liquid. The goniometer did, however, provide a relative measurement of the gravure inks. In addition to the inks, several mixtures of ink vehicle

and solvent were measured, as well as the solvent and ink vehicle separately. The mixtures of ink vehicle and solvent were measured as a baseline for the viscosity without the ITO nanoparticles added. The mix ratios of vehicle to solvent were the same as the inks used in the experiment, without the nanoparticles. Distilled water was also measured as a reference.

5.1.3.3: Ink Mixture Ratios

The solvent-based inks in this study were composed of solvent, ITO nanoparticles, and the ink vehicle. The ink vehicle also contained solvent in its received form. After solvent evaporation, the dried ink would then be composed of only ITO and a polymer binder, with some residual additives and impurities. Since the exact composition of the ink was not available, a drying factor, D, was introduced. D represented the dried weight of the ink vehicle after the solvent had been evaporated. This value was calculated by depositing small samples of the ink vehicle onto a substrate of known weight. The weight of the substrate and the ink vehicle sample was measured immediately after deposition and then again 24 hours later, after all the solvent had evaporated. The difference in weight between the ink vehicle before and after solvent evaporation could then be calculated. D was found to be about 0.2 on average for the five separate samples that were prepared. This implied the ink vehicle had about 80% solvent by weight, determined experimentally.

The two ratios of interest were the solid:solvent ratio, and the ITO:binder ratio. The solid: solvent ratio was of interest because the measured response of thickness was measured after the solvent was evaporated, and was expected to be affected by the

amount of initial solvent in the ink. The ITO:binder ratio was of interest because of its predicted influence on the conductivity of the printed ITO layer. If there is more binder relative to ITO, it was assumed that the conductive pathways between particles would be reduced. The two ratios were calculated as follows:

Solid:Solvent = [ITO wt% + D(Ink Vehicle wt%)]/[Solvent wt% + (1-D)*(Ink Vehicle wt%)]

ITO:binder = (ITO wt %)/(D*Ink Vehicle wt%)

5.1.4 Physical Parameters

In addition to the fundamental factors already listed, some of the response variables can themselves be seen as fundamental factors for the other responses. The sheet resistance and transparency, for example, are functional measures that are dependent on the thickness of the functional material. The surface morphology, i.e. the shape and features present in the film, can also influence these performance measures. Therefore the average thickness and roughness were also analyzed for their effect on the responses of sheet resistance and transparency.

5.1.5 Summary of Fundamental Factors

A full listing of all the fundamental parameters measured and used in the analysis is given in Table 5.4. These parameters became the potential variables for best subsets regression routines in MINITAB. Although the list of potential variables may not be exhaustive, it does represent a significant number of factors that are known to be important. The choice of potential variables was based on fundamental mechanics of the

gravure process, in an attempt to understand which forces and phenomena are most important to controlling the characteristics of a printed ITO nanoparticle film.

Table 5.4: Included variables in analysis of the four responses

	Response Variables			
Fundamental Variable	**Average Thickness**	**Average R_a**	**Sheet Resistance**	**Transparency**
Speed	x	x	x	x
Pressure	x	x	x	x
Cell Volume	x	x	x	x
Cell Aspect Ratio	x	x	x	x
Cell Surface Area	x	x	x	x
Dwell Time	x	x	x	x
Ink Density	x	x	x	x
Ink Viscosity	x	x	x	x
Ink Surface Tension	x	x	x	x
ITO/binder	x	x	x	x
Solid/Solvent	x	x	x	x
Average Thickness	N/A	x	x	x
Average R_a	N/A	N/A	x	x

From Table 5.4 it can be seen that for the responses of transparency and sheet resistance, the response variables of average thickness and roughness were included in the analysis, in addition to the other fundamental variables. For the response of average roughness, the thickness response was included as a potential variable as well. These response variables were seen as potential factors because of their fundamental effect on the other response. It was expected that the thickness would affect the roughness and that the thickness and roughness would both affect the sheet resistance and transparency.

5.2 Analysis

Once the potential variables had been measured and/or calculated, a statistical analysis was performed for each of the four responses: average film thickness, average film roughness, sheet resistance, and transparency. In order to determine which variables had an effect on the responses, a best subsets routine was performed using MINITAB. The best subsets routine tests the fit of different models by adding one factor at a time, and then selectively adding or deleting factors based on their statistical significance. The routine continues until all the variables are added. In general the "goodness-of-fit" of a given model can be judged by a variety of different criteria, such as R^2. However, R^2 tends to increase as variables are added to the model, even if the variables have no effect on the response [47]. Since a simpler model that does not include such extraneous variables was desired, a different model selection criterion was needed. Mallow's C_p is a selection criterion useful for such best subsets regression routines. The C_p value decreases as the model improves, but as more and more variables are added, the C_p begins to increase again. The best model will have a C_p that is small but is close to *p*, the number of variables in the model [47]. This selection criterion was used to choose the best models form the best subsets regression. After the factors in the chosen model were identified, a regression was performed on the data using the chosen factors. The results are presented in this chapter.

5.2.1 Response: Average Film Thickness

Although the effects of the experimental variables had relatively good correlation with the average thickness (see Chapter 4), the effect of several important parameters

were unclear. A best subsets routine was performed in MINITAB. The output is shown in Appendix B. A model was chosen using the afore-mentioned selection criteria. Out of a potential 11 variables, a model with seven variables was chosen. The regression output for the model is shown in Table 5.5.

Table 5.5: MINITAB output for thickness model

Predictor	Coef	SE Coef	T	P
Constant	-1935.7	373.6	-5.18	0.000
Speed	-17.126	5.085	-3.37	0.001
Dynamic Viscosity	-1250.4	284.9	-4.39	0.000
Density	1741.3	406.3	4.29	0.000
Cell Volume	0.0109435	0.0006586	16.62	0.000
Cell surface area	5.5982	0.7280	7.69	0.000
ITO/Binder	-130.94	32.45	-4.03	0.000
Solid/Solvent	588.9	130.6	4.51	0.000

S = 71.7263 R-Sq = 74.1% R-Sq(adj) = 73.3%

From Figure 5.5 it is clear that the cell volume is the largest factor. The larger the volume of the cell, the thicker the coating deposited. This agrees with the analysis in chapter four in which the cell geometry variables corresponding to larger cells also corresponded to higher thickness. The cell surface area was also a large factor, with higher cell surface area, i.e. lower bridge area, giving higher thickness. In the prior analysis, the cell geometry factors were all significant, but it was not immediately known why. It appears that the main effect was cell volume. This was masked in the prior analysis because all of the cell geometry factors were independently significant, but not as significant as ITO content. In this case the some of the ink properties are also significant, but not as significant as the cell volume. This result is interesting because it

suggests that film thickness can largely be controlled by controlling the cell shape and volume. However, material variables must also be taken into account.

A main effects plot for the analysis is also shown in Figure 5.10. There are several interesting features observed in the main effects plot. Most of the effects were not linear over the entire range of levels, but most did trend in a certain direction, i.e., either generally increasing or decreasing thickness. However, with an R^2 value over 70%, the model seems to explain most of the variation in the film thickness.

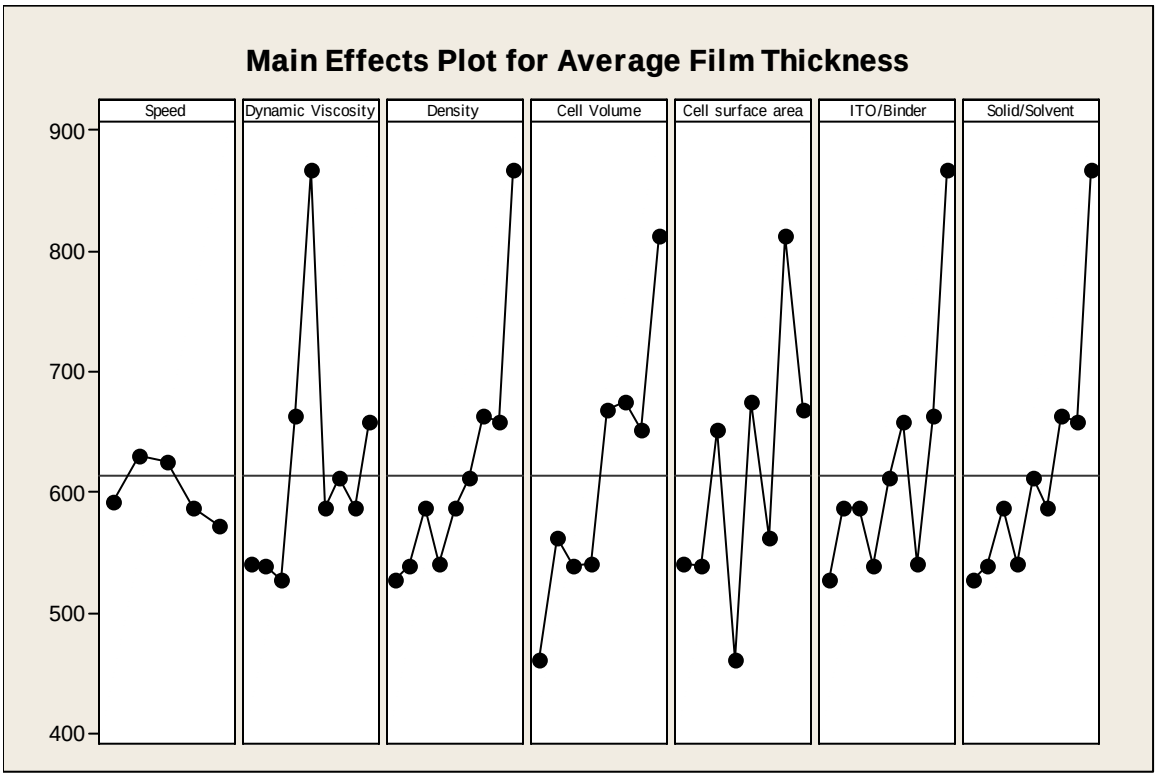

Figure 5.10: Regression model and main effects plot for thickness

From the main effects plot for viscosity, the effect seems unclear. It appears that the effect is significant, however. This is not surprising since the viscosity will affect how well the ink flows under shear, and may increase or decrease the amount of ink

transferred depending on the rate of shear and boundary conditions. The density of the ink appears to be important, with an increase in density corresponding to an increase in thickness. This is likely due to an increase in cohesion at higher densities causing more ink to be pulled out of the cells during ink transfer. The ITO/binder ratio and the solid/solvent ratio also correspond to higher thickness as the ratios increase. These ratios take into account the relative amount of material volume lost from solvent evaporation, as discussed in Chapter 4, so it is not surprising that at the amount of relative solvent decreases, the remaining layer thickness increases.

In Chapter 4 the process parameters of line screen, stylus geometry, and tone were all found to be significant. In this section both the cell volume and engraved cell area were found to be significant, suggesting that regardless of the internal shape of the cell, the larger the volume and wider the cell opening, the thicker the film. Therefore the cell geometry parameters can potentially be used to tune the amount of ink transferred, by making the cells larger or smaller, or by changing the size of the cell opening. However, the cell aspect ratio does not seem to directly have an effect, suggesting that increasing cell volume by making the cell deeper will not affect the thickness. The amount of ITO can also affect the thickness, in particular by increasing the proportion of solid material that is left after the solvent evaporates. The viscosity and the density also seem to have a significant effect, suggesting that the ink transfer dynamics also play an important role. However, the relatively minor effect of these variables compared to the cell volume suggests that the cell volume is the primary effect controlling ink thickness. It may also be worth noting that the interaction effect of pressure and speed on film thickness

discussed in Chapter 4 was probably not due to the change in dwell time, as this factor was not found to be significant.

5.2.2 Response: Average Roughness R_a

The MINITAB best subsets models for roughness can be found in Appendix D. The model chosen had 6 predictors out of a potential 12. The regression output for the chosen model is shown in Table 5.6. A main effects plot is shown in Figure 5.11.

Table 5.6: MINITAB output for roughness model

Predictor	Coef	SE Coef	T	P
Constant	-274.67	41.09	-6.68	0.000
Speed	-16.484	3.203	-5.15	0.000
Thick_ave	0.18490	0.01742	10.61	0.000
Density	299.34	51.08	5.86	0.000
Cell Volume	-0.0005740	0.0002877	-1.99	0.047
Dwell	-491.46	95.63	-5.14	0.000
Solid/Solvent	-105.03	35.71	-2.94	0.004

S = 21.4908 R-Sq = 70.2% R-Sq(adj) = 69.4%

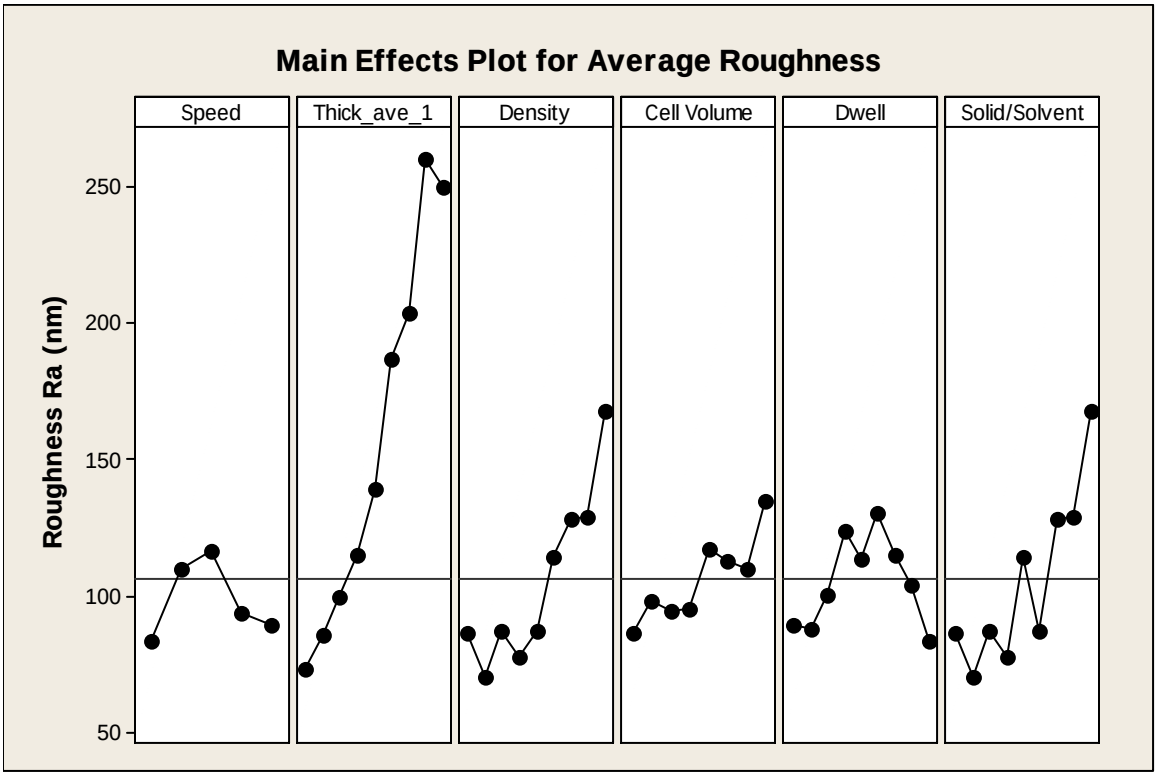

Figure 5.11: Main effects plot from MINITAB for average roughness

From the results we see that the roughness increases with thickness, which is the most significant effect. The density of the ink as well as the solid/solvent ratio also had a consistent effect on the roughness, with higher density and higher solid/solvent ratio corresponding to a higher average roughness. In general we can conclude that the roughness is primarily dependent on the material properties and the amount of ink transferred to the substrate. The amount of solvent and the effect the solvent has on the evaporation behavior of the ink significantly affects the final film roughness. Higher solid content will tend to give higher roughness. The effects of speed and dwell time are also significant, however the effect is not clear as evidenced by the inconsistent trends exhibited in the main effects plot. As discussed in Chapter 4, the roughness is likely dependent on the morphology of the ink as it is transferred onto the substrate, and amount

of solvent it has to evaporate before solidifying. The speed and dwell time may affect both of these variables. The fit of this model is reasonably good, with over 70% correlation. Since the R_a value is not a very descriptive parameter, it is not too surprising that the correlation is not higher. R_a only gives a relative measure of the non-uniformity in the printed film, and it is possible that two very different surface morphologies could give the same roughness value.

In Chapter 4 it was suggested that the cell geometry was an important factor. However, the fundamental analysis shows the cell volume to be only slightly significant compared to other fundamental parameters. The thickness was the parameter most highly correlated to the roughness. The thickness, in turn is most highly correlated to cell volume. So there appears to be an indirect effect of cell volume on roughness. But it appears that the roughness is mostly determined by the movement and behavior of the ink as it is drying. The amount of solvent relative to the amount of solid, as well as the speed of the press, will influence the way in which the ink will react once it is transferred to the substrate. Therefore in order to control the roughness the amount of solvent and he drying behavior of the solvent must be chosen. Since the ratio of ITO/Binder was not found to be significant, it may be assumed that the roughness is not directly related to ITO content. Rather it is the amount of solvent and the way in which the ink behaves under drying conditions, regardless of composition of the rest of the ink.

5.2.3 Response: Sheet Resistance

The sheet resistance of a material is simply a measure of the electrical resistance of a thin, uniform film of material such as ITO. Typical sheet resistance values of thin

films of ITO are less than 100 Ω/□ for sputter-deposited ITO on glass (17). ITO nanoparticles deposited on PET films using printing have been reported to have sheet resistance less than a few kΩ/□. However, in this study the films has sheet resistance values of several hundreds and even thousands of kΩ/□.

Sheet resistance of conductive thin films such as ITO is typically performed with a four point probe according to ASTM F390 or similar standards (48). However, the ITO films produced in this study were very soft compared to the rigid materials typically measured using a four point probe, due to the polymer binder employed. In measuring the electrical properties, the probe tips must come into sufficient contact with the material to form an electrical contact. If the tip is too sharp, it will pierce through the material and fail to make good contact. If the tip is too large, it will not be able to conform to the measured material and will again fail to make a good electrical contact. After several trial and error approaches it was determined that the four point probe method was not suitable for measuring the ITO nanoparticle films due to the softness of the dried ink. Therefore an alternate method of measuring sheet resistance was adopted.

The sheet resistance measurement was made by using the transfer length method (TLM), a commonly used technique to measure the sheet and contact resistance of thin films (49). An electron beam (E-beam) evaporator was used to deposit 200 nm thick lines of aluminum onto the samples. The lines were 1 mm wide and ran the width of the samples (see Figure 5.12).

Figure 5.12: E-beam deposited lines on ITO sample for TLM measurement

The lines were laid parallel to each other at 1mm, 4 mm, 9 mm, 16 mm, and 25 mm spacing from the first line. This pattern is used to enable measuring over longer distance with less fewer conductive lines, which have a non-negligible effect on the resistance measurement. The pattern was formed by applying a simple laser-cut mask onto the samples before deposition. After the e-beam electrodes were deposited, the resistance between the first line and each successive line was measured using a simple multi-meter. This measurement was divided by the area between the two electrodes to obtain the sheet resistance value. A plot of the resistance measured between each set of electrodes for three of the samples is shown in Figure 5.13. The plot is linear, as expected, showing the consistency of the sheet resistance. The y-intercept of the fitted line represents the contact resistance between the deposited lines and the ITO layer.

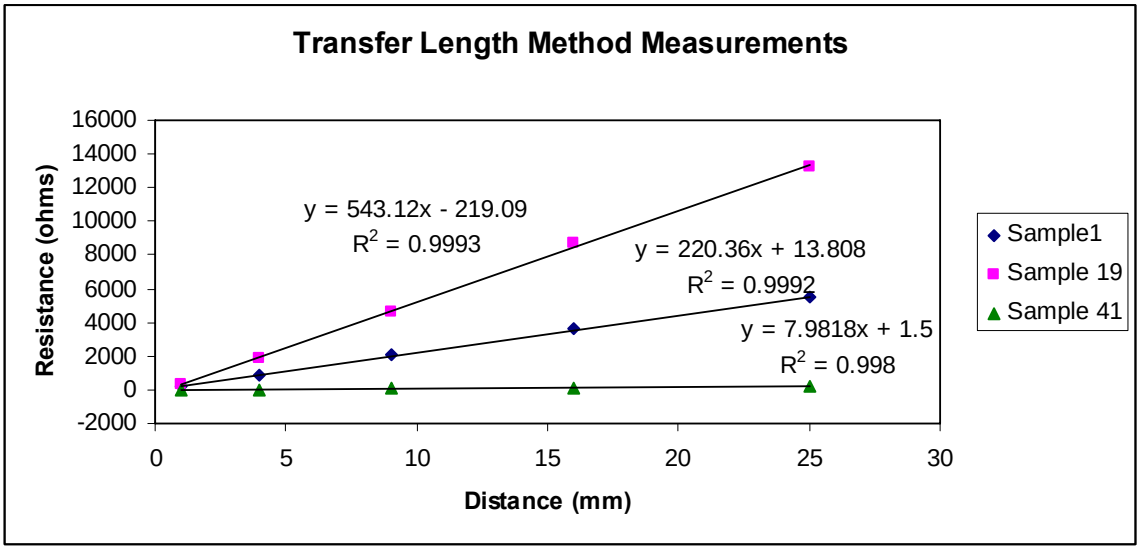

Figure 5.13: Transfer length method measurement plot

An initial best subsets analysis for the sheet resistance resulted in a very poor fitting model. Since the sheet resistance seemed to vary non-linearly, ranging from a few hundred kΩ/□ to a few MΩ/□, the analysis was performed a second time, using the square root of the sheet resistance as the response. This resulted in a much better fitting model from the best subsets analysis. Thus the model is nonlinear in nature, however it seems to fit the data reasonably well. It should also be noted that the analysis for sheet resistance was completed using only a subset of the data, or approximately 1/3 of the total samples produced in the experiment. This was due to limitations in measuring the sheet resistance of the films. The best subsets output can be found in Appendix D. Table 5.7shows the regression output, and a main effects plot is shown in Figure 5.14. The best subsets results from MINITAB are shown in Appendix D.

Table 5.7: MINITAB output for (sheet resistance)$^{1/2}$

Predictor	Coef	SE Coef	T	P
Constant	-628.1	171.4	-3.66	0.000
Dynamic Viscosity	-917.8	137.7	-6.67	0.000
Density	924.5	193.6	4.78	0.000
Cell Volume	0.0016142	0.0005661	2.85	0.006
Aspect Ratio	144.26	33.83	4.26	0.000
Cell surface area	-2.0026	0.4233	-4.73	0.000
ITO/Binder	-124.80	16.32	-7.65	0.000
Solid/Solvent	285.93	56.89	5.03	0.000

S = 18.3836 R-Sq = 76.3% R-Sq(adj) = 73.8%

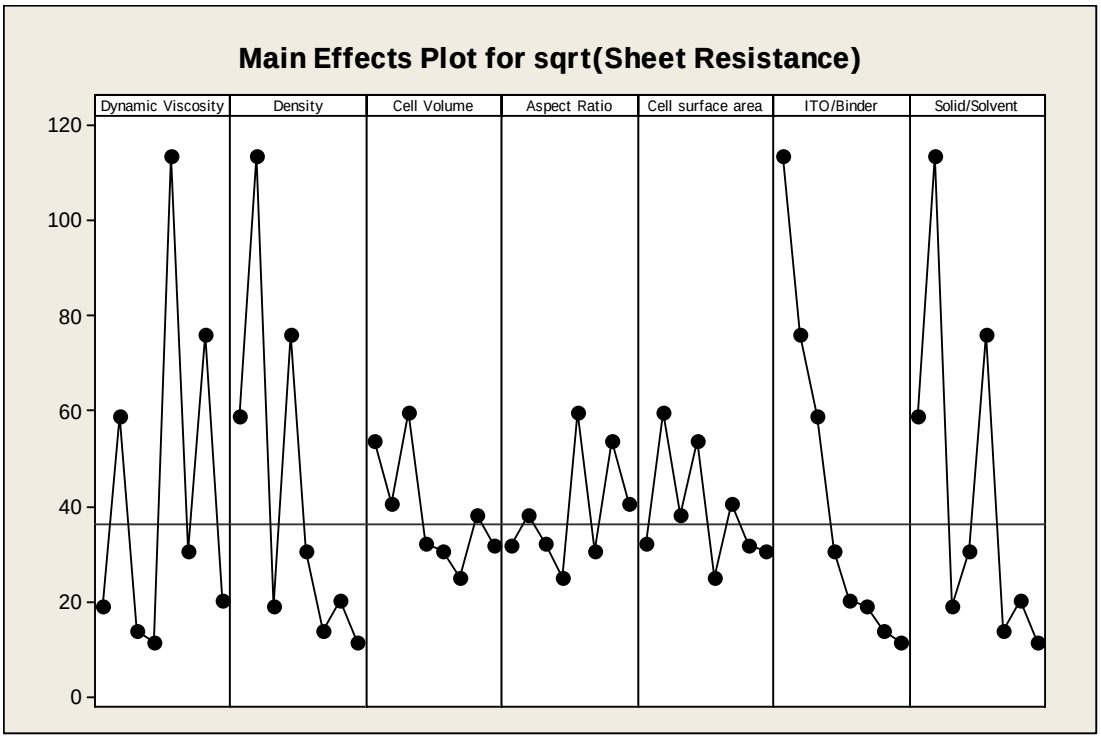

Figure 5.14: Main effects plot for (Sheet Resistance)$^{1/2}$

It is clear that the most significant, as well as the most straightforward effect, is the ratio of ITO to binder. This was expected from the outset, that the higher ITO ‘”loading”, the better the functional characteristics would be due to the increase in conductive pathways with higher ITO content. However, several cell geometry and ink

variables also seemed to have an effect, although the nature of the effects is unclear from the main effects plot. Surprisingly the film thickness was not found to be significant. This may suggest that the surface morphology determines the conductivity of the film more than the amount of material present. It seems reasonable to conclude that these variables all affect the surface morphology of the ITO films. The different cell geometry factors affect the shape of the ink as it is transferred to the substrate, while the viscosity and other variables affect how the ink flows and assumes its final form on the substrate. It can therefore be concluded that both material composition and surface layer morphology significantly affect the sheet resistance.

Although it is difficult to relate the sheet resistance directly back to the process parameters discussed in Chapter 4, it is interesting to note that the several cell geometry factors and the viscosity were significant, even though they were less significant with respect to roughness. It could be expected that these parameters would have a big effect on the surface morphology of the printed ITO, and the surface morphology would in turn have an effect on the sheet resistance. This is one possible explanation given the effects of these parameters on sheet resistance. However, since these parameters do not have significant correlation to surface roughness, it is likely that the surface roughness is not an adequate descriptor of the surface layer morphology. The roughness would not be able to characterize micro-cracks and other features that could directly influence the sheet resistance and other parameters. Therefore the sheet resistance of the film may potentially be partially controlled by cell geometry and viscosity of the ink, by controlling surface morphology effects. But the surface morphology will be more complex than can be measured using only roughness.

It should be noted that the sheet resistance values were extremely high compared to typical values for ITO. This is no doubt because of the significant amount of resistance added by the non-conductive polymer in the polymer-ITO matrix. As the amount of polymer relative to ITO particles increased, conductive pathways would necessarily be broken and the sheet resistance would increase. The decision was made to use a conventional ink without regard to its electrical characteristics in order to focus on the printing and ink transfer aspects of the process. Therefore the ink was not at all optimized for electrical performance. However, it was optimized for printing and therefore served as a good material for investigating the process aspects. It is suggested that future work incorporate ITO ink that has better electrical characteristics, perhaps using a conductive polymer as the binder material.

5.2.4 Response: Transparency

The relative transparency of the ITO films was apparent by simple observation of the printed films. However, all of the films had some degree of opacity. The transparency measurements were taken using a Cary spectrophotometer, or spectrometer. The spectrometer has the capability of measuring light intensity at a given light frequency over a range of frequency. The visible spectrum of approximately 300 to 1100 nm was chosen to scan. The spectrometer emitted a white light through the ITO films and then used a photo detector to capture the percentage of light transmitted at each wavelength of light. A figure showing the transparency plot for three of the samples is shown in Figure 5.15. There is a discontinuity in the data at 800 nm wavelength, representing the change

in optics in the machine to scan at higher wavelengths. This discontinuity can be considered a source of measurement error, and is a limitation of the spectrometer.

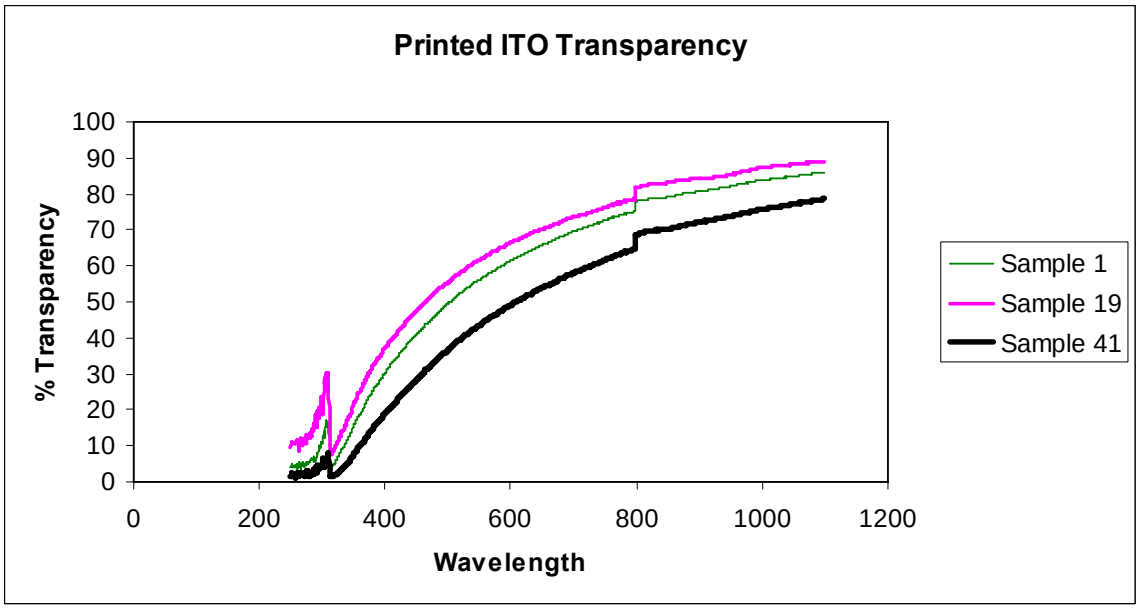

Figure 5.15: Transparency plots of several samples

The percentage of light transmitted at 550 nm wavelength was chosen as a standard response for comparison and analysis. Table 5.8 shows the regression results and Figure 5.16 shows a main effects plot. The best subsets output from MINITAB is included in Appendix D.

Table 5.8: MINITAB output for transparency

Predictor	Coef	SE Coef	T	P
Constant	7.35	22.08	0.33	0.740
Thick_ave	-0.022135	0.002842	-7.79	0.000
Ra_ave	-0.05621	0.01059	-5.31	0.000
Dynamic Viscosity	-82.15	18.71	-4.39	0.000
Surface Tension	0.2726	0.1083	2.52	0.014
Density	77.33	24.24	3.19	0.002
ITO/Binder	-9.764	2.109	-4.63	0.000
Solid/Solvent	21.485	8.183	2.63	0.011

S = 2.25818 R-Sq = 92.3% R-Sq(adj) = 91.5%

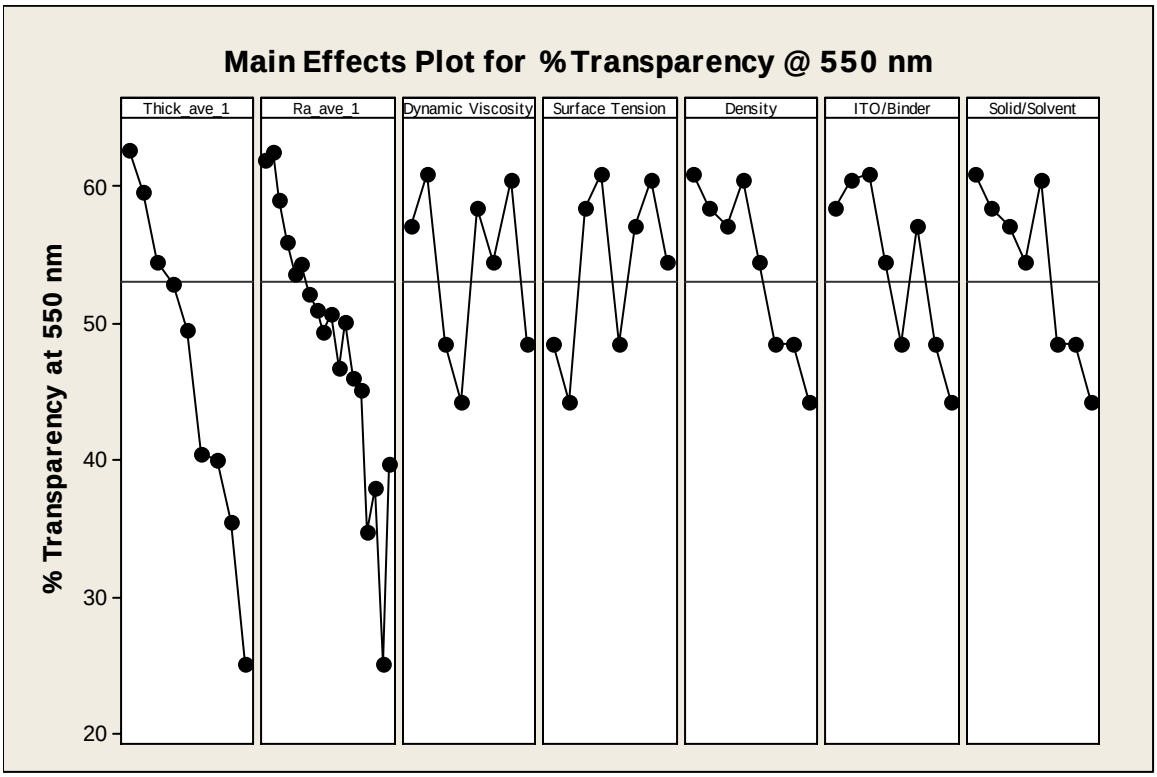

Figure 5.16: Main effects plot for transparency at 550 nm

From the above results it is clear that the transparency is highly dependent on the thickness and roughness. However, most of the ink property variables also seem to have a significant effect. This is an interesting correlation because it shows that the transparency

of the films is not directly affected by the process parameters. It is affected by the thickness and roughness, which in turn are affected by the process parameters, but the process factors such as cell geometry and speed, etc., do not significantly alter the transparency directly. Furthermore, of all the responses analyzed using the best subsets regression approach, the transparency model chosen had the highest R^2 value of over 90%. Additionally, the surface tension of the ink had a significant effect on the transparency, but not for any of the other responses, although the effect of surface tension was not clear. Still, from the main effects plots it appears that most of the effects of surface tension and other material parameters are quite complex, and conclusions about the nature of the effects are very limited. However, it seems reasonable to say that the thickness, surface morphology and the composition directly affect the transparency, with a high degree of correlation. The thinner and smoother film will have higher transparency, and the higher proportion of ITO the higher will be the transparency. However it would be difficult to alter the transparency of the film by altering any of the cell geometry or process factors, other than indirectly changing the thickness or roughness.

5.2.5 Summary

A best subsets regression approach was taken to fit a statistical model to the data. The effects of fundamental variables on the chosen responses were investigated. For each of the four responses, a model was chosen with R^2 values above 70% for each, and over 90% in the case of transparency. For sheet resistance, a nonlinear model was developed by regressing the predictor variables on the square root of the sheet resistance rather than

the measured value. This dramatically increased the goodness of fit for the model. The general conclusions for each response are summarized in this section.

For the response of average thickness, the cell volume was the single most important factor, with larger volumes corresponding to higher thickness. The composition of the ink was found to be important, with higher solvent content leading to a decrease in thickness, most likely due to the removal of volume by solvent evaporation. The material properties also seem slightly significant, with viscosity playing a role, although the exact effect is still unclear.

The average roughness is most highly correlated with the thickness of the printed layer, with higher thickness giving a higher roughness value. ITO content and ink density are also significant factors, with higher ITO content and higher density in general corresponding to higher roughness. The speed and dwell time were significant, but had a nonlinear effect at different factor levels.

The sheet resistance model was nonlinear, with the analysis being performed on a modified response variable, the square root of the sheet resistance. The amount of ITO relative to the binder is the most significant effect, while thickness was not found to be significant. The surface morphology, as affected by cell geometry and ink material properties, was also important. The exact effect of these factors was not clear.

The model selected for the response of percent transparency at 550 nm wavelength had the highest R^2 value of any of the models for other responses. The surface tension was found to be significant for this response, unlike the other variables, but the nature of the effect was unclear. The transparency model did not include any process parameters. Only material related parameters are included, suggesting that

transparency cannot be directly affected by changing cell geometry or processing conditions.

The analysis described in this chapter gave more insight into the gravure process and helped to identify fundamental parameters that help to control the characteristics of gravure printed ITO films. Many of these parameters can be directly controlled by changing the experimental parameters discussed in Chapter 4. Although some of the mechanisms responsible for certain effects were clarified by the analysis, some of the mechanisms remain unclear.

CHAPTER 6

MECHANISTIC MODEL OF THE GRAVURE PROCESS

In this chapter a mechanistic description of the gravure process is presented. In this case mechanistic is meant to imply a physical explanation of the gravure process, including the fundamental physical mechanisms responsible for the behavior of the ink during the ink transfer phase. An understanding of the behavior of the gravure ink during the process will be critical to successfully applying the gravure process to printed electronics. By understanding the process mechanics, materials and methods can potentially be developed that exploit or enhance the characteristics of the process.

6.1 Phases of the Gravure Process

The gravure process as a whole can be thought of as consisting of three separate phases. The first is the inking/doctoring phase, during which the ink is applied to the gravure image and subsequently doctored, leaving the remaining ink to come to a steady state. The second phase is the ink transfer phase, during which the ink comes into with and wets the substrate. The ink is then pulled or "picked out" of the cell, leaving only a fraction of the ink behind. The final phase relates to the ink behavior on the substrate, including ink spreading and drying or curing. These three phases will be discussed in the following sections. The discussion is based on the printing of a conventional, evaporative solvent-based ink being printed onto a non-absorbent substrate. Bery [8,50] presented many aspects of this model previously. However, he did not present the model in this form, and did not discuss the aspect of ink spreading and drying after ink transfer, and the

resulting dried ink layer morphology. Therefore this model is based off both Bery's work and the current work, in which many of the relevant effects and phenomena were observed firsthand. This model also makes some simplifying assumptions not made by Bery, which are detailed in the following sections.

6.1.1 Gravure Phase 1: Inking and Doctoring

The first phase comprises the series of processes from before the gravure image has been inked until it has been inked and doctored and is prepared for transfer. There are several different potential methods for inking and doctoring the image, usually dependent on the type of ink being used and the type of image carrier. The most common inking system, as used in rotogravure printing, is an ink well or bath. In this system, the gravure image is engraved onto a roller and simply rolls through the ink well, usually located underneath the center of the roll, and the ink simply wets the roller, and a thin layer of liquid is applied, with any excess simply falling back into the well. The amount of ink on the roller, or rather the thickness of the ink layer after coming out of the ink well this time is dependent on the speed of the roller and the viscosity of the ink. When the ink comes out of the fountain the surface is not yet horizontal, and therefore the ink layer is free to flow under the influence of gravity, thereby continuously decreasing its thickness.

In other systems without a gravure roller, such as the lab scale press used in this study, the ink is applied by hand. It then spreads on the surface under the influence of the surface wetting force. Whether the ink is applied in this manner or the previous manner, the result is the same. There is a layer of ink of some thickness covering the image, and the ink wets and fills the cells, as shown in Figure 6.1.

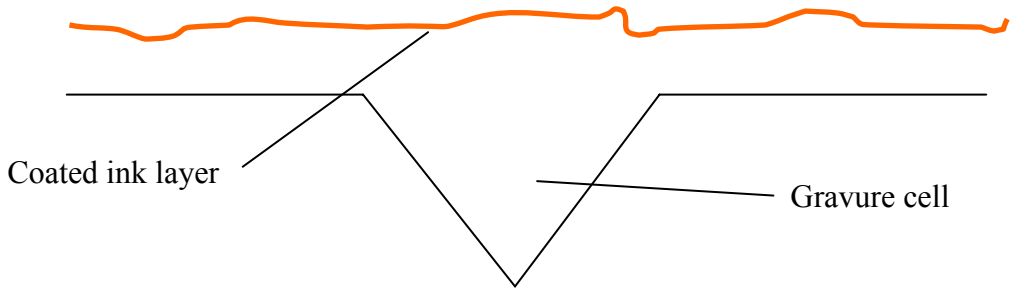

Figure 6.1: Ink covering the cell area

It should be noted here that depending on the cell size and ink properties, the ink will not necessarily fill the cells. Especially if the ink is very viscous or the ink has a high surface tension, it may not flow into the cells, or may not flow quickly enough. If the cells are too small, the ink will likewise have difficulty flowing in. In these cases, special procedures may be required, e.g. pressurizing the ink well or agitating the ink as it wets the image. However, for the purposes of this presentation, it will be assumed that the ink completely wets and fills the gravure cells before being doctored.

The doctoring step is most often achieved by the use of a flexible blade. The blade can be either steel or plastic, and it is most often a consumable part, i.e. it has to be replaced periodically. For most commercial gravure systems, the blade also oscillates back and forth across the gravure image. This ensures a more even pressure across the blade, which also ensures more even wear of the blade. This is important for complete doctoring, in which there is no ink left on the outer surface of the roller, i.e. only the cells contain ink. The doctoring process is illustrated in Figure 6.2.

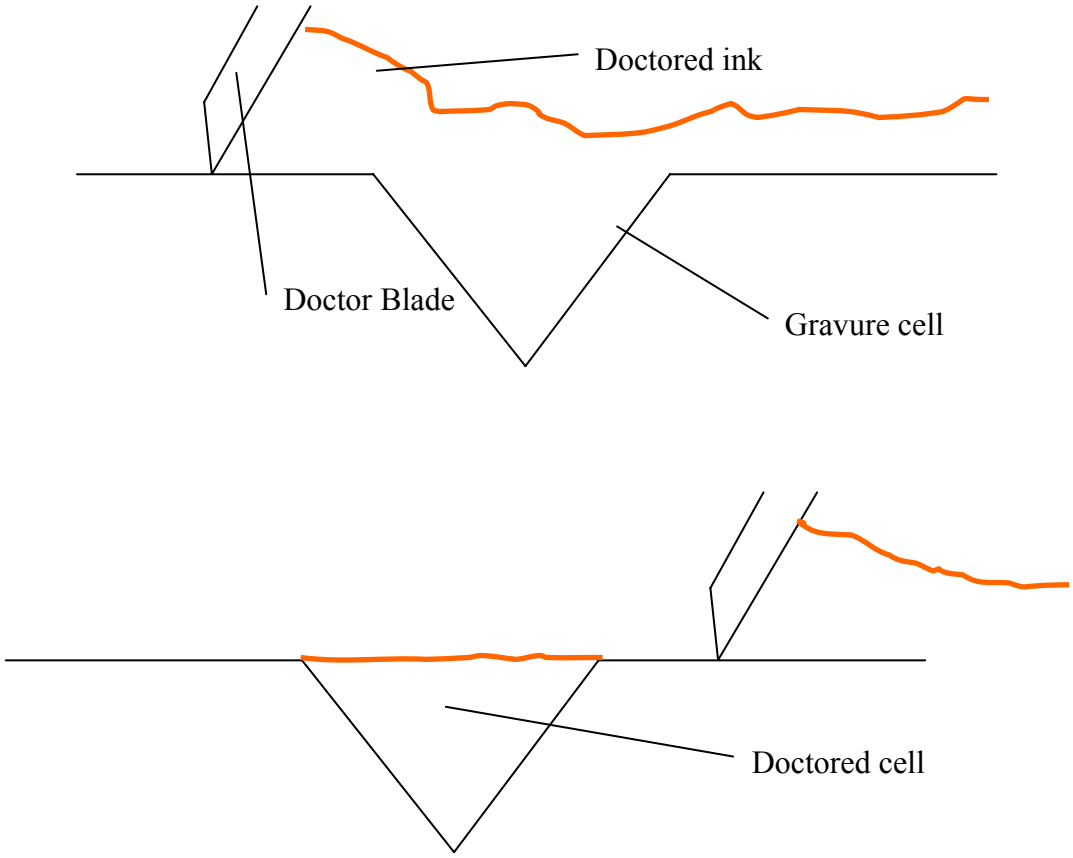

Figure 6.2: Doctoring process with a doctor blade

For the purposes of this explanation, it is assumed that the volume of ink in the cell is equal to the volume of the cell. In reality, there are two phenomena that complicate this assumption. The first is the possibility of excess ink remaining on the surface of the gravure image. This could happen if there is insufficient pressure on the doctor blade, or if the doctoring process happens too fast. As the ink begins to build up behind the doctor blade, there is a hydrodynamic force that acts to push it away from the gravure surface. This force is dependent on the size and angle of the blade, as well as the amount and viscosity of the ink. In general a shallower angle will result in a greater hydrodynamic force, as will a larger blade area and higher ink viscosity and volume. Therefore there

must be sufficient pressure on the blade and the angle to resist the force generated by the ink. However, greater pressure will also lead to increased friction and heat generation, as well as increased blade wear. A higher blade angle will likewise produce the same effects. Therefore there should be just enough pressure and an appropriate blade angle to prevent ink "leaking" under the blade, but not much more than that. It may also be noted that although in theory there should not be any ink remaining on the non-cell area, in reality it is nearly impossible to prevent this. However, if only a microscopically thin layer of ink remains on the surface, it will likely not transfer to the substrate during ink transfer, and therefore it is acceptable for all practical considerations. Such a thin layer may also serve to lubricate the doctor blade and prevent excessive wear or heat generation.

The second phenomenon that complicates the doctored ink volume assumption is the presence of an ink wetting force on the back side of the doctor blade. As the blade passes over the cell, the doctored ink in the cell remains in contact with the tip of the blade. If there is a sufficient wetting energy, the ink may wet the back of the blade and be pulled from the cell onto the back edge of the blade due to the wetting force, thereby evacuating some of the ink from the cell. The ink will also tend to be pulled up out of the cell by the blade, thus leaving the cells unfilled, and leaving a small amount of ink on the rear edge of the cell, above the surface of the image.

After the doctor blade has passed over the cells, the ink in the cell is left under the influence of the surface wetting force. As the ink wets the top edges of the cell, it will also wet the regions between cells and begin to flow outwards. If left undisturbed, it will eventually reach an equilibrium state between the wetting forces and cohesion forces.

However, the ink is also continuously changing at this stage as the solvent evaporates from the ink. The ink volume will begin to decrease, and the properties at the surface of the ink will be different from the properties below the surface of the ink. Some authors [50] have discussed the issue of frictional heating of the surface of the ink due to the doctor blade passing over the gravure cells. Estimates have put the temperature rise due to friction at up to 200 °C, depending on the process conditions. Such a temperature rise could cause a temporary sharp increase in the evaporation of solvent, further decreasing the volume of ink and changing the surface properties of the doctored ink layer. If the cells are close enough together, the ink will begin to coalesce in the areas between cells, forming a continuous layer of ink. The ink will remain in this state until the substrate comes in contact with the gravure cells (see Figure 6.3).

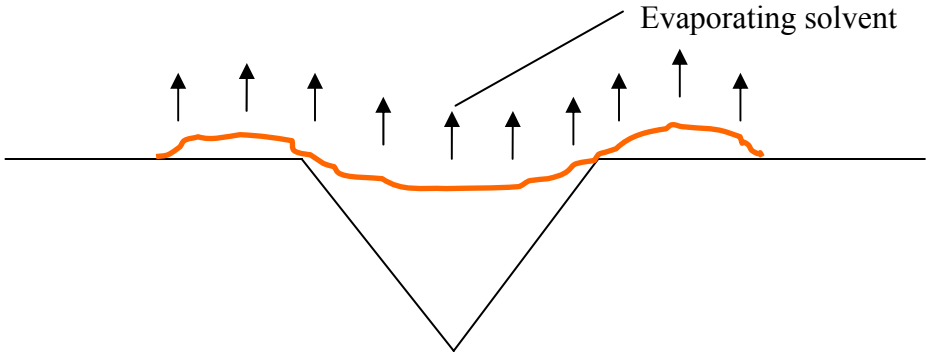

Figure 6.3: Ink wetting edges of the cell as solvent evaporates

6.1.2 Gravure Phase 2: Ink Transfer

After the ink has been doctored, the substrate moves into contact with the surface of the cell. The time between doctoring and contact with the substrate is dependent on several factors. The first factor is the distance between the doctor blade and the

impression roller. Depending on the size and configuration of the press, this distance could be considerable. The printing speed will also affect the time between doctoring and contact. The last factor is the size of the printing nip, or the region in which the compliant impression roller is in contact with the gravure roller. The nip size in turn is dependent on the amount of pressure on the impression roller and the compliance of the roller. As the nip increases in size it moves the point of initial contact closer to the doctor blade, thereby reducing the time between doctoring and substrate contact.

The ink wets the substrate as it moves close to the cell. Since the ink has wetted the outside edges of the cell, the ink will come into contact with the substrate slightly before the substrate reaches the edge of the cell, as shown in Figure 6.4. This may be an important consideration for precision ink placement because the ink that is transferred to the substrate is not constrained by the cell area. This must therefore be taken into consideration when designing and manufacturing the engraved cells for precise patterns.

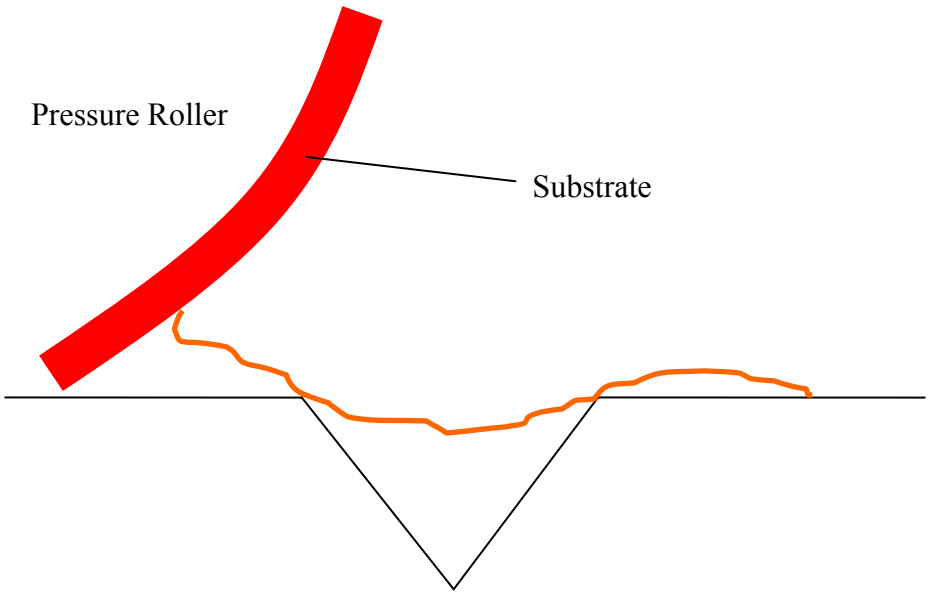

Figure 6.4: The substrate comes into contact with the ink

As the substrate continues to roll across the cell, the ink that has wet the substrate will tend to be squeezed back into the cell. The substrate will then come into its most intimate contact with the cell, completely covering and sealing the cell off with the ink trapped inside. However, it is important to realize the ink flow is not completely constrained as it is squeezed by the rolling substrate. Therefore the ink may not completely transfer back into the cell. Furthermore the ink will have had some of the solvent evaporate during the time immediately after the cell was doctored. The net effect is that there is not enough ink to fill the cell volume, and a void space is created in the cell by the substrate as it passes over the cell (see Figure 6.5). The size of this void is dependent on the properties of the ink, especially its evaporative properties. The void phenomenon has been documented by Bery [8] and others using high speed photography (see Figure 6.6), and can also explain some of the printed layer patterns presented in this

study (see Chapter 3), in which a small pinhole void is shown in locations on the substrate corresponding to the location of the center portion of the cells during ink transfer. The location of these pinholes is shown to be slightly offset from the center of the cell, in the direction of substrate travel.

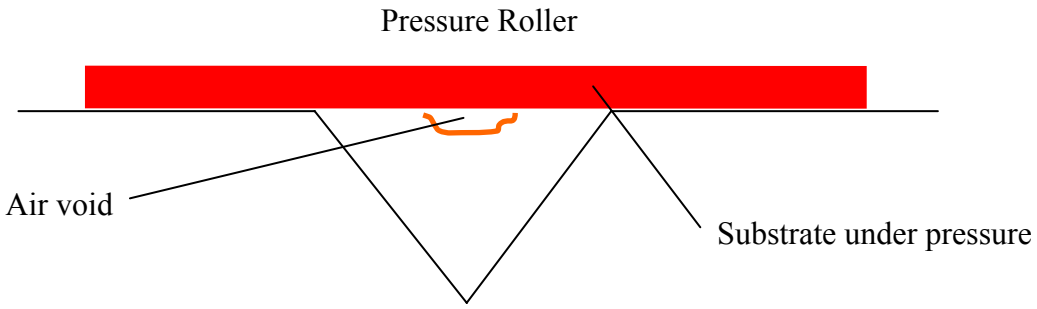

Figure 6.5: Substrate presses against cell

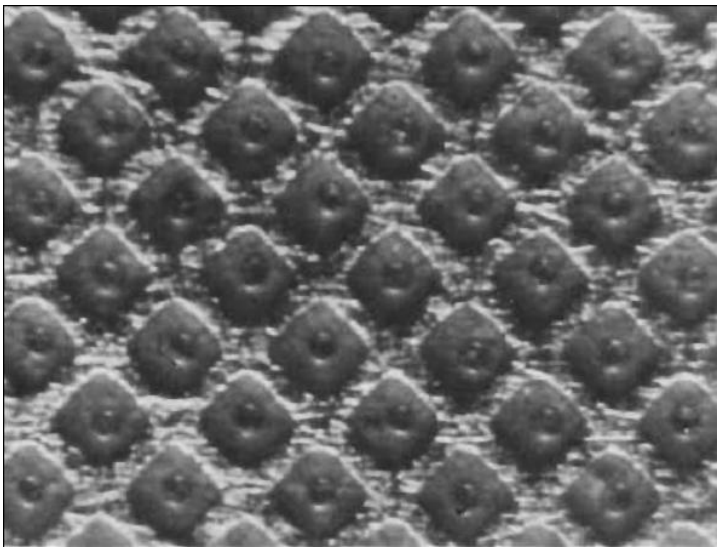

Figure 6.6: Void area in gravure cells while in contact with a substrate [8]

After the substrate has come into full contact with the cell, it will begin to lift off and separate from the cell as it exits the printing nip. Due to the wetting of the substrate,

some of the ink will be pulled out of the cell, as illustrated in Figure 6.7. If the substrate is non-porous, like the PET films used in this study, the air void will remain in the ink until the ink is transferred.

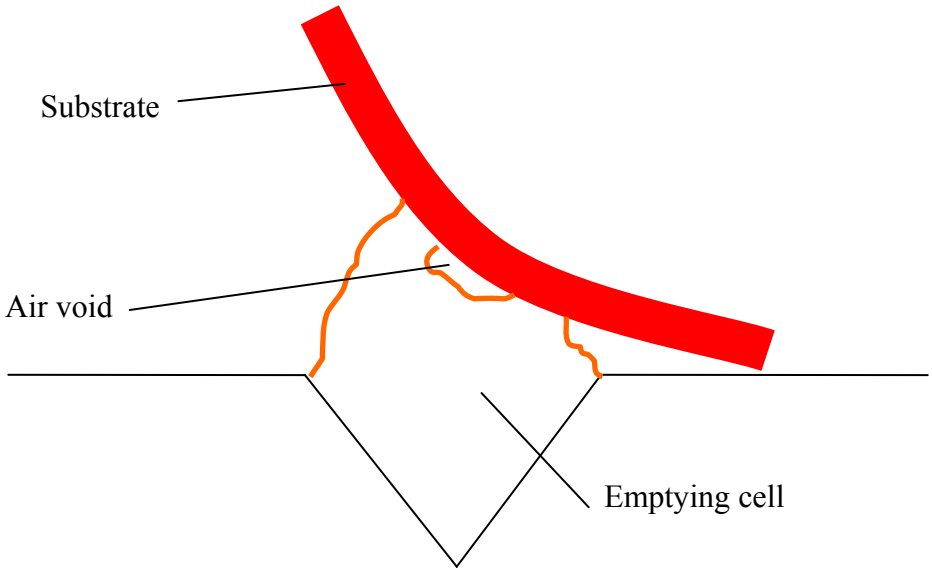

Figure 6.7: Separation of substrate from engraved cell

As the substrate continues to lift away from the cell, the ink will begin to form a filament and be stretched as ink continues to be pulled from the cell (see Figure 6.8). The filament will eventually break, when an equilibrium point is reached between the competing forces of wetting forces, inertial forces, and ink cohesion. When the filament breaks the ink will either stay on the substrate or return to the cell. The amount of ink transferred is a complex problem involving the surface energies of both the cell walls and the substrate, the surface tension of the ink, and many other ink properties. It will also be affected by the void space created in the top of the cell. The larger the void space, the less contact area the ink has with the substrate. The greater the surface area that is wetted by the cell, the more ink will be transferred form the cell.

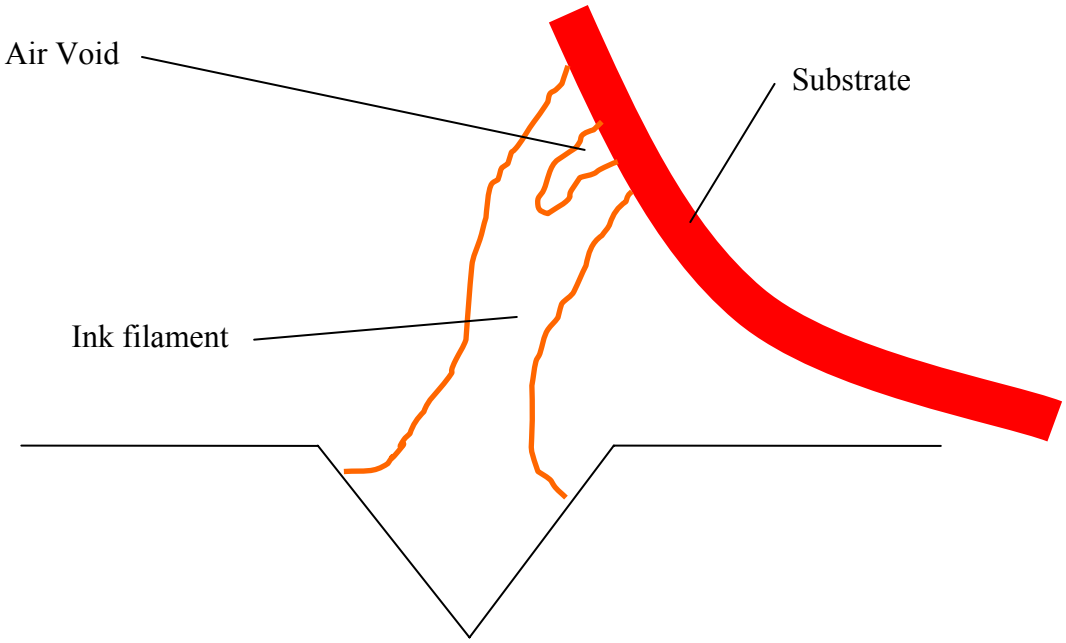

Figure 6.8: Filament formed as substrate separates from cell

6.1.3: Gravure Phase 3: Ink Spreading and Solvent Evaporation

After the ink has been transferred from the gravure cell, it will continue to wet the substrate and begin to spread. The initial profile of the ink will be uneven due to the ink transfer process and the split of the ink from the cell. The spreading dynamics may also be affected by the motion of the substrate after it exits the printing nip. If the ink layer is subjected to a relative air flow over the substrate or acceleration forces the spreading dynamics may be altered.

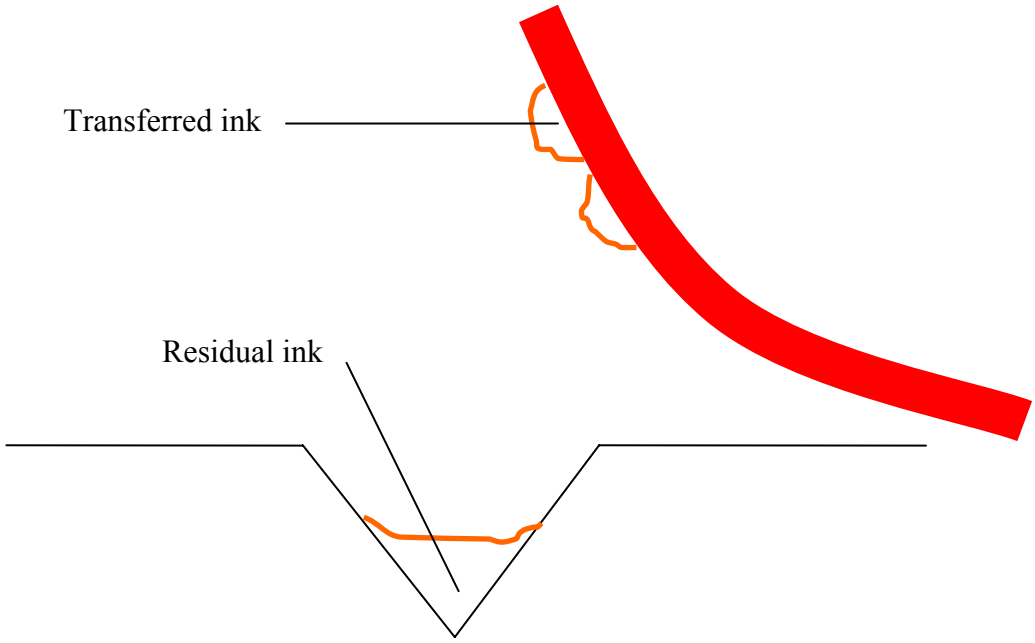

Figure 6.9: Completion of ink transfer

Due to the void created when the substrate was pressed onto the cell, there may also be small craters of ink created with pinholes in the center. The wetting forces will tend to force the ink to spread evenly and coalesce with adjacent cells. These forces will be resisted, however, by the internal cohesion of the ink, which will continue to increase as the solvent from the ink evaporates and the ink begins to cure. Therefore the final printed ink layer will have some profile that is a function of film thickness and the drying behavior of the ink. The ink may or may not coalesce and will have gaps and voids where the distances between the discrete areas of ink are too large to be covered due to wetting.

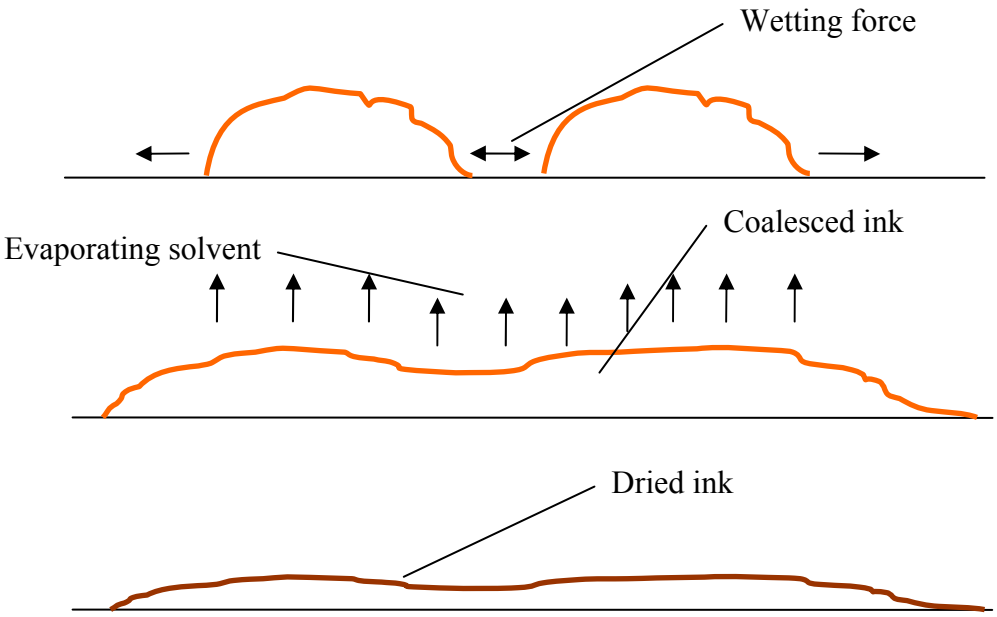

Figure 6.10: Spreading and coalescing of the ink on the substrate

The spreading of ink into a continuous film has also been documented for inkjet printing in the manufacture of printed electronics [90]. A schematic of the film formation process is shown in Figure 6.11. The schematic also illustrates the continuous evaporation of solvent from the ink layer. This illustrates one of the challenges of printed electronics. Regardless of the printing process used, the final properties of the deposited film are going to be dependent on the behavior of the ink after it has been transferred. Printing processes in general do not deposit material in a thin, uniform layer. The ink morphology at the point of transfer can be quite uneven, but the final layer could be very smooth.

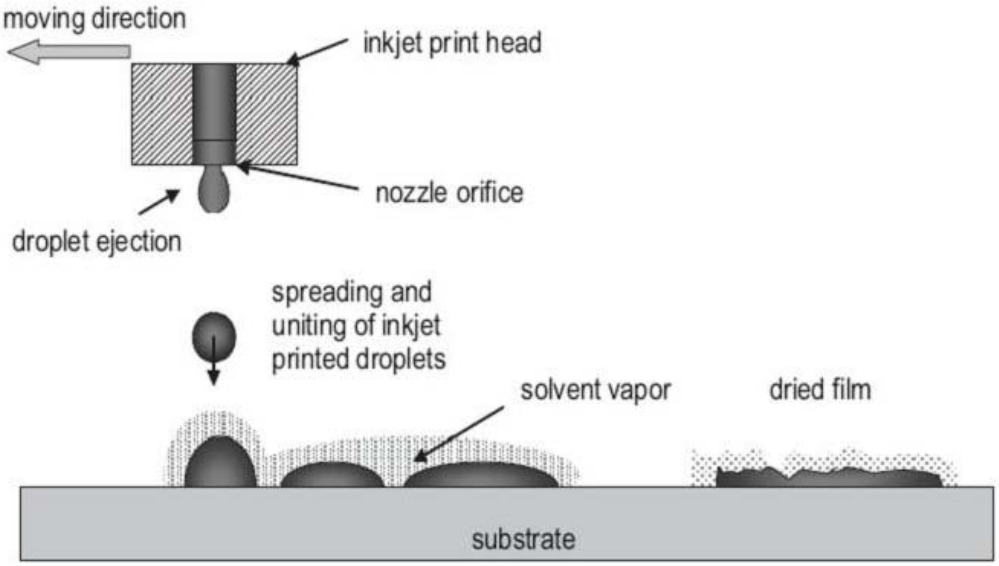

Figure 6.11: Film formation in inkjet printing [51]

6.2: Analysis of Printed ITO

In order to more fully understand the physical characteristics of the printed ITO layer, some of the films were studied under a scanning electron microscope (SEM) to view the surface layer morphology and composition. Because of the lack of conductivity of the samples, only the thickest films with the lowest sheet resistance could be viewed adequately. The films were viewed under up to 7000x magnification. Some of the images obtained can be seen in Figure 6.6. The image was focused on some of the clumps that were visible under the light microscope (see Figure 6.12). This allowed characterization of the clumps and their morphology.

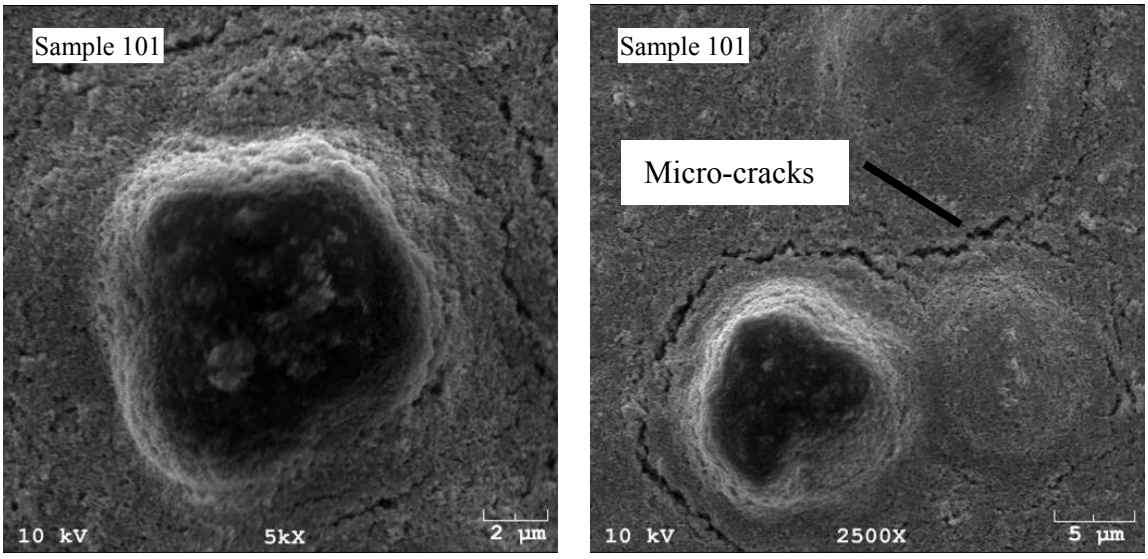

Figure 6.12: SEM micrographs of ITO films, focused on clumped areas

The SEM analysis highlighted several interesting features. The first was that all of the clumps had circular edges and were all several microns in diameter. One of the most interesting features is the ring of cracks visible around the edge of each clump. These cracks suggest that as the film dried, it formed clumps and solidified, and then continued to cure and contract. The clumps then seemed to act as stress concentrations, points at which the film cannot relax and instead forms micro-cracks. Such cracks almost certainly affect the conductivity of the film adversely. Conductive pathways between nanoparticles are broken as the film develops these cracks. Therefore a rough film with many clumps may be expected to be less conductive. Another feature of interest was the relatively smooth micro-roughness. Most of the surface variation occurs at the clumps, with the rest of the film forming relatively smooth micro-surface. This gives some insight into the drying behavior of the nanoparticle inks.

In related studies that investigate the drying of ink-jet drops of solvent-based inks [52-54] the phenomenon of the "coffee-ring" effect is reported. In a circular ink-jet drop

on a non-absorbing substrate, the drop forms a "coffee-ring" shape as the solvent evaporates, with thicker profile around the edge of the drop, and a thinner depression in the middle. This effect can be observed for an inkjet drop in Figure 6.13. This is caused by the flow of ink to the edges of the drop during solvent evaporation.

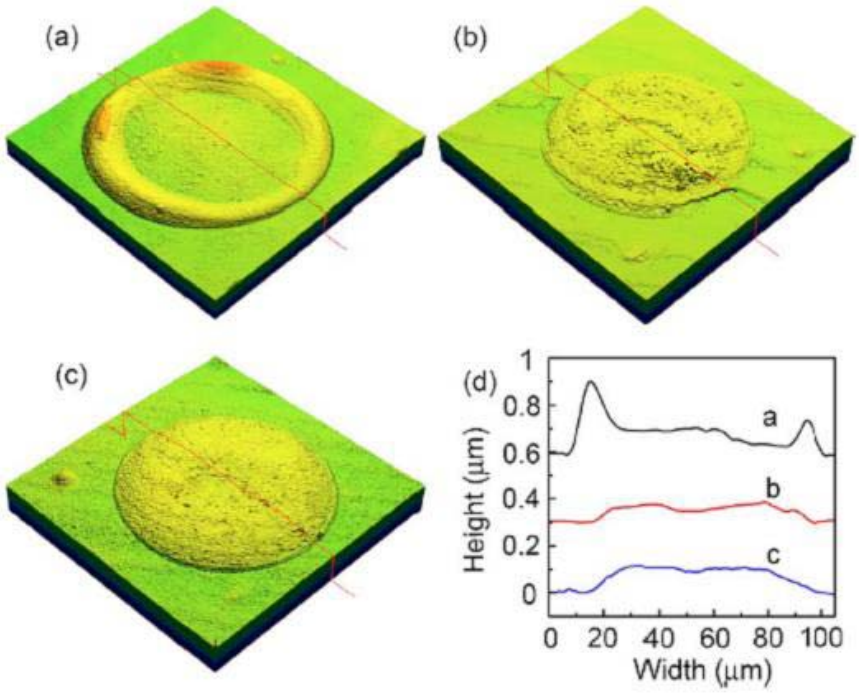

Figure 6.13: Illustration of "coffee-ring" effect for an inkjet drop [52]

Due to the disproportionately high evaporation rate close to the ink-surface contact line, the solid ink particles flow to the edges of the cell due to convection of the solvent. The ink then solidifies before the film can equalize and the coffee ring is formed. Other studies in ink drying report similar irregularities in dried ink films (see Figure 6.14), due mainly to high evaporation rates. Some studies have shown that replacing the quick-

evaporating solvents typically used with slower evaporating solvents can eliminate the coffee-ring effect and other irregularities.

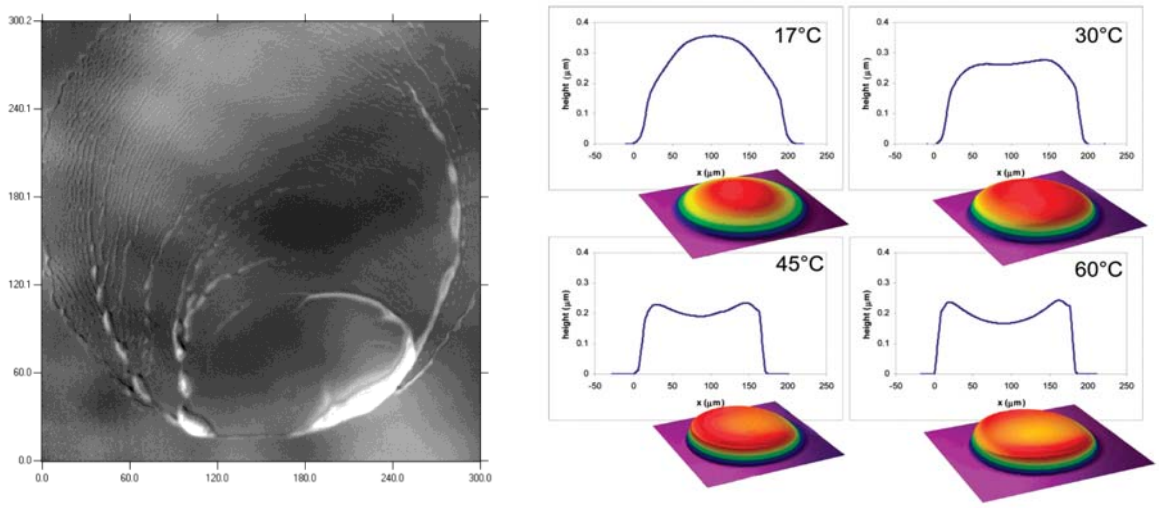

Figure 6.14: Surface irregularities in printed ink films [53,54]

Due to the related studies on irregular surface morphology, as well as the SEM analysis, there is good reason to believe that most of the clumps and irregularities are due to drying behavior of the ITO ink. Ethanol mixed with acetone used in the ink is a relatively quick-evaporating solvent. This may be useful in graphics printing where the image must travel through several print stations within a few seconds, with the ink drying in between each station. However, in functional printing, a slower evaporation cycle could greatly improve the uniformity of the printed layer.

6.3 Summary

This chapter describes the ink transfer in the gravure process mechanistically. The process can be described in a series of steps as illustrated in Figure 6.15.

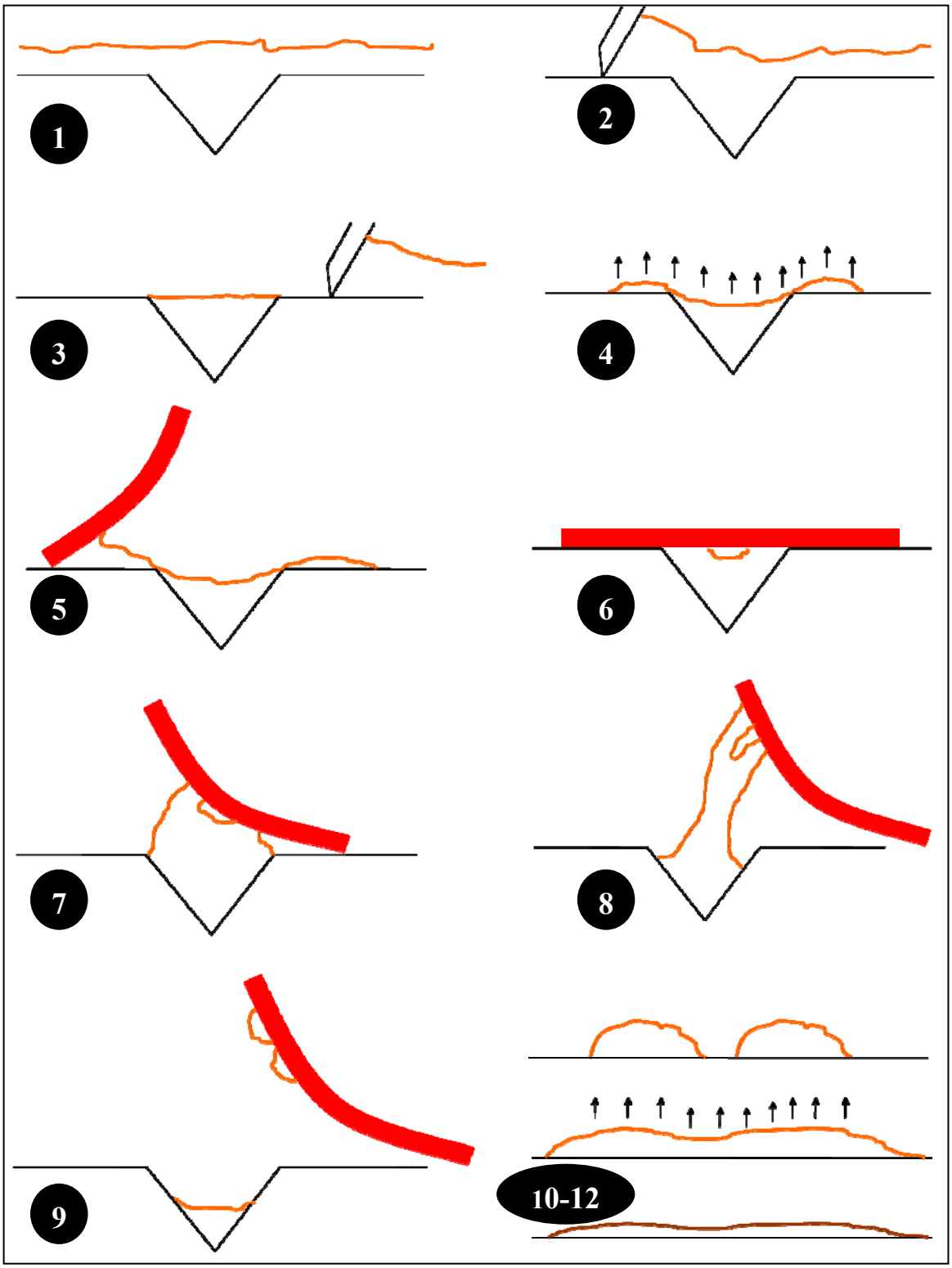

Figure 6.15: Summary of steps in mechanistic model of gravure printing

This mechanistic view is useful to understand the gravure process and how thin films and patterns are created. The processes of ink doctoring, ink transfer, and ink spreading on the substrate all contribute to the characteristics of the printed film of material. This mechanistic view complements the experimental results described in this work, by identifying the governing mechanisms responsible for certain effects. The significant parameters identified by the analysis of the experimental data can be partially explained by understanding the mechanisms that have been documented in gravure printing.

CHAPTER 7

CONCLUSIONS AND RECOMMENDATIONS

This thesis described an investigation of the gravure process for printed flexible electronics. Two experiments were performed to investigate the effects of several key process parameters on several different responses of interest. The first experiment was a screening experiment that was used to explore the process and identify factor levels that could print thin, uniform layers of ITO ink without voids or pinholes. The second experiment was designed to further investigate the effect of process parameters on the physical characteristics of the improved, void- and pinhole-free films.

Further analysis was performed on the experimental data from the main experiment in order to relate fundamental properties of the process to physical and functional characteristics of the printed films. This analysis gave further insight into the process and identified key process factors that corresponded to certain properties of the printed films. A mechanistic description of the gravure process was also given that was based on prior work and verified by the experiments performed in this work.

7.1 Experimental Findings

Some of the key findings from the experiments are summarized here.

- ITO nanoparticles suspended in a conventional printing ink can be successfully printed using the gravure process.
- High ITO content can lead to the presence of pinholes, which are generally undesirable.

- ITO nanoparticle films ranging in thickness from 300 nm to 1300 nm and in average roughness from ~90 nm to ~300nm were successfully printed.
- The printed films had extremely high sheet resistance and relatively poor transparency, resulting in poor functionality.
- The evaporation of solvent during the process can affect several different process mechanisms, from the transfer of ink from the cell to drying on the substrate.
- The volume of the gravure cells is highly correlated to the amount of ink transferred to the substrate, while the geometry of the cells can also affect the roughness of the films.
- The sheet resistance is most highly correlated to the ratio of ITO relative to ink binder, and is not highly correlated to the thickness or roughness of the film.
- The transparency is most highly correlated to the thickness and roughness of the ITO films
- Small air voids can be trapped between the substrate and ink surface that will appear as pinholes in the printed ink layer. These voids occur at the interior of each individual cell area and the pinholes will remain unless the ink can spread and coalesce on the substrate after printing.

7.2: Further Observations

- The ink transfer phase can be separated into ink doctoring, ink transfer, and ink spreading, with each phase having different effects on the characteristics of the printed layer.

- The films could potentially be made smoother by reducing the solvent evaporation rate.
- The dried films had microcracks viewed with an SEM likely due to contraction of the dried ink, which most likely affect the conductivity of the film adversely.
- There is a direct tradeoff between the ITO content and the printability of the ITO ink. More content is better for performance, but diminishes printability.

7.3: Recommendations for Future Work

In the course of completing this study there were several key areas identified that have potential for future study. The field of printed flexible electronics is still quite nascent, and there is still a large gap in knowledge between traditional printing processes and electronics manufacturing. Several recommendations for future work will be discussed here.

The material used in this study was ITO. This material was chosen for its conductivity and transparency. However, the choice of this material limited the scope of this study only to inorganic solid nanoparticles mixed with an organic binder. There are many materials, such as purely organic active materials, that are potentially even more suited to printing processes that may give even better results. Furthermore, the organic binder used in this study was a commercially available ink vehicle that was chosen based on the likelihood that it would print easily. Since the combination of the ink vehicle and ITO nanoparticles created a truly unique "ink", there was no way to know what to expect in terms of ink properties. The ink proved to be very difficult to characterize, due to the

rapid solvent evaporation, and in the future a more familiar or fully optimized material may be more useful and provide better results.

The ITO films were rougher than desired, and this was at least partially due to the rapidly evaporating solvent used. A more slowly evaporating ink would most likely provide better roughness values, and this would be an interesting study to pursue. The use of a UV-curing ink or something that did not rely on solvent evaporation may also be an interesting area to investigate.There were also several process variables, such as doctor blade angle and blade load, that were not investigated. There are likely other factors that may have a significant impact on the properties of the printed film that were not included in this study.

There are also some issues related to printed electronics that should be pursued in the future. The printing of multiple layers of functional materials on top of each other would make possible the production of an all printed electronic device. However, this introduces issues such as registration between printing steps, and printed layer durability within the printing process. The general durability and failure modes of printed electronics are also of interest.

APPENDIX A

EXPERIMENTAL DESIGNS

A.1: Screening Experiment Design

The following table A.1 presents the experimental design for the screening experiment, which was a 2^{8-1} fractional factorial experiment. The low and high levels for each factor are represented by a "-" and "+" sign, respectively. The actual levels of the factors as used in the experiment are shown in Figure 3.2. The treatments were randomized and performed in the random order. It should be noted that each eight treatments represented the eight different sections of the printing plate and were printed simultaneously, i.e. there were 16 sheets printed with 8 treatments each, for a total of 128 treatments.

Table A.1: Screening experiment design

	Tone	Stylus	Line Screen	Roller Pressure	Speed	Binder	ITO %	Solvent
Treatment	X1	X2	X3	X4	X5	X6	X7	X8
1	+	+	+	+	+	+	+	+
2	-	+	+	+	+	+	+	+
3	+	-	+	+	+	+	+	+
4	-	-	+	+	+	+	+	+
5	+	+	-	+	+	+	+	+
6	-	+	-	+	+	+	+	+
7	+	-	-	+	+	+	+	+
8	-	-	-	+	+	+	+	+
9	+	+	+	-	+	+	+	-
10	-	+	+	-	+	+	+	-
11	+	-	+	-	+	+	+	-
12	-	-	+	-	+	+	+	-
13	+	+	-	-	+	+	+	-
14	-	+	-	-	+	+	+	-
15	+	-	-	-	+	+	+	-

	Tone	Stylus	Line Screen	Roller Pressure	Speed	Binder	ITO %	Solvent
Treatment	X1	X2	X3	X4	X5	X6	X7	X8
16	-	-	-	-	+	+	+	-
17	+	+	+	+	-	+	+	-
18	-	+	+	+	-	+	+	-
19	+	-	+	+	-	+	+	-
20	-	-	+	+	-	+	+	-
21	+	+	-	+	-	+	+	-
22	-	+	-	+	-	+	+	-
23	+	-	-	+	-	+	+	-
24	-	-	-	+	-	+	+	-
25	+	+	+	-	-	+	+	+
26	-	+	+	-	-	+	+	+
27	+	-	+	-	-	+	+	+
28	-	-	+	-	-	+	+	+
29	+	+	-	-	-	+	+	+
30	-	+	-	-	-	+	+	+
31	+	-	-	-	-	+	+	+
32	-	-	-	-	-	+	+	+
33	+	+	+	+	+	-	+	-
34	-	+	+	+	+	-	+	-
35	+	-	+	+	+	-	+	-
36	-	-	+	+	+	-	+	-
37	+	+	-	+	+	-	+	-
38	-	+	-	+	+	-	+	-
39	+	-	-	+	+	-	+	-
40	-	-	-	+	+	-	+	-
41	+	+	+	-	+	-	+	+
42	-	+	+	-	+	-	+	+
43	+	-	+	-	+	-	+	+
44	-	-	+	-	+	-	+	+
45	+	+	-	-	+	-	+	+
46	-	+	-	-	+	-	+	+
47	+	-	-	-	+	-	+	+
48	-	-	-	-	+	-	+	+
49	+	+	+	+	-	-	+	+
50	-	+	+	+	-	-	+	+
51	+	-	+	+	-	-	+	+
52	-	-	+	+	-	-	+	+
53	+	+	-	+	-	-	+	+
54	-	+	-	+	-	-	+	+
55	+	-	-	+	-	-	+	+
56	-	-	-	+	-	-	+	+
57	+	+	+	-	-	-	+	-
58	-	+	+	-	-	-	+	-

	Tone	Stylus	Line Screen	Roller Pressure	Speed	Binder	ITO %	Solvent
Treatment	X1	X2	X3	X4	X5	X6	X7	X8
59	+	-	+	-	-	-	+	-
60	-	-	+	-	-	-	+	-
61	+	+	-	-	-	-	+	-
62	-	+	-	-	-	-	+	-
63	+	-	-	-	-	-	+	-
64	-	-	-	-	-	-	+	-
65	+	+	+	+	+	+	-	-
66	-	+	+	+	+	+	-	-
67	+	-	+	+	+	+	-	-
68	-	-	+	+	+	+	-	-
69	+	+	-	+	+	+	-	-
70	-	+	-	+	+	+	-	-
71	+	-	-	+	+	+	-	-
72	-	-	-	+	+	+	-	-
73	+	+	+	-	+	+	-	+
74	-	+	+	-	+	+	-	+
75	+	-	+	-	+	+	-	+
76	-	-	+	-	+	+	-	+
77	+	+	-	-	+	+	-	+
78	-	+	-	-	+	+	-	+
79	+	-	-	-	+	+	-	+
80	-	-	-	-	+	+	-	+
81	+	+	+	+	-	+	-	+
82	-	+	+	+	-	+	-	+
83	+	-	+	+	-	+	-	+
84	-	-	+	+	-	+	-	+
85	+	+	-	+	-	+	-	+
86	-	+	-	+	-	+	-	+
87	+	-	-	+	-	+	-	+
88	-	-	-	+	-	+	-	+
89	+	+	+	-	-	+	-	-
90	-	+	+	-	-	+	-	-
91	+	-	+	-	-	+	-	-
92	-	-	+	-	-	+	-	-
93	+	+	-	-	-	+	-	-
94	-	+	-	-	-	+	-	-
95	+	-	-	-	-	+	-	-
96	-	-	-	-	-	+	-	-
97	+	+	+	+	+	-	-	+
98	-	+	+	+	+	-	-	+
99	+	-	+	+	+	-	-	+
100	-	-	+	+	+	-	-	+
101	+	+	-	+	+	-	-	+

	Tone	Stylus	Line Screen	Roller Pressure	Speed	Binder	ITO %	Solvent
Treatment	X1	X2	X3	X4	X5	X6	X7	X8
102	-	+	-	+	+	-	-	+
103	+	-	-	+	+	-	-	+
104	-	-	-	+	+	-	-	+
105	+	+	+	-	+	-	-	-
106	-	+	+	-	+	-	-	-
107	+	-	+	-	+	-	-	-
108	-	-	+	-	+	-	-	-
109	+	+	-	-	+	-	-	-
110	-	+	-	-	+	-	-	-
111	+	-	-	-	+	-	-	-
112	-	-	-	-	+	-	-	-
113	+	+	+	+	-	-	-	-
114	-	+	+	+	-	-	-	-
115	+	-	+	+	-	-	-	-
116	-	-	+	+	-	-	-	-
117	+	+	-	+	-	-	-	-
118	-	+	-	+	-	-	-	-
119	+	-	-	+	-	-	-	-
120	-	-	-	+	-	-	-	-
121	+	+	+	-	-	-	-	+
122	-	+	+	-	-	-	-	+
123	+	-	+	-	-	-	-	+
124	-	-	+	-	-	-	-	+
125	+	+	-	-	-	-	-	+
126	-	+	-	-	-	-	-	+
127	+	-	-	-	-	-	-	+
128	-	-	-	-	-	-	-	+

A.2: Main Experiment Design

The experimental design for the main experiment is given in Table A.2. The corresponding factor levels are given in Table 4.1. It should be noted that there were a total of 28 printing runs in the original design, with 8 treatments for each print, for a total of 224 treatments. During the course of the experiment, one additional was performed that was a replicate of one of the other runs. It was added to the original design, so there was a total of 29 print runs comprising 232 total treatments.

Table A.2: Main experiment design

Treatment	Pressure	Speed	ITO %	Solvent	Line Screen	Stylus	Tone
1	-1	-1	-1	-1	1	1	1
2	-1	-1	-1	-1	1	1	-1
3	-1	-1	-1	-1	1	-1	1
4	-1	-1	-1	-1	1	-1	-1
5	-1	-1	-1	-1	-1	1	1
6	-1	-1	-1	-1	-1	1	-1
7	-1	-1	-1	-1	-1	-1	1
8	-1	-1	-1	-1	-1	-1	-1
9	1	-1	-1	-1	1	1	1
10	1	-1	-1	-1	1	1	-1
11	1	-1	-1	-1	1	-1	1
12	1	-1	-1	-1	1	-1	-1
13	1	-1	-1	-1	-1	1	1
14	1	-1	-1	-1	-1	1	-1
15	1	-1	-1	-1	-1	-1	1
16	1	-1	-1	-1	-1	-1	-1
17	-1	1	-1	-1	1	1	1
18	-1	1	-1	-1	1	1	-1
19	-1	1	-1	-1	1	-1	1
20	-1	1	-1	-1	1	-1	-1
21	-1	1	-1	-1	-1	1	1
22	-1	1	-1	-1	-1	1	-1
23	-1	1	-1	-1	-1	-1	1
24	-1	1	-1	-1	-1	-1	-1
25	1	1	-1	-1	1	1	1
26	1	1	-1	-1	1	1	-1
27	1	1	-1	-1	1	-1	1
28	1	1	-1	-1	1	-1	-1
29	1	1	-1	-1	-1	1	1
30	1	1	-1	-1	-1	1	-1
31	1	1	-1	-1	-1	-1	1
32	1	1	-1	-1	-1	-1	-1
33	-1	-1	1	-1	1	1	1
34	-1	-1	1	-1	1	1	-1
35	-1	-1	1	-1	1	-1	1
36	-1	-1	1	-1	1	-1	-1
37	-1	-1	1	-1	-1	1	1
38	-1	-1	1	-1	-1	1	-1
39	-1	-1	1	-1	-1	-1	1
40	-1	-1	1	-1	-1	-1	-1
41	1	-1	1	-1	1	1	1
42	1	-1	1	-1	1	1	-1
43	1	-1	1	-1	1	-1	1

Treatment	Pressure	Speed	ITO %	Solvent	Line Screen	Stylus	Tone
44	1	-1	1	-1	1	-1	-1
45	1	-1	1	-1	-1	1	1
46	1	-1	1	-1	-1	1	-1
47	1	-1	1	-1	-1	-1	1
48	1	-1	1	-1	-1	-1	-1
49	-1	1	1	-1	1	1	1
50	-1	1	1	-1	1	1	-1
51	-1	1	1	-1	1	-1	1
52	-1	1	1	-1	1	-1	-1
53	-1	1	1	-1	-1	1	1
54	-1	1	1	-1	-1	1	-1
55	-1	1	1	-1	-1	-1	1
56	-1	1	1	-1	-1	-1	-1
57	1	1	1	-1	1	1	1
58	1	1	1	-1	1	1	-1
59	1	1	1	-1	1	-1	1
60	1	1	1	-1	1	-1	-1
61	1	1	1	-1	-1	1	1
62	1	1	1	-1	-1	1	-1
63	1	1	1	-1	-1	-1	1
64	1	1	1	-1	-1	-1	-1
65	-1	-1	-1	1	1	1	1
66	-1	-1	-1	1	1	1	-1
67	-1	-1	-1	1	1	-1	1
68	-1	-1	-1	1	1	-1	-1
69	-1	-1	-1	1	-1	1	1
70	-1	-1	-1	1	-1	1	-1
71	-1	-1	-1	1	-1	-1	1
72	-1	-1	-1	1	-1	-1	-1
73	1	-1	-1	1	1	1	1
74	1	-1	-1	1	1	1	-1
75	1	-1	-1	1	1	-1	1
76	1	-1	-1	1	1	-1	-1
77	1	-1	-1	1	-1	1	1
78	1	-1	-1	1	-1	1	-1
79	1	-1	-1	1	-1	-1	1
80	1	-1	-1	1	-1	-1	-1
81	-1	1	-1	1	1	1	1
82	-1	1	-1	1	1	1	-1
83	-1	1	-1	1	1	-1	1
84	-1	1	-1	1	1	-1	-1
85	-1	1	-1	1	-1	1	1
86	-1	1	-1	1	-1	1	-1
87	-1	1	-1	1	-1	-1	1
88	-1	1	-1	1	-1	-1	-1
89	1	1	-1	1	1	1	1

Treatment	Pressure	Speed	ITO %	Solvent	Line Screen	Stylus	Tone
90	1	1	-1	1	1	1	-1
91	1	1	-1	1	1	-1	1
92	1	1	-1	1	1	-1	-1
93	1	1	-1	1	-1	1	1
94	1	1	-1	1	-1	1	-1
95	1	1	-1	1	-1	-1	1
96	1	1	-1	1	-1	-1	-1
97	-1	-1	1	1	1	1	1
98	-1	-1	1	1	1	1	-1
99	-1	-1	1	1	1	-1	1
100	-1	-1	1	1	1	-1	-1
101	-1	-1	1	1	-1	1	1
102	-1	-1	1	1	-1	1	-1
103	-1	-1	1	1	-1	-1	1
104	-1	-1	1	1	-1	-1	-1
105	1	-1	1	1	1	1	1
106	1	-1	1	1	1	1	-1
107	1	-1	1	1	1	-1	1
108	1	-1	1	1	1	-1	-1
109	1	-1	1	1	-1	1	1
110	1	-1	1	1	-1	1	-1
111	1	-1	1	1	-1	-1	1
112	1	-1	1	1	-1	-1	-1
113	-1	1	1	1	1	1	1
114	-1	1	1	1	1	1	-1
115	-1	1	1	1	1	-1	1
116	-1	1	1	1	1	-1	-1
117	-1	1	1	1	-1	1	1
118	-1	1	1	1	-1	1	-1
119	-1	1	1	1	-1	-1	1
120	-1	1	1	1	-1	-1	-1
121	1	1	1	1	1	1	1
122	1	1	1	1	1	1	-1
123	1	1	1	1	1	-1	1
124	1	1	1	1	1	-1	-1
125	1	1	1	1	-1	1	1
126	1	1	1	1	-1	1	-1
127	1	1	1	1	-1	-1	1
128	1	1	1	1	-1	-1	-1
129	-2	0	0	0	1	1	1
130	-2	0	0	0	1	1	-1
131	-2	0	0	0	1	-1	1
132	-2	0	0	0	1	-1	-1
133	-2	0	0	0	-1	1	1
134	-2	0	0	0	-1	1	-1
135	-2	0	0	0	-1	-1	1

Treatment	Pressure	Speed	ITO %	Solvent	Line Screen	Stylus	Tone
136	-2	0	0	0	-1	-1	-1
137	2	0	0	0	1	1	1
138	2	0	0	0	1	1	-1
139	2	0	0	0	1	-1	1
140	2	0	0	0	1	-1	-1
141	2	0	0	0	-1	1	1
142	2	0	0	0	-1	1	-1
143	2	0	0	0	-1	-1	1
144	2	0	0	0	-1	-1	-1
145	0	-2	0	0	1	1	1
146	0	-2	0	0	1	1	-1
147	0	-2	0	0	1	-1	1
148	0	-2	0	0	1	-1	-1
149	0	-2	0	0	-1	1	1
150	0	-2	0	0	-1	1	-1
151	0	-2	0	0	-1	-1	1
152	0	-2	0	0	-1	-1	-1
153	0	2	0	0	1	1	1
154	0	2	0	0	1	1	-1
155	0	2	0	0	1	-1	1
156	0	2	0	0	1	-1	-1
157	0	2	0	0	-1	1	1
158	0	2	0	0	-1	1	-1
159	0	2	0	0	-1	-1	1
160	0	2	0	0	-1	-1	-1
161	0	0	-2	0	1	1	1
162	0	0	-2	0	1	1	-1
163	0	0	-2	0	1	-1	1
164	0	0	-2	0	1	-1	-1
165	0	0	-2	0	-1	1	1
166	0	0	-2	0	-1	1	-1
167	0	0	-2	0	-1	-1	1
168	0	0	-2	0	-1	-1	-1
169	0	0	2	0	1	1	1
170	0	0	2	0	1	1	-1
171	0	0	2	0	1	-1	1
172	0	0	2	0	1	-1	-1
173	0	0	2	0	-1	1	1
174	0	0	2	0	-1	1	-1
175	0	0	2	0	-1	-1	1
176	0	0	2	0	-1	-1	-1
177	0	0	0	-2	1	1	1
178	0	0	0	-2	1	1	-1
179	0	0	0	-2	1	-1	1
180	0	0	0	-2	1	-1	-1
181	0	0	0	-2	-1	1	1

Treatment	Pressure	Speed	ITO %	Solvent	Line Screen	Stylus	Tone
182	0	0	0	-2	-1	1	-1
183	0	0	0	-2	-1	-1	1
184	0	0	0	-2	-1	-1	-1
185	0	0	0	2	1	1	1
186	0	0	0	2	1	1	-1
187	0	0	0	2	1	-1	1
188	0	0	0	2	1	-1	-1
189	0	0	0	2	-1	1	1
190	0	0	0	2	-1	1	-1
191	0	0	0	2	-1	-1	1
192	0	0	0	2	-1	-1	-1
193	0	0	0	0	1	1	1
194	0	0	0	0	1	1	-1
195	0	0	0	0	1	-1	1
196	0	0	0	0	1	-1	-1
197	0	0	0	0	-1	1	1
198	0	0	0	0	-1	1	-1
199	0	0	0	0	-1	-1	1
200	0	0	0	0	-1	-1	-1
201	0	0	0	0	1	1	1
202	0	0	0	0	1	1	-1
203	0	0	0	0	1	-1	1
204	0	0	0	0	1	-1	-1
205	0	0	0	0	-1	1	1
206	0	0	0	0	-1	1	-1
207	0	0	0	0	-1	-1	1
208	0	0	0	0	-1	-1	-1
209	0	0	0	0	1	1	1
210	0	0	0	0	1	1	-1
211	0	0	0	0	1	-1	1
212	0	0	0	0	1	-1	-1
213	0	0	0	0	-1	1	1
214	0	0	0	0	-1	1	-1
215	0	0	0	0	-1	-1	1
216	0	0	0	0	-1	-1	-1
217	0	0	0	0	1	1	1
218	0	0	0	0	1	1	-1
219	0	0	0	0	1	-1	1
220	0	0	0	0	1	-1	-1
221	0	0	0	0	-1	1	1
222	0	0	0	0	-1	1	-1
223	0	0	0	0	-1	-1	1
224	0	0	0	0	-1	-1	-1
225	-1	-1	-1	-1	1	1	1
226	-1	-1	-1	-1	1	1	-1
227	-1	-1	-1	-1	1	-1	1

Treatment	Pressure	Speed	ITO %	Solvent	Line Screen	Stylus	Tone
228	-1	-1	-1	-1	1	-1	-1
229	-1	-1	-1	-1	-1	1	1
230	-1	-1	-1	-1	-1	1	-1
231	-1	-1	-1	-1	-1	-1	1
232	-1	-1	-1	-1	-1	-1	-1

APPENDIX B

EXPERIMENTAL DATA AND ANALYSIS

B.1: Screening Experiment Data and Analysis

The response data for the screening experiments is given in Table B.1, including average void area and pinhole area data. The MINITAB regression output for the two responses of void area and pinhole area are shown in Tables B.2 and B.3. Main effects plots for the two responses of void area and pinhole area, as well as interaction plots, are shown in Figures B.1-B.4.

Table B.1: Screening Experiment Data

Sample #	Void Area (mm^2)	Pinhole Area (pixels)	Sample #	Void Area (mm^2)	Pinhole Area (pixels)	Sample #	Void Area (mm^2)	Pinhole Area (pixels)
1	0.2262	8158	44	3.5024	65065	87	0.1521	4
2	0	9744	45	0.3081	27483	88	0	2
3	1.5913	8950	46	0.7761	60936	89	0.0507	8
4	0.0098	10795	47	1.6576	32412	90	0.4544	6
5	0	14946	48	4.1849	72154	91	2.424	469
6	0	15216	49	0.0254	37226	92	1.1662	5651
7	0.1073	2415	50	0	24932	93	0.353	13585
8	13.971	11039	51	1.3183	17115	94	1.8828	4479
9	11.706	4027	52	2.2134	19787	95	0.1584	1263
10	1.4743	48460	53	0.5012	33411	96	2.5078	6451
11	1.1896	56012	54	0.5499	28965	97	0.5285	4024
12	5.665	66149	55	0.977	14279	98	1.4099	4777
13	0.8444	30660	56	3.3171	10328	99	1.0843	11524
14	0.08	37372	57	4.1986	21493	100	4.9045	8048
15	6.6479	26963	58	1.9501	17062	101	0.4797	21286
16	2.4415	68529	59	2.8998	20777	102	0.9282	5943
17	0.9438	5607	60	0.7742	18785	103	6.0726	11121
18	0.4485	14046	61	0.3842	37885	104	3.0714	9523
19	1.3709	3254	62	2.5858	42006	105	3.3971	9132
20	0.3705	5653	63	2.1763	20734	106	1.2071	16809
21	0.117	13536	64	0.5967	48404	107	7.2427	18793
22	0.5519	9953	65	2.0086	5680	108	4.7465	18634
23	0.0059	394	66	1.6985	3091	109	1.6966	17059
24	1.1779	21	67	3.0519	3645	110	4.6278	35048
25	1.7772	8338	68	0.0507	5035	111	3.6857	23396
26	1.3124	16338	69	0.6981	15088	112	0.3335	28962
27	5.3023	15523	70	0.2516	19117	113	0.1287	693
28	4.844	36515	71	0.1911	5995	114	0.0917	1521
29	0.9854	48822	72	0.351	3343	115	0.002	5025
30	4.1713	26567	73	1.0063	6849	116	0.4399	6628
31	4.0328	10893	74	12.229	6927	117	0.0722	10210
32	11.978	14554	75	1.3085	5822	118	0	8805
33	0.1385	35920	76	2.4123	5688	119	0.1287	2924
34	2.4766	31709	77	0.3432	22424	120	0.2399	1037
35	0.0078	41670	78	0.7332	12518	121	1.2968	37778
36	6.488	77847	79	11.34	1971	122	5.6241	25050
37	0.0195	41028	80	8.5375	4685	123	0.3159	4295
38	2.3245	67492	81	0.2639	571	124	9.5457	2264
39	0.0624	23090	82	0.1716	1314	125	1.9696	19190
40	4.1303	46585	83	0.3842	29	126	2.3616	24999
41	1.1174	43854	84	0	66	127	1.0901	2872
42	0.1248	45448	85	0.5631	10133	128	11.088	7656
43	0.6511	27132	86	0.0546	1716			

Table B.2: MINITAB regression output for void area

Factorial Fit: Void Area versus Tone, Stylus, ...

Estimated Effects and Coefficients for Void Area (coded units)

Term	Effect	Coef	SE Coef	T	P
Constant		2.1437	0.2229	9.62	0.000
Tone	-0.9505	-0.4753	0.2229	-2.13	0.036
Stylus	-1.4529	-0.7265	0.2229	-3.26	0.002
Line Screen	-0.0135	-0.0067	0.2229	-0.03	0.976
Roller Pressure	-1.9463	-0.9731	0.2229	-4.37	0.000
Speed	0.8861	0.4431	0.2229	1.99	0.050
Binder	0.1546	0.0773	0.2229	0.35	0.730
ITO %	0.0183	0.0092	0.2229	0.04	0.967
Solvent	0.8002	0.4001	0.2229	1.80	0.076
Tone*Stylus	0.5004	0.2502	0.2229	1.12	0.265
Tone*Line Screen	0.3615	0.1808	0.2229	0.81	0.419
Tone*Roller Pressure	0.0608	0.0304	0.2229	0.14	0.892
Tone*Speed	0.1776	0.0888	0.2229	0.40	0.691
Tone*Binder	0.3302	0.1651	0.2229	0.74	0.461
Tone*ITO %	-0.0245	-0.0122	0.2229	-0.05	0.956
Tone*Solvent	-1.0885	-0.5443	0.2229	-2.44	0.017
Stylus*Line Screen	0.8970	0.4485	0.2229	2.01	0.047
Stylus*Roller Pressure	0.2163	0.1082	0.2229	0.49	0.629
Stylus*Speed	-0.2918	-0.1459	0.2229	-0.65	0.514
Stylus*Binder	-0.0264	-0.0132	0.2229	-0.06	0.953
Stylus*ITO %	-0.2203	-0.1101	0.2229	-0.49	0.622
Stylus*Solvent	-1.0197	-0.5099	0.2229	-2.29	0.024
Line Screen*Roller Pressure	-0.2121	-0.1061	0.2229	-0.48	0.635
Line Screen*Speed	0.1309	0.0655	0.2229	0.29	0.770
Line Screen*Binder	-0.2464	-0.1232	0.2229	-0.55	0.582
Line Screen*ITO %	-0.1598	-0.0799	0.2229	-0.36	0.721
Line Screen*Solvent	-0.9178	-0.4589	0.2229	-2.06	0.042
Roller Pressure*Speed	0.4186	0.2093	0.2229	0.94	0.350
Roller Pressure*Binder	-0.5717	-0.2859	0.2229	-1.28	0.203
Roller Pressure*ITO %	0.4807	0.2403	0.2229	1.08	0.284
Roller Pressure*Solvent	-0.3366	-0.1683	0.2229	-0.76	0.452
Speed*Binder	0.4323	0.2161	0.2229	0.97	0.335
Speed*ITO %	-0.5715	-0.2858	0.2229	-1.28	0.203
Speed*Solvent	-0.6852	-0.3426	0.2229	-1.54	0.128
Binder*ITO %	0.8737	0.4369	0.2229	1.96	0.053
Binder*Solvent	0.3708	0.1854	0.2229	0.83	0.408

S = 2.52141 PRESS = 1144.63
R-Sq = 47.13% R-Sq(pred) = 0.00% R-Sq(adj) = 26.21%

Analysis of Variance for Void Area (coded units)

Source	DF	Seq SS	Adj SS	Adj MS	F	P
Main Effects	8	264.1	264.1	33.010	5.19	0.000
2-Way Interactions	28	251.6	251.6	8.984	1.41	0.113
Residual Error	91	578.5	578.5	6.358		
Total	127	1094.2				

Unusual Observations for Void Area

Obs	StdOrder	Void Area	Fit	SE Fit	Residual	St Resid
8	8	13.9705	5.7217	1.3556	8.2488	3.88R

Table B.3: MINITAB regression output for pinhole area

Factorial Fit: Pinhole Area (pixels) versus Tone, Stylus, ...

Estimated Effects and Coefficients for Pinhole Area (pixels) (coded units)

Term	Effect	Coef	SE Coef	T	P
Constant		18602	789.1	23.58	0.000
Tone	-5115	-2558	789.1	-3.24	0.002
Stylus	2622	1311	789.1	1.66	0.100
Line Screen	-3166	-1583	789.1	-2.01	0.048
Roller Pressure	-9923	-4961	789.1	-6.29	0.000
Speed	10646	5323	789.1	6.75	0.000
Binder	-11484	-5742	789.1	-7.28	0.000
ITO %	19122	9561	789.1	12.12	0.000
Solvent	-2817	-1409	789.1	-1.79	0.078
Tone*Stylus	3170	1585	789.1	2.01	0.048
Tone*Line Screen	414	207	789.1	0.26	0.794
Tone*Roller Pressure	3393	1696	789.1	2.15	0.034
Tone*Speed	-4702	-2351	789.1	-2.98	0.004
Tone*Binder	1396	698	789.1	0.88	0.379
Tone*ITO %	-5336	-2668	789.1	-3.38	0.001
Tone*Solvent	2656	1328	789.1	1.68	0.096
Stylus*Line Screen	-5624	-2812	789.1	-3.56	0.001
Stylus*Roller Pressure	1712	856	789.1	1.08	0.281
Stylus*Speed	-4959	-2479	789.1	-3.14	0.002
Stylus*Binder	-1137	-569	789.1	-0.72	0.473
Stylus*ITO %	-2159	-1080	789.1	-1.37	0.175
Stylus*Solvent	3983	1991	789.1	2.52	0.013
Line Screen*Roller Pressure	1764	882	789.1	1.12	0.267
Line Screen*Speed	29	15	789.1	0.02	0.985
Line Screen*Binder	471	236	789.1	0.30	0.766
Line Screen*ITO %	801	401	789.1	0.51	0.613
Line Screen*Solvent	1275	638	789.1	0.81	0.421
Roller Pressure*Speed	-1438	-719	789.1	-0.91	0.365
Roller Pressure*Binder	-2764	-1382	789.1	-1.75	0.083
Roller Pressure*ITO %	-3585	-1792	789.1	-2.27	0.025
Roller Pressure*Solvent	-2128	-1064	789.1	-1.35	0.181
Speed*Binder	-2160	-1080	789.1	-1.37	0.175
Speed*ITO %	5481	2741	789.1	3.47	0.001
Speed*Solvent	-7604	-3802	789.1	-4.82	0.000
Binder*ITO %	-4253	-2126	789.1	-2.69	0.008
Binder*Solvent	-1683	-842	789.1	-1.07	0.289
ITO %*Solvent	-2301	-1151	789.1	-1.46	0.148

S = 8927.28 PRESS = 14348857443
R-Sq = 82.58% R-Sq(pred) = 65.53% R-Sq(adj) = 75.68%

Analysis of Variance for Pinhole Area (pixels) (coded units)

Source	DF	Seq SS	Adj SS	Adj MS	F	P
Main Effects	8	24330463789	24330463789	3041307974	38.16	0.000
2-Way Interactions	28	10038482870	10038482870	358517245	4.50	0.000
Residual Error	91	7252373565	7252373565	79696413		
Total	127	41621320224				

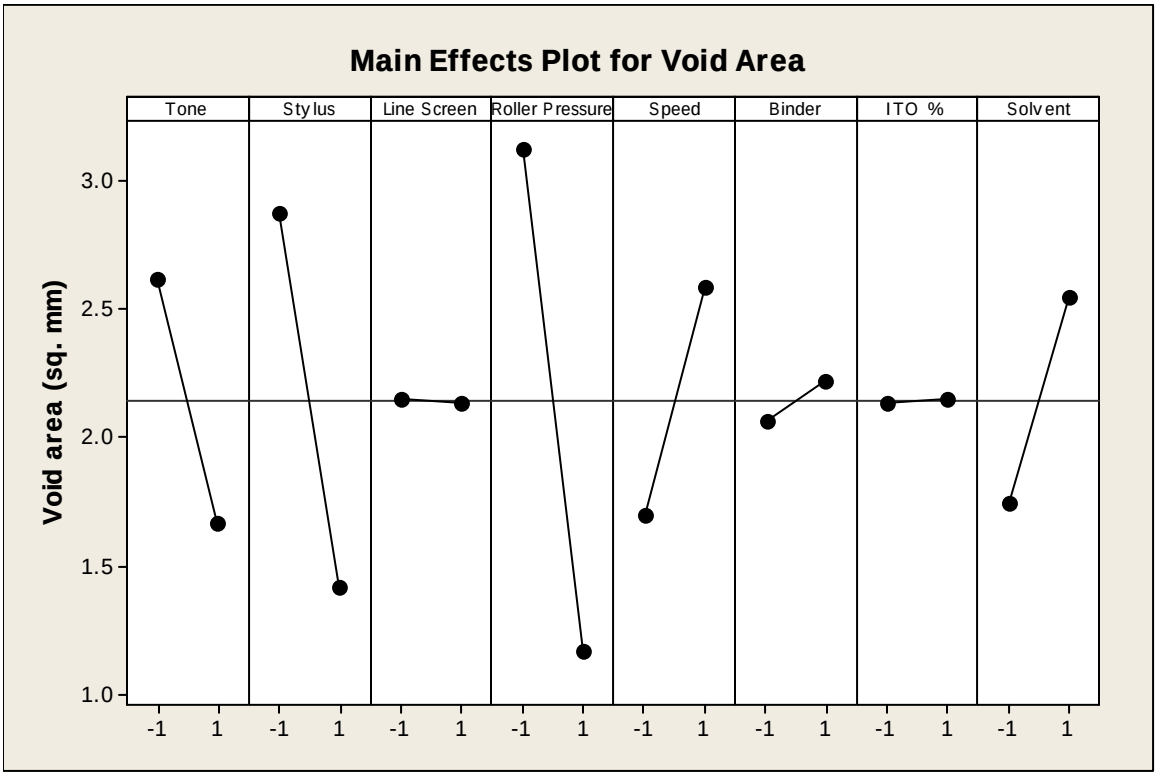

Figure B.1: Main effects plot for void area

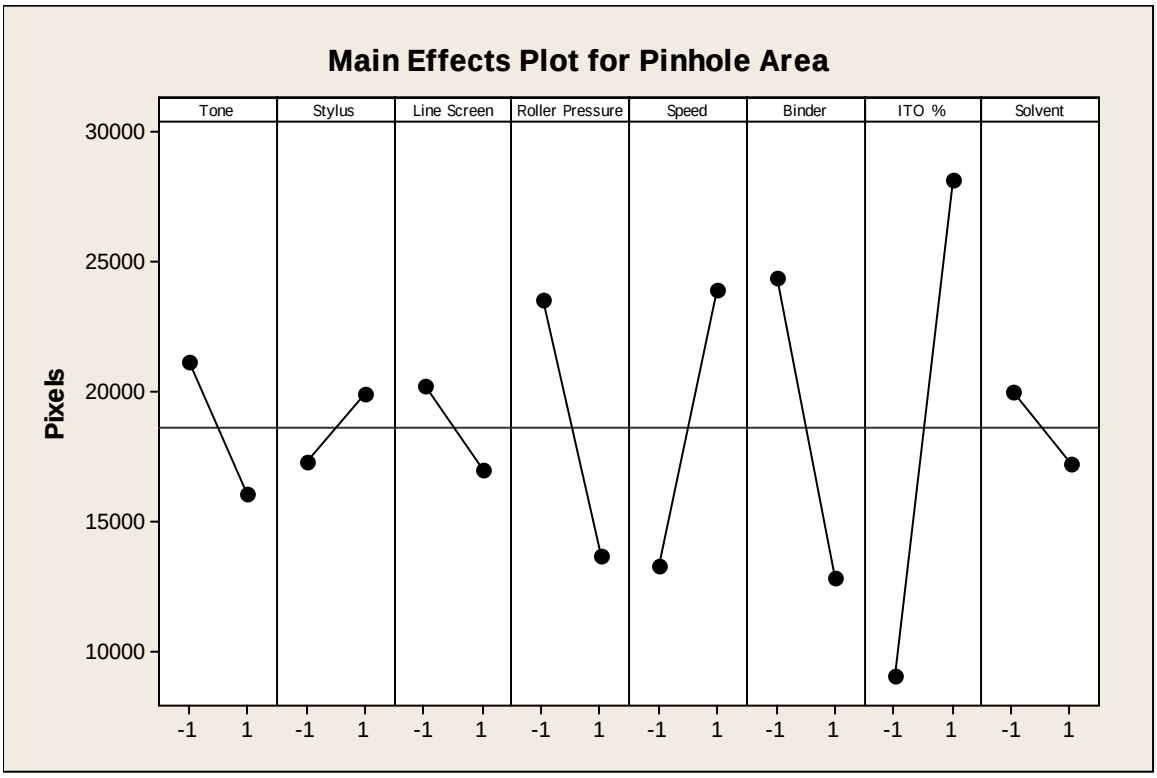

Figure B.2: Main effects plots for pinhole area

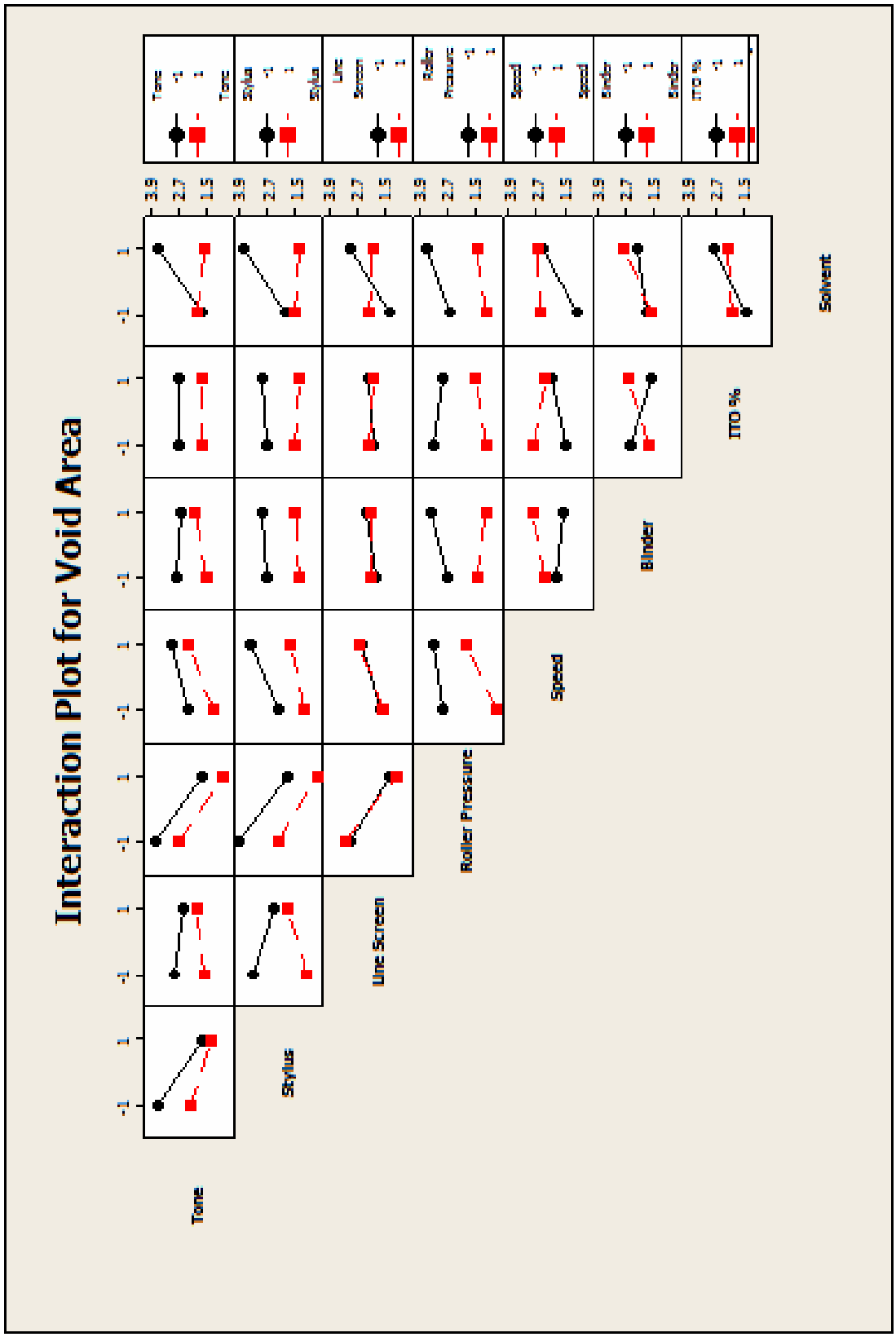

Figure B.3: Interaction Plot for Void Area

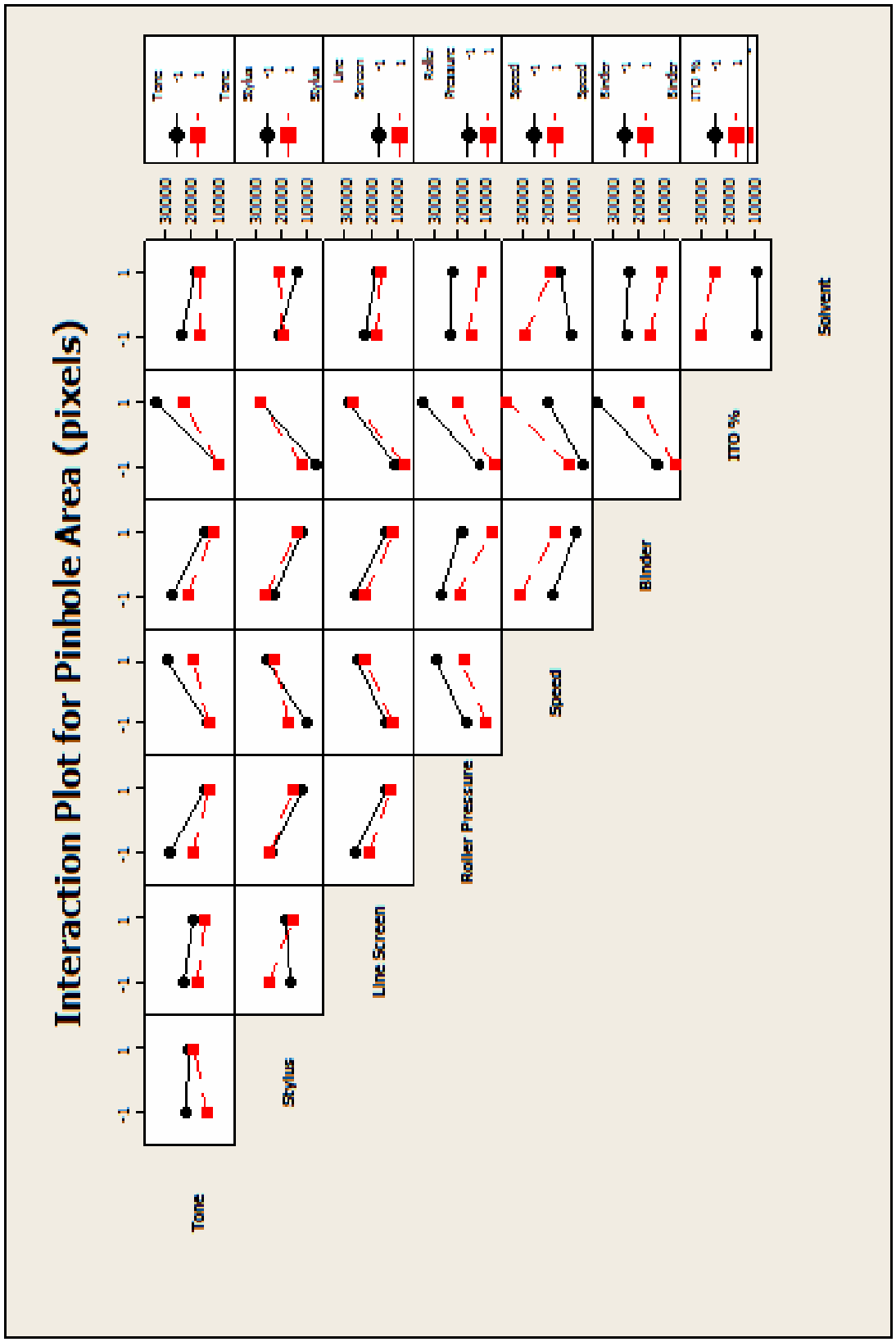

Figure B.4: Interaction Plot for Pinhole Area

B.2 Main Experiment Data and Analysis

The response data for the main experiment is given in Table B.4, including average roughness and thickness data. Table B.5 shows the subset of data taken for sheet resistance and transparency at 550 nm. The MINITAB regression output for the two responses of average thickness and roughness are shown in Tables B.6 and B.7. The main effects plots and interaction plots are shown in Figures B.5-B.8.

Table B.4: Main Experiment Data

Sample #	Ave. thick (nm)	R_a_ave (nm)
1	675	90
2	639	76
3	566	70
4	476	74
5	841	109
6	745	76
7	663	77
8	510	66
9	685	69
10	533	106
11	498	67
12	449	72
13	843	125
14	681	112
15	630	71
16	491	82
17	574	81
18	450	59
19	524	81
20	437	71
21	676	93
22	484	72
23	621	74
24	488	64
25	674	115
26	466	83
27	527	113
28	480	88
29	781	128
30	635	101
31	658	107
32	553	86
33	764	237
34	581	140
35	685	147
36	466	102
37	999	238
38	618	151
39	855	190
40	547	126
41	743	157
42	588	132
43	647	143
44	595	101
45	849	194
46	826	125
47	793	157
48	624	118
49	662	98
50	536	87
51	590	104
52	452	84
53	788	116
54	532	110
55	729	124
56	559	102
57	710	102
58	556	84
59	640	122
60	461	90
61	827	99
62	642	101
63	648	124
64	571	110
65	603	83
66	548	66
67	515	67
68	371	79
69	717	78
70	639	72
71	549	70
72	451	69
73	563	58
74	471	67
75	491	71
76	379	63
77	688	84
78	774	69
79	525	78
80	484	82
81	581	73
82	497	60
83	456	67
84	398	60
85	745	87
86	578	72
87	595	76
88	485	66
89	599	63
90	473	62
91	506	73
92	386	56
93	632	70
94	581	74
95	533	72
96	441	65
97	767	163
98	613	106
99	576	93
100	492	122
101	1264	250
102	891	216
103	939	199
104	571	162
105	623	107
106	538	111
107	492	82
108	418	77
109	809	181
110	763	153
111	678	119
112	571	105
113	533	101
114	506	80
115	553	95
116	457	83
117	783	166
118	580	104
119	714	101
120	591	102
121	731	140
122	575	128
123	712	131
124	601	109
125	924	148
126	681	123
127	660	139
128	631	105
129	692	127

Table B.4 Cont'd

Sample #	Ave. thick (nm)	R_a_ave (nm)	Sample #	Ave. thick (nm)	R_a_ave (nm)	Sample #	Ave. thick (nm)	R_a_ave (nm)
130	502	90	174	878	182	218	558	71
131	560	116	175	1052	276	219	518	76
132	450	91	176	756	129	220	405	72
133	765	194	177	548	84	221	732	93
134	588	120	178	463	109	222	636	92
135	712	139	179	630	99	223	585	80
136	559	112	180	510	78	224	496	80
137	783	181	181	793	101	225	667	103
138	643	112	182	525	72	226	588	91
139	610	136	183	682	84	227	503	86
140	538	108	184	546	68	228	391	80
141	747	148	185	641	90	229	779	103
142	620	126	186	586	78	230	581	92
143	686	135	187	491	66	231	588	89
144	520	98	188	408	63	232	483	89
145	629	80	189	606	92			
146	553	75	190	560	89			
147	491	75	191	550	82			
148	432	80	192	490	59			
149	840	80	193	697	128			
150	703	83	194	525	117			
151	586	92	195	569	113			
152	500	107	196	470	103			
153	695	94	197	791	144			
154	449	97	198	666	148			
155	532	84	199	624	148			
156	422	81	200	533	109			
157	788	98	201	758	138			
158	620	98	202	525	110			
159	596	90	203	615	122			
160	482	74	204	466	127			
161	642	93	205	794	121			
162	456	82	206	661	126			
163	454	88	207	695	148			
164	385	81	208	596	118			
165	704	101	209	758	193			
166	557	89	210	539	138			
167	538	81	211	587	153			
168	487	77	212	518	104			
169	971	151	213	969	220			
170	731	138	214	684	142			
171	780	112	215	692	176			
172	650	109	216	616	124			
173	1120	244	217	624	79			

Table B.5: Transparency and conductivity data

Sample #	Sheet Resistance (kΩ/□)	%T 550 nm	%T 1100 nm
1	5341	56.7	86.7
5	12067	56.0	86.4
14	17208	56.1	86.0
19	12321	61.5	89.1
20	45812	64.8	90.5
33	120	42.3	77.2
34	240	48.2	83.2
37	149	40.1	74.2
41	205	44.0	78.7
42	275	51.7	84.5
45	125	42.8	77.7
46	269	48.2	82.7
47	243	46.4	81.0
50	972	55.4	87.3
51	897	51.7	84.8
52	1627	55.8	87.7
60	1302	56.1	87.7
61	232	47.0	81.6
63	417	48.2	83.0
65	706	59.7	89.0
69	1489	57.3	87.9
74	7039	63.1	91.2
77	3549	58.9	88.7
78	4306	59.9	89.0
82	4233	61.2	90.3
84	6612	65.3	91.3
87	2937	60.3	89.4
89	2146	59.4	89.5
91	4925	63.9	91.0
97	56	50.0	83.6
101	79	25.1	73.3
102	107	34.7	81.4
107	509	58.6	88.4
108	830	60.0	89.2
117	126	50.1	83.8
118	225	52.4	86.1
121	104	45.7	82.4
122	206	53.0	87.6

Sample #	Sheet Resistance (kΩ/□)	%T 550 nm	%T 1100 nm
123	183	51.3	87.0
124	405	56.6	89.9
125	74	44.6	81.3
127	147	48.8	85.0
129	328	52.1	84.0
132	1200	61.4	89.4
135	442	51.8	83.6
138	547	56.0	86.6
170	85	49.9	88.0
171	96	47.8	86.8
172	181	52.9	89.8
173	99	31.4	78.9
174	167	41.8	84.8
175	165	39.7	82.7
176	152	45.9	87.0
177	631	57.7	86.5
181	3090	57.1	86.6
183	8217	61.7	89.4
184	17690	65.3	91.2
185	137	53.7	87.2
187	468	58.6	90.2
188	756	61.9	91.4
190	252	54.1	87.9
193	378	51.5	82.7
195	1038	55.5	85.6
199	740	53.5	83.7
201	389	51.8	82.8
203	1090	55.6	85.9
208	1153	56.8	85.6
209	193	47.5	78.3
211	622	54.1	83.5
212	1624	57.4	86.5
215	410	50.3	80.8
217	1253	56.0	86.4
219	6409	60.5	88.6
221	1716	54.2	85.5
225	1785	55.7	85.5

Table B.6: MINITAB output for average thickness

Response Surface Regression: Thick_ave versus Pressure, Speed, ITO%, ...

The following terms cannot be estimated, and were removed.

Line Screen*Line Screen
Stylus*Stylus
Tone*Tone

Estimated Regression Coefficients for Thick_ave

Term	Coef	SE Coef	T	P
Constant	621.971	10.623	58.547	0.000
Pressure	8.098	8.559	0.946	0.345
Speed	-34.867	8.559	-4.074	0.000
ITO%	122.124	8.559	14.268	0.000
Solvent	-21.708	8.559	-2.536	0.012
Line Screen	-54.102	3.955	-13.679	0.000
Stylus	56.181	3.955	14.204	0.000
Tone	65.816	3.955	16.640	0.000
Pressure*Pressure	-1.753	17.334	-0.101	0.920
Speed*Speed	-42.919	17.334	-2.476	0.014
ITO%*ITO%	72.252	17.334	4.168	0.000
Solvent*Solvent	-60.872	17.334	-3.512	0.001
Pressure*Speed	79.695	20.823	3.827	0.000
Pressure*ITO%	-8.340	20.823	-0.401	0.689
Pressure*Solvent	-43.101	20.823	-2.070	0.040
Pressure*Line Screen	13.171	8.522	1.545	0.124
Pressure*Stylus	3.992	8.522	0.468	0.640
Pressure*Tone	-18.010	8.522	-2.113	0.036
Speed*ITO%	-33.092	20.823	-1.589	0.114
Speed*Solvent	29.319	20.823	1.408	0.161
Speed*Line Screen	19.172	8.522	2.250	0.026
Speed*Stylus	-31.955	8.522	-3.750	0.000
Speed*Tone	5.589	8.522	0.656	0.513
ITO%*Solvent	51.926	20.823	2.494	0.013
ITO%*Line Screen	-22.679	8.522	-2.661	0.008
ITO%*Stylus	-8.761	8.522	-1.028	0.305
ITO%*Tone	28.533	8.522	3.348	0.001
Solvent*Line Screen	-6.264	8.522	-0.735	0.463
Solvent*Stylus	18.140	8.522	2.128	0.035
Solvent*Tone	-18.339	8.522	-2.152	0.033
Line Screen*Stylus	-8.258	3.945	-2.093	0.038
Line Screen*Tone	-6.663	3.945	-1.689	0.093
Stylus*Tone	8.066	3.945	2.044	0.042

S = 60.0954 PRESS = 988655
R-Sq = 83.88% R-Sq(pred) = 77.82% R-Sq(adj) = 81.29%

Analysis of Variance for Thick_ave

Source	DF	Seq SS	Adj SS	Adj MS	F	P
Regression	32	3739337	3739337	116854	32.36	0.000
Linear	7	3227962	3212068	458867	127.06	0.000
Square	4	169519	169807	42452	11.75	0.000
Interaction	21	341855	341855	16279	4.51	0.000
Residual Error	199	718679	718679	3611		
Lack-of-Fit	167	618219	618219	3702	1.18	0.298
Pure Error	32	100460	100460	3139		
Total	231	4458016				

Table B.7: MINITAB output for average roughness

Response Surface Regression: Ra_ave versus Pressure, Speed, ITO%, Solvent,

The following terms cannot be estimated, and were removed.

Line Screen*Line Screen
Stylus*Stylus
Tone*Tone

The analysis was done using coded units.

Estimated Regression Coefficients for Ra_ave

Term	Coef	SE Coef	T	P
Constant	122.276	3.907	31.295	0.000
Pressure	-0.422	3.148	-0.134	0.893
Speed	-11.617	3.148	-3.690	0.000
ITO%	46.678	3.148	14.828	0.000
Solvent	-7.287	3.148	-2.315	0.022
Line Screen	-8.138	1.455	-5.595	0.000
Stylus	6.961	1.455	4.786	0.000
Tone	9.738	1.455	6.695	0.000
Pressure*Pressure	3.242	6.375	0.509	0.612
Speed*Speed	-37.143	6.375	-5.826	0.000
ITO%*ITO%	3.284	6.375	0.515	0.607
Solvent*Solvent	-41.560	6.375	-6.519	0.000
Pressure*Speed	29.684	7.659	3.876	0.000
Pressure*ITO%	-19.129	7.659	-2.498	0.013
Pressure*Solvent	-9.181	7.659	-1.199	0.232
Pressure*Line Screen	5.602	3.134	1.787	0.075
Pressure*Stylus	-1.113	3.134	-0.355	0.723
Pressure*Tone	-2.475	3.134	-0.789	0.431
Speed*ITO%	-36.931	7.659	-4.822	0.000
Speed*Solvent	9.371	7.659	1.224	0.223
Speed*Line Screen	5.644	3.134	1.801	0.073
Speed*Stylus	-4.856	3.134	-1.549	0.123
Speed*Tone	-0.134	3.134	-0.043	0.966
ITO%*Solvent	16.184	7.659	2.113	0.036
ITO%*Line Screen	-13.617	3.134	-4.344	0.000
ITO%*Stylus	5.585	3.134	1.782	0.076
ITO%*Tone	11.043	3.134	3.523	0.001
Solvent*Line Screen	-5.603	3.134	-1.788	0.075
Solvent*Stylus	1.189	3.134	0.379	0.705
Solvent*Tone	-3.402	3.134	-1.085	0.279
Line Screen*Stylus	-1.193	1.451	-0.822	0.412
Line Screen*Tone	-2.124	1.451	-1.464	0.145
Stylus*Tone	1.040	1.451	0.716	0.475

S = 22.1022 PRESS = 128353
R-Sq = 72.10% R-Sq(pred) = 63.16% R-Sq(adj) = 67.61%

Analysis of Variance for Ra_ave

Source	DF	Seq SS	Adj SS	Adj MS	F	P
Regression	32	251202	251202	7850.1	16.07	0.000
Linear	7	163826	163047	23292.5	47.68	0.000
Square	4	38273	38176	9544.0	19.54	0.000
Interaction	21	49104	49104	2338.3	4.79	0.000
Residual Error	199	97213	97213	488.5		
Lack-of-Fit	167	65948	65948	394.9	0.40	1.000
Pure Error	32	31265	31265	977.0		
Total	231	348415				

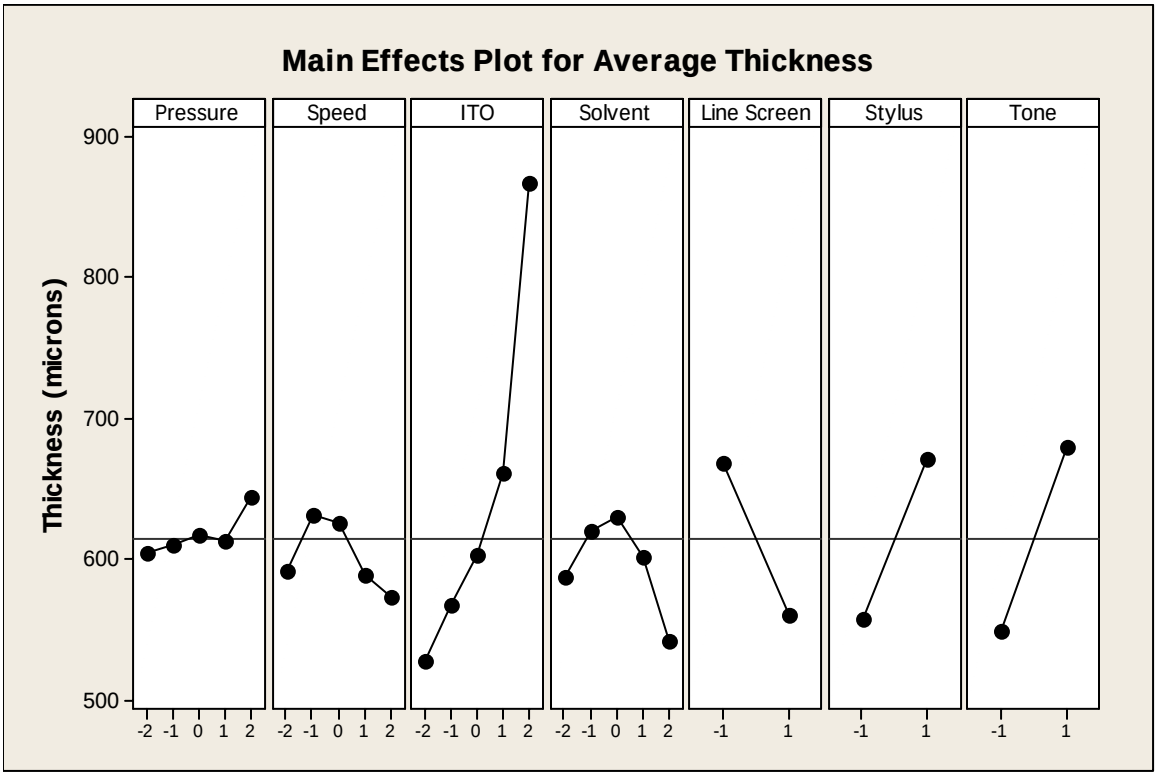

Figure B.5: Main effects plot for average thickness

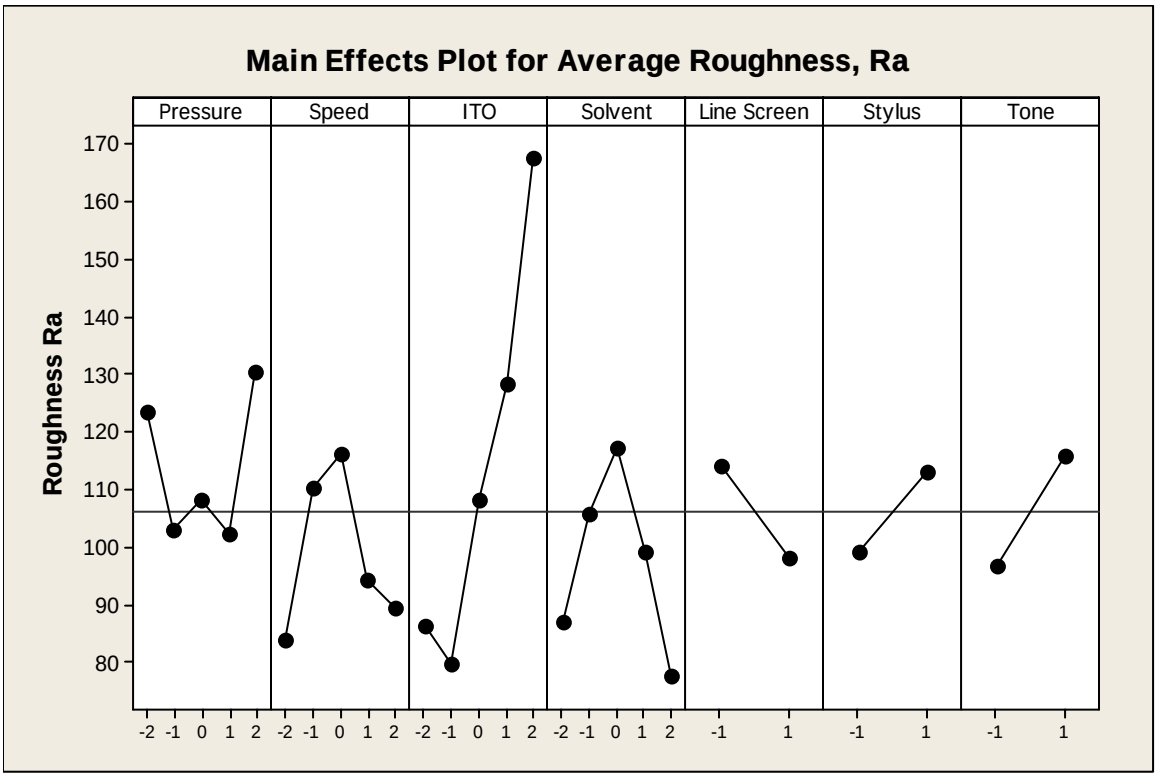

Figure B.6: Main effects plot for average roughness

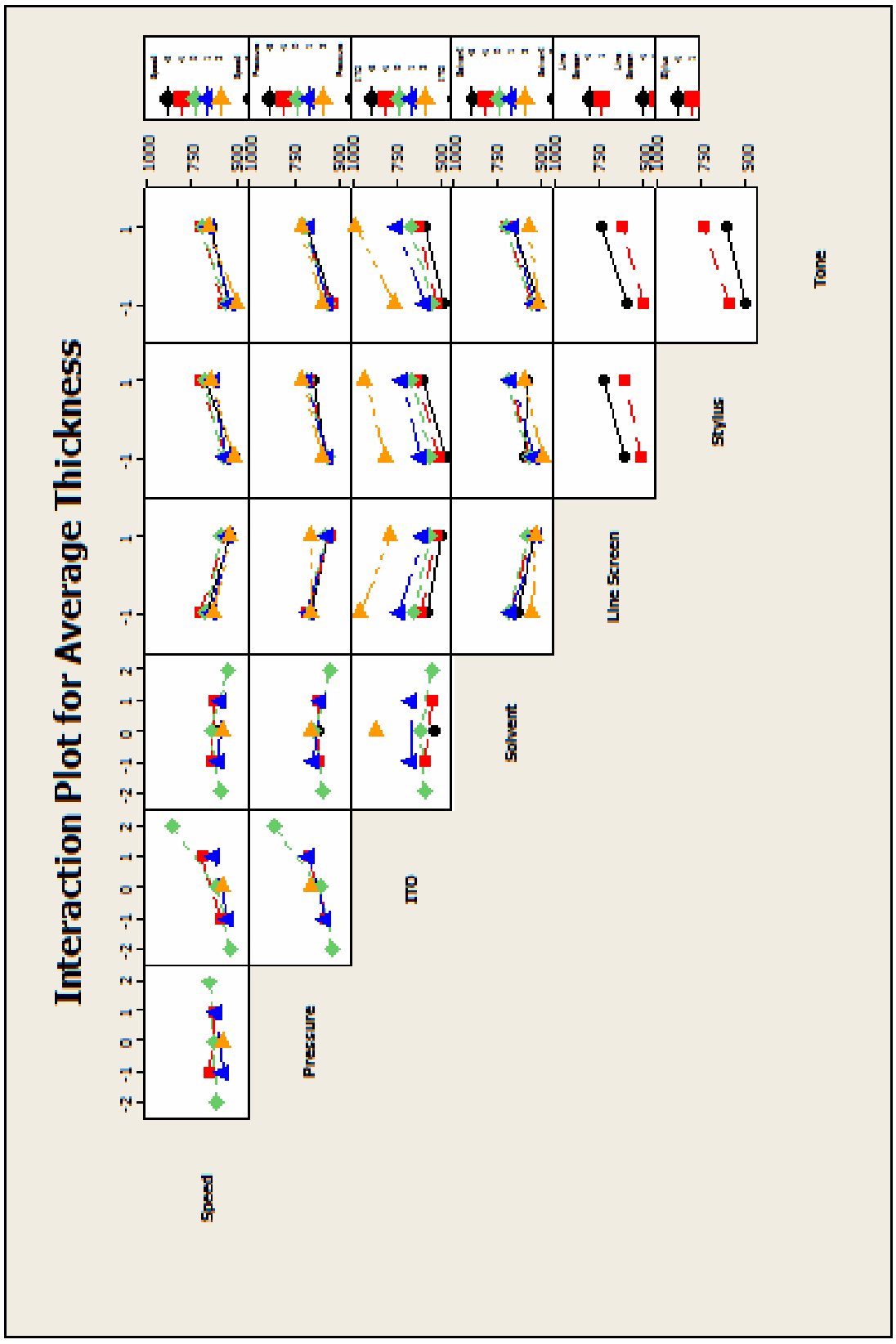

Figure B.7: Interaction plot for average thickness

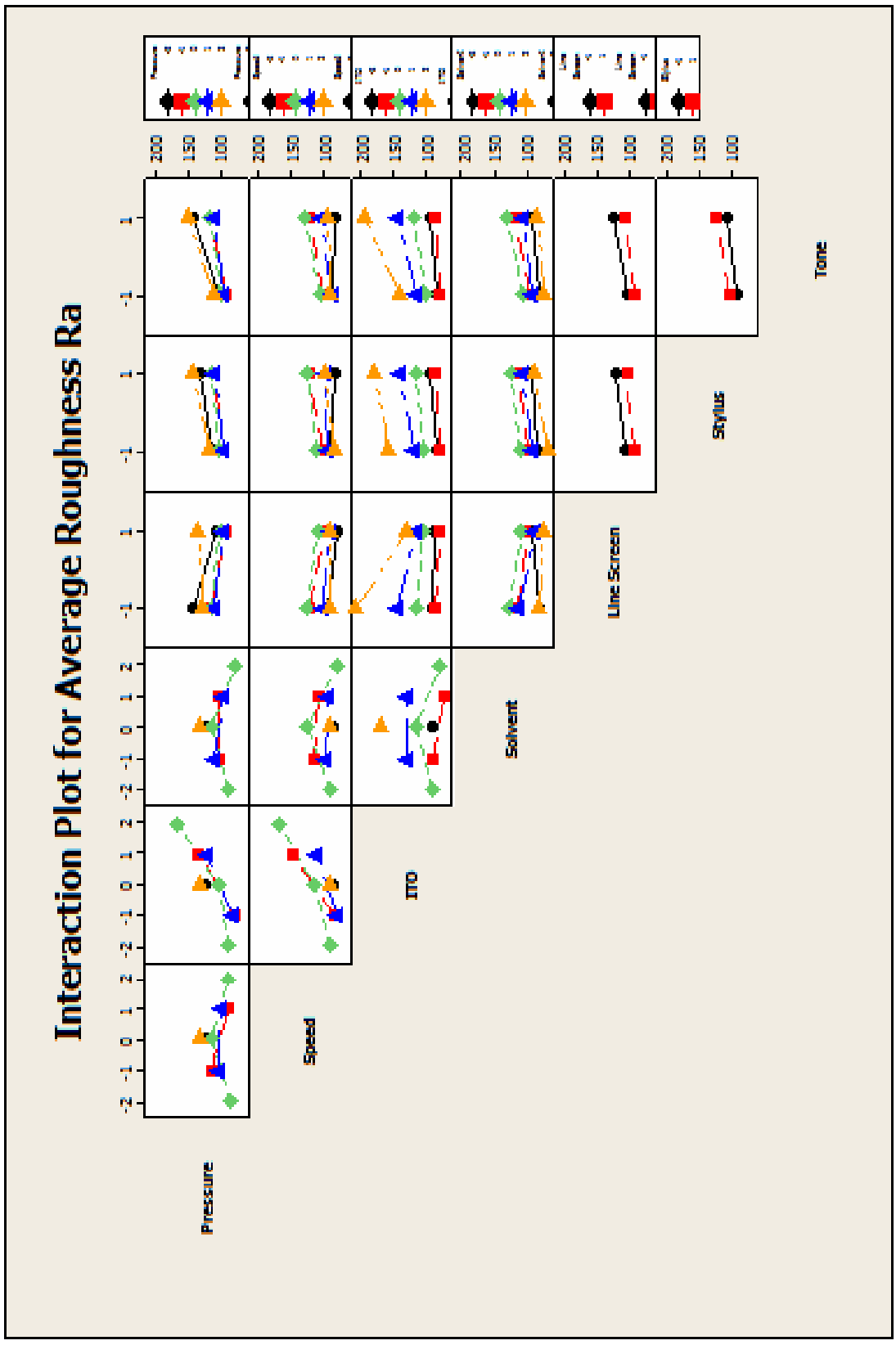

Figure B.8: Interaction plot for average roughness, R_a

APPENDIX C

FUNDAMENTAL PARAMETER ANALYSIS

This section contains MINITAB results from the best subsets regression routines and regression of chosen fundamental parameter models. Models were chosen for the responses of average thickness, roughness R_a, the square root of sheet resistance, and the percent transparency at 550 nm. The final models were chosen based on their R^2 and C_p values. For those cases in which the addition of variables resulted in only a very small improvement in R^2 or C_p, a simpler model using fewer variables was chosen, based on R^2 values. This eliminated any unnecessarily complex models that offered hardly any improvement over a simpler model with a similar R^2 value. Tables C.1-C.4 contain the best subsets output with the chosen models highlighted in red. Tables C.5-C.8 contain regression analysis data for the chosen models. Tables C.9-C.12 show the data used for the fundamental parameter analysis. Main effects plots for the models can be found in Chapter 5.

Table C.1: MINITAB best subsets regression results for average thickness

Best Subsets Regression: Thick_ave versus Pressure, Speed, ...

Response is Thick_ave

Vars	R-Sq	R-Sq(adj)	Mallows Cp	S	Pressure	Speed	Dynamic Viscosity	Surface Tension	Cell Density	Cell Velocity	Aspect Ratio	Cell Surface Area	Cell Diameter	ITO/Bin Width	Solid/Solvent
1	46.3	46.0	260.4	102.04						X					
1	23.5	23.1	468.0	121.81							X				
2	63.4	63.1	106.6	84.394						X					X
2	62.5	62.1	115.3	85.480					X	X					
3	70.2	69.8	46.6	76.283						X		X			X
3	69.3	68.9	55.2	77.488					X	X		X			
4	71.7	71.2	35.6	74.599		X				X		X			X
4	70.8	70.3	43.8	75.766						X	X	X			X
5	72.4	71.8	31.0	73.800		X				X		X	X		X
5	72.2	71.6	32.8	74.060		X				X	X	X			X
6	72.9	72.2	28.2	73.249		X				X	X	X	X		X
6	72.8	72.1	28.9	73.356			X		X	X		X		X	X
7	**74.1**	**73.3**	**19.0**	**71.726**		**X**	**X**		**X**	**X**		**X**		**X**	**X**
7	73.4	72.5	26.1	72.798			X		X	X	X	X		X	X
8	74.7	73.8	15.7	71.064		X	X		X	X		X	X	X	X
8	74.7	73.8	16.2	71.145		X	X		X	X	X	X		X	X
9	75.3	74.3	12.9	70.472		X	X		X	X	X	X	X	X	X
9	75.0	74.0	15.2	70.833		X	X	X	X	X		X	X	X	X
10	75.5	74.4	12.3	70.235		X	X	X	X	X	X	X	X	X	X
10	75.5	74.4	12.4	70.243	X	X	X		X	X	X	X	X	X	X
11	75.8	74.6	12.0	70.023	X	X	X	X	X	X	X	X	X	X	X

Table C.2: MINITAB best subsets regression results for average roughness

Best Subsets Regression: Ra_ave versus Pressure, Speed, ...

Response is Ra_ave

Vars	R-Sq	R-Sq(adj)	Mallows Cp	S	Pressure	Speed	Dynamic Viscosity	Surface Tension	Thickness_Ave	Cell Density	Cell Velocity	Aspect Ratio	Cell Surface Area	Cell Diameter	ITO/Bilayer Thickness	Solid/Solvent
1	54.1	53.9	121.0	26.364					X							
1	35.6	35.3	261.9	31.235						X						
2	64.9	64.6	40.9	23.108					X	X						
2	62.1	61.8	62.4	24.018					X							X
3	65.8	65.4	36.0	22.856					X	X	X					
3	65.5	65.0	38.7	22.973					X	X		X				
4	68.6	68.1	16.5	21.936		X			X	X				X		
4	66.4	65.8	33.3	22.698					X	X	X					X
5	69.6	69.0	10.9	21.632		X			X	X				X		X
5	69.0	68.3	15.6	21.852		X			X	X	X			X		
6	**70.2**	**69.4**	**8.9**	**21.491**		**X**			**X**	**X**	**X**			**X**		**X**
6	70.0	69.2	10.0	21.545		X			X	X		X		X		X
7	70.4	69.4	9.5	21.474		X			X	X		X	X	X		X
7	70.3	69.4	9.7	21.483	X	X			X	X	X			X		X
8	70.6	69.5	10.0	21.449		X	X	X	X	X	X			X		X
8	70.6	69.5	10.0	21.450		X	X	X	X		X			X	X	X
9	70.8	69.6	10.2	21.412		X	X	X	X			X	X	X	X	X
9	70.8	69.6	10.4	21.421		X	X	X	X	X	X			X	X	X
10	71.0	69.7	10.8	21.393		X	X	X	X	X		X	X	X	X	X
10	70.9	69.6	11.1	21.407	X	X	X	X	X	X	X			X	X	X
11	71.1	69.7	11.6	21.382	X	X	X	X	X	X		X	X	X	X	X
11	71.1	69.6	12.2	21.410		X	X	X	X	X	X	X	X	X	X	X
12	71.2	69.6	13.0	21.403	X	X	X	X	X	X	X	X	X	X	X	X

Table C.3: MINITAB best subsets regression results for (sheet resistance)$^{1/2}$

Best Subsets Regression: sqrt_SR versus Pressure, Speed, ...

Response is sqrt_SR

Vars	R-Sq	R-Sq(adj)	Mallows Cp	S	Pressure	Speed	Thick_ave	RA_ave	Dynamic Vis	Surface Tension	Cell Density	Cell Viol	Aspect Ratio	Cell asurface	Dwell Time	ITO/Bind	Sol id/Sol vent
1	43.4	42.6	93.3	27.206											X		
1	35.6	34.7	115.9	29.019							X						
2	49.5	48.1	77.7	25.889						X						X	
2	49.0	47.6	79.1	26.010										X		X	
3	55.8	54.0	61.3	24.374					X							X	X
3	54.7	52.7	64.6	24.693						X			X			X	
4	64.1	62.0	39.3	22.137					X		X					X	X
4	61.0	58.8	48.2	23.058					X				X			X	X
5	69.1	66.8	26.9	20.695			X		X		X					X	X
5	68.9	66.7	27.3	20.741					X		X			X		X	X
6	73.4	71.1	16.2	19.323					X		X		X	X		X	X
6	71.0	68.5	23.2	20.175		X			X		X			X		X	X
7	**76.3**	**73.8**	**9.9**	**18.384**					**X**		**X**	**X**	**X**	**X**		**X**	**X**
7	74.0	71.3	16.5	19.247		X			X		X		X	X		X	X
8	76.8	74.0	10.4	18.320		X			X		X	X	X	X		X	X
8	76.7	73.8	10.8	18.376					X	X	X	X	X	X		X	X
9	77.6	74.4	10.2	18.159		X			X		X	X	X	X	X	X	X
9	77.1	73.9	11.5	18.337		X			X	X	X	X	X	X		X	X
10	78.1	74.7	10.6	18.072	X	X			X		X	X	X	X	X	X	X
10	77.6	74.1	12.1	18.282		X	X		X		X	X	X	X	X	X	X
11	79.0	75.3	10.0	17.846	X	X			X	X	X	X	X	X	X	X	X
11	78.1	74.3	12.5	18.206	X	X		X	X		X	X	X	X	X	X	X
12	79.0	74.9	12.0	17.987	X	X	X		X	X	X	X	X	X	X	X	X
12	79.0	74.9	12.0	17.988	X	X		X	X	X	X	X	X	X	X	X	X
13	79.0	74.5	14.0	18.134	X	X	X	X	X	X	X	X	X	X	X	X	X

Table C.4: MINITAB best subsets regression results for average thickness

Best Subsets Regression: %T 550 nm versus Pressure, Speed, ...

Response is %T 550 nm

Vars	R-Sq	R-Sq(adj)	Mallows Cp	S	Pressure	Speed	Thick_Rate	Thick_Avg	Dynamic Viscosity	Surfactant Concentration	Dendrimer Volume	Cell Temperature	Aspect Ratio	Cell Surface Area	Dwell Time	IT0/Bind Time	Sol Vol/Sol Vol
1	79.5	79.3	109.0	3.5166				X									
1	71.4	71.0	181.0	4.1605			X										
2	84.9	84.4	64.3	3.0475			X	X									
2	84.6	84.1	67.0	3.0773			X				X						
3	89.3	88.9	27.1	2.5780			X	X								X	
3	89.0	88.5	29.7	2.6140			X	X			X						
4	90.3	89.8	20.1	2.4688			X	X	X							X	
4	89.9	89.3	23.9	2.5232			X	X			X					X	
5	91.2	90.6	14.3	2.3704			X	X	X		X					X	
5	91.1	90.5	15.2	2.3836			X	X	X				X			X	
6	91.7	91.0	12.2	2.3232			X	X	X		X		X			X	
6	91.5	90.8	13.6	2.3450			X	X	X		X					X	X
7	**92.3**	**91.5**	**9.1**	**2.2582**			**X**	**X**	**X**	**X**	**X**					**X**	**X**
7	92.0	91.1	11.7	2.2998			X	X	X		X		X			X	X
8	92.5	91.6	8.9	2.2375			X	X	X	X	X		X			X	X
8	92.5	91.5	9.4	2.2456	X		X	X	X	X	X					X	X
9	92.8	91.7	8.8	2.2188			X	X	X	X	X	X	X			X	X
9	92.7	91.7	9.2	2.2263	X		X	X	X	X	X		X			X	X
10	93.0	91.9	9.0	2.2034	X		X	X	X	X	X	X	X			X	X
10	92.8	91.7	10.3	2.2279			X	X	X	X	X	X	X		X	X	X
11	93.0	91.8	10.6	2.2148	X		X	X	X	X	X	X	X	X		X	X
11	93.0	91.8	10.8	2.2183	X	X	X	X	X	X	X	X	X			X	X
12	93.0	91.7	12.3	2.2269	X	X	X	X	X		X	X	X	X	X	X	X
12	93.0	91.7	12.4	2.2287	X	X	X	X	X	X	X	X	X		X	X	X
13	93.1	91.6	14.0	2.2394	X	X	X	X	X	X	X	X	X	X	X	X	X

Table C.5: MINITAB regression results for % transparency at 550 nm

Regression Analysis: Thick_ave versus Speed, Dynamic Viscosity, ...

```
The regression equation is
Thick_ave = - 1936 - 17.1 Speed - 1250 Dynamic Viscosity + 1741 Density
            + 0.0109 Cell Volume + 5.60 Cell surface area - 131 ITO/Binder
            + 589 Solid/Solvent


Predictor               Coef    SE Coef      T      P
Constant             -1935.7      373.6  -5.18  0.000
Speed                -17.126      5.085  -3.37  0.001
Dynamic Viscosity    -1250.4      284.9  -4.39  0.000
Density               1741.3      406.3   4.29  0.000
Cell Volume        0.0109435  0.0006586  16.62  0.000
Cell surface area     5.5982     0.7280   7.69  0.000
ITO/Binder           -130.94      32.45  -4.03  0.000
Solid/Solvent          588.9      130.6   4.51  0.000

S = 71.7263   R-Sq = 74.1%   R-Sq(adj) = 73.3%

Analysis of Variance

Source           DF       SS      MS      F      P
Regression        7  3305612  472230  91.79  0.000
Residual Error  224  1152404    5145
Total           231  4458016
```

Table C.6: MINITAB regression results for average roughness model

Regression Analysis: Ra_ave versus Speed, Thick_ave, ...

```
The regression equation is
Ra_ave = - 275 - 16.5 Speed + 0.185 Thick_ave + 299 Density
         - 0.000574 Cell Volume - 491 Dwell - 105 Solid/Solvent


Predictor            Coef    SE Coef      T      P
Constant          -274.67      41.09  -6.68  0.000
Speed             -16.484      3.203  -5.15  0.000
Thick_ave         0.18490    0.01742  10.61  0.000
Density            299.34      51.08   5.86  0.000
Cell Volume    -0.0005740  0.0002877  -1.99  0.047
Dwell             -491.46      95.63  -5.14  0.000
Solid/Solvent     -105.03      35.71  -2.94  0.004

S = 21.4908   R-Sq = 70.2%   R-Sq(adj) = 69.4%


Analysis of Variance

Source           DF      SS     MS      F      P
Regression        6  244498  40750  88.23  0.000
Residual Error  225  103918    462
Total           231  348415
```

Table C.7: MINITAB regression results for (sheet resistance)$^{1/2}$

Regression Analysis: sqrt_SR versus Dynamic Viscosity, Density, ...

The regression equation is
sqrt_SR = - 628 - 918 Dynamic Viscosity + 925 Density + 0.00161 Cell Volume
+ 144 Aspect Ratio - 2.00 Cell surface area - 125 ITO/Binder
+ 286 Solid/Solvent

Predictor	Coef	SE Coef	T	P
Constant	-628.1	171.4	-3.66	0.000
Dynamic Viscosity	-917.8	137.7	-6.67	0.000
Density	924.5	193.6	4.78	0.000
Cell Volume	0.0016142	0.0005661	2.85	0.006
Aspect Ratio	144.26	33.83	4.26	0.000
Cell surface area	-2.0026	0.4233	-4.73	0.000
ITO/Binder	-124.80	16.32	-7.65	0.000
Solid/Solvent	285.93	56.89	5.03	0.000

S = 18.3836 R-Sq = 76.3% R-Sq(adj) = 73.8%

Analysis of Variance

Source	DF	SS	MS	F	P
Regression	7	72848	10407	30.79	0.000
Residual Error	67	22643	338		
Total	74	95491			

Source	DF	Seq SS
Dynamic Viscosity	1	0
Density	1	39556
Cell Volume	1	1632
Aspect Ratio	1	1864
Cell surface area	1	9029
ITO/Binder	1	12229
Solid/Solvent	1	8538

Unusual Observations

Obs	Dynamic Viscosity	sqrt_SR	Fit	SE Fit	Residual	St Resid
5	0.235	214.04	124.46	7.04	89.58	5.28R
54	0.300	25.11	62.78	6.85	-37.66	-2.21R
73	0.290	80.06	38.29	4.83	41.77	2.35R
75	0.235	42.24	86.21	6.86	-43.97	-2.58R

R denotes an observation with a large standardized residual.

Table C.8: MINITAB regression results for transparency at 550 nm

Regression Analysis: %T 550 nm versus Thick_ave, Ra_ave, ...

The regression equation is
%T 550 nm = 7.4 - 0.0221 Thick_ave - 0.0562 Ra_ave - 82.1 Dynamic Viscosity
+ 0.273 Surface Tension + 77.3 Density - 9.76 ITO/Binder
+ 21.5 Solid/Solvent

Predictor	Coef	SE Coef	T	P
Constant	7.35	22.08	0.33	0.740
Thick_ave	-0.022135	0.002842	-7.79	0.000
Ra_ave	-0.05621	0.01059	-5.31	0.000
Dynamic Viscosity	-82.15	18.71	-4.39	0.000
Surface Tension	0.2726	0.1083	2.52	0.014
Density	77.33	24.24	3.19	0.002
ITO/Binder	-9.764	2.109	-4.63	0.000
Solid/Solvent	21.485	8.183	2.63	0.011

S = 2.25818 R-Sq = 92.3% R-Sq(adj) = 91.5%

Analysis of Variance

Source	DF	SS	MS	F	P
Regression	7	4072.32	581.76	114.08	0.000
Residual Error	67	341.66	5.10		
Total	74	4413.98			

Source	DF	Seq SS
Thick_ave	1	3150.36
Ra_ave	1	594.95
Dynamic Viscosity	1	0.10
Surface Tension	1	80.10
Density	1	137.33
ITO/Binder	1	74.32
Solid/Solvent	1	35.16

Unusual Observations

Obs	Thick_ave	%T 550 nm	Fit	SE Fit	Residual	St Resid
31	1264	25.086	30.114	1.128	-5.028	-2.57R
32	891	34.739	40.278	0.756	-5.539	-2.60R
35	783	50.089	45.475	0.593	4.613	2.12R
52	1052	39.690	34.011	1.128	5.679	2.90R

R denotes an observation with a large standardized residual.

Table C.9: Fundamental parameters for thickness and roughness, part 1

	Process Parameters		Material Properties			Responses	
Sample	Linear Pressure (lb/in.)	Speed (m/min)	Dynamic Viscosity (mPa-s)	Surface Tension dynes/cm	Density (g/cm^3)	Thick_ave (nm)	Ra_ave (nm)
1	35	10	0.24	23.55	1.25	675	90
2	35	10	0.24	23.55	1.25	639	76
3	35	10	0.24	23.55	1.25	566	70
4	35	10	0.24	23.55	1.25	476	74
5	35	10	0.24	23.55	1.25	841	109
6	35	10	0.24	23.55	1.25	745	76
7	35	10	0.24	23.55	1.25	663	77
8	35	10	0.24	23.55	1.25	510	66
9	45	10	0.24	23.55	1.25	685	69
10	45	10	0.24	23.55	1.25	533	106
11	45	10	0.24	23.55	1.25	498	67
12	45	10	0.24	23.55	1.25	449	72
13	45	10	0.24	23.55	1.25	843	125
14	45	10	0.24	23.55	1.25	681	112
15	45	10	0.24	23.55	1.25	630	71
16	45	10	0.24	23.55	1.25	491	82
17	35	20	0.24	23.55	1.25	574	81
18	35	20	0.24	23.55	1.25	450	59
19	35	20	0.24	23.55	1.25	524	81
20	35	20	0.24	23.55	1.25	437	71
21	35	20	0.24	23.55	1.25	676	93
22	35	20	0.24	23.55	1.25	484	72
23	35	20	0.24	23.55	1.25	621	74
24	35	20	0.24	23.55	1.25	488	64
25	45	20	0.24	23.55	1.25	674	115
26	45	20	0.24	23.55	1.25	466	83
27	45	20	0.24	23.55	1.25	527	113
28	45	20	0.24	23.55	1.25	480	88
29	45	20	0.24	23.55	1.25	781	128
30	45	20	0.24	23.55	1.25	635	101
31	45	20	0.24	23.55	1.25	658	107
32	45	20	0.24	23.55	1.25	553	86
33	35	10	0.34	23.76	1.41	764	237
34	35	10	0.34	23.76	1.41	581	140
35	35	10	0.34	23.76	1.41	685	147
36	35	10	0.34	23.76	1.41	466	102
37	35	10	0.34	23.76	1.41	999	238
38	35	10	0.34	23.76	1.41	618	151
39	35	10	0.34	23.76	1.41	855	190
40	35	10	0.34	23.76	1.41	547	126
41	45	10	0.34	23.76	1.41	743	157
42	45	10	0.34	23.76	1.41	588	132

	Process Parameters		Material Properties			Responses	
Sample	Linear Pressure (lb/in.)	Speed (m/min)	Dynamic Viscosity (mPa-s)	Surface Tension dynes/cm	Density (g/cm^3)	Thick_ave (nm)	Ra_ave (nm)
43	45	10	0.34	23.76	1.41	647	143
44	45	10	0.34	23.76	1.41	595	101
45	45	10	0.34	23.76	1.41	849	194
46	45	10	0.34	23.76	1.41	826	125
47	45	10	0.34	23.76	1.41	793	157
48	45	10	0.34	23.76	1.41	624	118
49	35	20	0.34	23.76	1.41	662	98
50	35	20	0.34	23.76	1.41	536	87
51	35	20	0.34	23.76	1.41	590	104
52	35	20	0.34	23.76	1.41	452	84
53	35	20	0.34	23.76	1.41	788	116
54	35	20	0.34	23.76	1.41	532	110
55	35	20	0.34	23.76	1.41	729	124
56	35	20	0.34	23.76	1.41	559	102
57	45	20	0.34	23.76	1.41	710	102
58	45	20	0.34	23.76	1.41	556	84
59	45	20	0.34	23.76	1.41	640	122
60	45	20	0.34	23.76	1.41	461	90
61	45	20	0.34	23.76	1.41	827	99
62	45	20	0.34	23.76	1.41	642	101
63	45	20	0.34	23.76	1.41	648	124
64	45	20	0.34	23.76	1.41	571	110
65	35	10	0.12	23.67	1.19	603	83
66	35	10	0.12	23.67	1.19	548	66
67	35	10	0.12	23.67	1.19	515	67
68	35	10	0.12	23.67	1.19	371	79
69	35	10	0.12	23.67	1.19	717	78
70	35	10	0.12	23.67	1.19	639	72
71	35	10	0.12	23.67	1.19	549	70
72	35	10	0.12	23.67	1.19	451	69
73	45	10	0.12	23.67	1.19	563	58
74	45	10	0.12	23.67	1.19	471	67
75	45	10	0.12	23.67	1.19	491	71
76	45	10	0.12	23.67	1.19	379	63
77	45	10	0.12	23.67	1.19	688	84
78	45	10	0.12	23.67	1.19	774	69
79	45	10	0.12	23.67	1.19	525	78
80	45	10	0.12	23.67	1.19	484	82
81	35	20	0.12	23.67	1.19	581	73
82	35	20	0.12	23.67	1.19	497	60
83	35	20	0.12	23.67	1.19	456	67
84	35	20	0.12	23.67	1.19	398	60
85	35	20	0.12	23.67	1.19	745	87

	Process Parameters		Material Properties			Responses	
Sample	Linear Pressure (lb/in.)	Speed (m/min)	Dynamic Viscosity (mPa-s)	Surface Tension dynes/cm	Density (g/cm^3)	Thick_ave (nm)	Ra_ave (nm)
86	35	20	0.12	23.67	1.19	578	72
87	35	20	0.12	23.67	1.19	595	76
88	35	20	0.12	23.67	1.19	485	66
89	45	20	0.12	23.67	1.19	599	63
90	45	20	0.12	23.67	1.19	473	62
91	45	20	0.12	23.67	1.19	506	73
92	45	20	0.12	23.67	1.19	386	56
93	45	20	0.12	23.67	1.19	632	70
94	45	20	0.12	23.67	1.19	581	74
95	45	20	0.12	23.67	1.19	533	72
96	45	20	0.12	23.67	1.19	441	65
97	35	10	0.14	18.28	1.40	767	163
98	35	10	0.14	18.28	1.40	613	106
99	35	10	0.14	18.28	1.40	576	93
100	35	10	0.14	18.28	1.40	492	122
101	35	10	0.14	18.28	1.40	1264	250
102	35	10	0.14	18.28	1.40	891	216
103	35	10	0.14	18.28	1.40	939	199
104	35	10	0.14	18.28	1.40	571	162
105	45	10	0.14	18.28	1.40	623	107
106	45	10	0.14	18.28	1.40	538	111
107	45	10	0.14	18.28	1.40	492	82
108	45	10	0.14	18.28	1.40	418	77
109	45	10	0.14	18.28	1.40	809	181
110	45	10	0.14	18.28	1.40	763	153
111	45	10	0.14	18.28	1.40	678	119
112	45	10	0.14	18.28	1.40	571	105
113	35	20	0.14	18.28	1.40	533	101
114	35	20	0.14	18.28	1.40	506	80
115	35	20	0.14	18.28	1.40	553	95
116	35	20	0.14	18.28	1.40	457	83
117	35	20	0.14	18.28	1.40	783	166
118	35	20	0.14	18.28	1.40	580	104
119	35	20	0.14	18.28	1.40	714	101
120	35	20	0.14	18.28	1.40	591	102
121	45	20	0.14	18.28	1.40	731	140
122	45	20	0.14	18.28	1.40	575	128
123	45	20	0.14	18.28	1.40	712	131
124	45	20	0.14	18.28	1.40	601	109
125	45	20	0.14	18.28	1.40	924	148
126	45	20	0.14	18.28	1.40	681	123
127	45	20	0.14	18.28	1.40	660	139
128	45	20	0.14	18.28	1.40	631	105

	Process Parameters		Material Properties			Responses	
Sample	Linear Pressure (lb/in.)	Speed (m/min)	Dynamic Viscosity (mPa-s)	Surface Tension dynes/cm	Density (g/cm^3)	Thick_ave (nm)	Ra_ave (nm)
129	30	15	0.29	29.04	1.36	692	127
130	30	15	0.29	29.04	1.36	502	90
131	30	15	0.29	29.04	1.36	560	116
132	30	15	0.29	29.04	1.36	450	91
133	30	15	0.29	29.04	1.36	765	194
134	30	15	0.29	29.04	1.36	588	120
135	30	15	0.29	29.04	1.36	712	139
136	30	15	0.29	29.04	1.36	559	112
137	50	15	0.29	29.04	1.36	783	181
138	50	15	0.29	29.04	1.36	643	112
139	50	15	0.29	29.04	1.36	610	136
140	50	15	0.29	29.04	1.36	538	108
141	50	15	0.29	29.04	1.36	747	148
142	50	15	0.29	29.04	1.36	620	126
143	50	15	0.29	29.04	1.36	686	135
144	50	15	0.29	29.04	1.36	520	98
145	40	5	0.29	29.04	1.36	629	80
146	40	5	0.29	29.04	1.36	553	75
147	40	5	0.29	29.04	1.36	491	75
148	40	5	0.29	29.04	1.36	432	80
149	40	5	0.29	29.04	1.36	840	80
150	40	5	0.29	29.04	1.36	703	83
151	40	5	0.29	29.04	1.36	586	92
152	40	5	0.29	29.04	1.36	500	107
153	40	25	0.29	29.04	1.36	695	94
154	40	25	0.29	29.04	1.36	449	97
155	40	25	0.29	29.04	1.36	532	84
156	40	25	0.29	29.04	1.36	422	81
157	40	25	0.29	29.04	1.36	788	98
158	40	25	0.29	29.04	1.36	620	98
159	40	25	0.29	29.04	1.36	596	90
160	40	25	0.29	29.04	1.36	482	74
161	40	15	0.14	22.57	1.16	642	93
162	40	15	0.14	22.57	1.16	456	82
163	40	15	0.14	22.57	1.16	454	88
164	40	15	0.14	22.57	1.16	385	81
165	40	15	0.14	22.57	1.16	704	101
166	40	15	0.14	22.57	1.16	557	89
167	40	15	0.14	22.57	1.16	538	81
168	40	15	0.14	22.57	1.16	487	77
169	40	15	0.20	22.60	1.49	971	151
170	40	15	0.20	22.60	1.49	731	138
171	40	15	0.20	22.60	1.49	780	112

	Process Parameters		Material Properties			Responses	
Sample	Linear Pressure (lb/in.)	Speed (m/min)	Dynamic Viscosity (mPa-s)	Surface Tension dynes/cm	Density (g/cm^3)	Thick_ave (nm)	Ra_ave (nm)
172	40	15	0.20	22.60	1.49	650	109
173	40	15	0.20	22.60	1.49	1120	244
174	40	15	0.20	22.60	1.49	878	182
175	40	15	0.20	22.60	1.49	1052	276
176	40	15	0.20	22.60	1.49	756	129
177	40	15	0.30	27.46	1.30	548	84
178	40	15	0.30	27.46	1.30	463	109
179	40	15	0.30	27.46	1.30	630	99
180	40	15	0.30	27.46	1.30	510	78
181	40	15	0.30	27.46	1.30	793	101
182	40	15	0.30	27.46	1.30	525	72
183	40	15	0.30	27.46	1.30	682	84
184	40	15	0.30	27.46	1.30	546	68
185	40	15	0.07	27.29	1.28	641	90
186	40	15	0.07	27.29	1.28	586	78
187	40	15	0.07	27.29	1.28	491	66
188	40	15	0.07	27.29	1.28	408	63
189	40	15	0.07	27.29	1.28	606	92
190	40	15	0.07	27.29	1.28	560	89
191	40	15	0.07	27.29	1.28	550	82
192	40	15	0.07	27.29	1.28	490	59
193	40	15	0.29	29.04	1.36	697	128
194	40	15	0.29	29.04	1.36	525	117
195	40	15	0.29	29.04	1.36	569	113
196	40	15	0.29	29.04	1.36	470	103
197	40	15	0.29	29.04	1.36	791	144
198	40	15	0.29	29.04	1.36	666	148
199	40	15	0.29	29.04	1.36	624	148
200	40	15	0.29	29.04	1.36	533	109
201	40	15	0.29	29.04	1.36	758	138
202	40	15	0.29	29.04	1.36	525	110
203	40	15	0.29	29.04	1.36	615	122
204	40	15	0.29	29.04	1.36	466	127
205	40	15	0.29	29.04	1.36	794	121
206	40	15	0.29	29.04	1.36	661	126
207	40	15	0.29	29.04	1.36	695	148
208	40	15	0.29	29.04	1.36	596	118
209	40	15	0.29	29.04	1.36	758	193
210	40	15	0.29	29.04	1.36	539	138
211	40	15	0.29	29.04	1.36	587	153
212	40	15	0.29	29.04	1.36	518	104
213	40	15	0.29	29.04	1.36	969	220
214	40	15	0.29	29.04	1.36	684	142

	Process Parameters		Material Properties			Responses	
Sample	Linear Pressure (lb/in.)	Speed (m/min)	Dynamic Viscosity (mPa-s)	Surface Tension dynes/cm	Density (g/cm^3)	Thick_ave (nm)	Ra_ave (nm)
215	40	15	0.29	29.04	1.36	692	176
216	40	15	0.29	29.04	1.36	616	124
217	40	15	0.29	29.04	1.36	624	79
218	40	15	0.29	29.04	1.36	558	71
219	40	15	0.29	29.04	1.36	518	76
220	40	15	0.29	29.04	1.36	405	72
221	40	15	0.29	29.04	1.36	732	93
222	40	15	0.29	29.04	1.36	636	92
223	40	15	0.29	29.04	1.36	585	80
224	40	15	0.29	29.04	1.36	496	80
225	35	10	0.24	23.55	1.25	667	103
226	35	10	0.24	23.55	1.25	588	91
227	35	10	0.24	23.55	1.25	503	86
228	35	10	0.24	23.55	1.25	391	80
229	35	10	0.24	23.55	1.25	779	103
230	35	10	0.24	23.55	1.25	581	92
231	35	10	0.24	23.55	1.25	588	89
232	35	10	0.24	23.55	1.25	483	89

Table C.10: Fundamental parameters for thickness and roughness, part 2

	Cell factors			Ratios		Other
Sample	Cell Volume (μm^3)	Aspect Ratio	Cell surface area (%)	ITO/ Binder	Solid/ Solvent	Dwell Time (s)
1	16427	0.35	79.46	2.73	0.69	0.09
2	13139	0.32	64.82	2.73	0.69	0.09
3	10026	0.58	79.79	2.73	0.69	0.09
4	8311	0.55	68.34	2.73	0.69	0.09
5	33044	0.25	80.33	2.73	0.69	0.09
6	22815	0.27	66.56	2.73	0.69	0.09
7	16070	0.51	80.37	2.73	0.69	0.09
8	12111	0.51	66.25	2.73	0.69	0.09
9	16427	0.35	79.46	2.73	0.69	0.102
10	13139	0.32	64.82	2.73	0.69	0.102
11	10026	0.58	79.79	2.73	0.69	0.102
12	8311	0.55	68.34	2.73	0.69	0.102
13	33044	0.25	80.33	2.73	0.69	0.102
14	22815	0.27	66.56	2.73	0.69	0.102
15	16070	0.51	80.37	2.73	0.69	0.102
16	12111	0.51	66.25	2.73	0.69	0.102
17	16427	0.35	79.46	2.73	0.69	0.045
18	13139	0.32	64.82	2.73	0.69	0.045
19	10026	0.58	79.79	2.73	0.69	0.045
20	8311	0.55	68.34	2.73	0.69	0.045
21	33044	0.25	80.33	2.73	0.69	0.045
22	22815	0.27	66.56	2.73	0.69	0.045
23	16070	0.51	80.37	2.73	0.69	0.045
24	12111	0.51	66.25	2.73	0.69	0.045
25	16427	0.35	79.46	2.73	0.69	0.051
26	13139	0.32	64.82	2.73	0.69	0.051
27	10026	0.58	79.79	2.73	0.69	0.051
28	8311	0.55	68.34	2.73	0.69	0.051
29	33044	0.25	80.33	2.73	0.69	0.051
30	22815	0.27	66.56	2.73	0.69	0.051
31	16070	0.51	80.37	2.73	0.69	0.051
32	12111	0.51	66.25	2.73	0.69	0.051
33	16427	0.35	79.46	4.44	0.96	0.09
34	13139	0.32	64.82	4.44	0.96	0.09
35	10026	0.58	79.79	4.44	0.96	0.09
36	8311	0.55	68.34	4.44	0.96	0.09
37	33044	0.25	80.33	4.44	0.96	0.09
38	22815	0.27	66.56	4.44	0.96	0.09
39	16070	0.51	80.37	4.44	0.96	0.09
40	12111	0.51	66.25	4.44	0.96	0.09
41	16427	0.35	79.46	4.44	0.96	0.102
42	13139	0.32	64.82	4.44	0.96	0.102

	Cell factors			Ratios		Other
Sample	Cell Volume (μm^3)	Aspect Ratio	Cell surface area (%)	ITO/ Binder	Solid/ Solvent	Dwell Time (s)
43	10026	0.58	79.79	4.44	0.96	0.102
44	8311	0.55	68.34	4.44	0.96	0.102
45	33044	0.25	80.33	4.44	0.96	0.102
46	22815	0.27	66.56	4.44	0.96	0.102
47	16070	0.51	80.37	4.44	0.96	0.102
48	12111	0.51	66.25	4.44	0.96	0.102
49	16427	0.35	79.46	4.44	0.96	0.045
50	13139	0.32	64.82	4.44	0.96	0.045
51	10026	0.58	79.79	4.44	0.96	0.045
52	8311	0.55	68.34	4.44	0.96	0.045
53	33044	0.25	80.33	4.44	0.96	0.045
54	22815	0.27	66.56	4.44	0.96	0.045
55	16070	0.51	80.37	4.44	0.96	0.045
56	12111	0.51	66.25	4.44	0.96	0.045
57	16427	0.35	79.46	4.44	0.96	0.051
58	13139	0.32	64.82	4.44	0.96	0.051
59	10026	0.58	79.79	4.44	0.96	0.051
60	8311	0.55	68.34	4.44	0.96	0.051
61	33044	0.25	80.33	4.44	0.96	0.051
62	22815	0.27	66.56	4.44	0.96	0.051
63	16070	0.51	80.37	4.44	0.96	0.051
64	12111	0.51	66.25	4.44	0.96	0.051
65	16427	0.35	79.46	3.33	0.64	0.09
66	13139	0.32	64.82	3.33	0.64	0.09
67	10026	0.58	79.79	3.33	0.64	0.09
68	8311	0.55	68.34	3.33	0.64	0.09
69	33044	0.25	80.33	3.33	0.64	0.09
70	22815	0.27	66.56	3.33	0.64	0.09
71	16070	0.51	80.37	3.33	0.64	0.09
72	12111	0.51	66.25	3.33	0.64	0.09
73	16427	0.35	79.46	3.33	0.64	0.102
74	13139	0.32	64.82	3.33	0.64	0.102
75	10026	0.58	79.79	3.33	0.64	0.102
76	8311	0.55	68.34	3.33	0.64	0.102
77	33044	0.25	80.33	3.33	0.64	0.102
78	22815	0.27	66.56	3.33	0.64	0.102
79	16070	0.51	80.37	3.33	0.64	0.102
80	12111	0.51	66.25	3.33	0.64	0.102
81	16427	0.35	79.46	3.33	0.64	0.045
82	13139	0.32	64.82	3.33	0.64	0.045
83	10026	0.58	79.79	3.33	0.64	0.045
84	8311	0.55	68.34	3.33	0.64	0.045
85	33044	0.25	80.33	3.33	0.64	0.045
86	22815	0.27	66.56	3.33	0.64	0.045

	Cell factors			Ratios		Other
Sample	Cell Volume (μm^3)	Aspect Ratio	Cell surface area (%)	ITO/ Binder	Solid/ Solvent	Dwell Time (s)
87	16070	0.51	80.37	3.33	0.64	0.045
88	12111	0.51	66.25	3.33	0.64	0.045
89	16427	0.35	79.46	3.33	0.64	0.051
90	13139	0.32	64.82	3.33	0.64	0.051
91	10026	0.58	79.79	3.33	0.64	0.051
92	8311	0.55	68.34	3.33	0.64	0.051
93	33044	0.25	80.33	3.33	0.64	0.051
94	22815	0.27	66.56	3.33	0.64	0.051
95	16070	0.51	80.37	3.33	0.64	0.051
96	12111	0.51	66.25	3.33	0.64	0.051
97	16427	0.35	79.46	5.71	0.89	0.09
98	13139	0.32	64.82	5.71	0.89	0.09
99	10026	0.58	79.79	5.71	0.89	0.09
100	8311	0.55	68.34	5.71	0.89	0.09
101	33044	0.25	80.33	5.71	0.89	0.09
102	22815	0.27	66.56	5.71	0.89	0.09
103	16070	0.51	80.37	5.71	0.89	0.09
104	12111	0.51	66.25	5.71	0.89	0.09
105	16427	0.35	79.46	5.71	0.89	0.102
106	13139	0.32	64.82	5.71	0.89	0.102
107	10026	0.58	79.79	5.71	0.89	0.102
108	8311	0.55	68.34	5.71	0.89	0.102
109	33044	0.25	80.33	5.71	0.89	0.102
110	22815	0.27	66.56	5.71	0.89	0.102
111	16070	0.51	80.37	5.71	0.89	0.102
112	12111	0.51	66.25	5.71	0.89	0.102
113	16427	0.35	79.46	5.71	0.89	0.045
114	13139	0.32	64.82	5.71	0.89	0.045
115	10026	0.58	79.79	5.71	0.89	0.045
116	8311	0.55	68.34	5.71	0.89	0.045
117	33044	0.25	80.33	5.71	0.89	0.045
118	22815	0.27	66.56	5.71	0.89	0.045
119	16070	0.51	80.37	5.71	0.89	0.045
120	12111	0.51	66.25	5.71	0.89	0.045
121	16427	0.35	79.46	5.71	0.89	0.051
122	13139	0.32	64.82	5.71	0.89	0.051
123	10026	0.58	79.79	5.71	0.89	0.051
124	8311	0.55	68.34	5.71	0.89	0.051
125	33044	0.25	80.33	5.71	0.89	0.051
126	22815	0.27	66.56	5.71	0.89	0.051
127	16070	0.51	80.37	5.71	0.89	0.051
128	12111	0.51	66.25	5.71	0.89	0.051
129	16427	0.35	79.46	3.89	0.79	0.054
130	13139	0.32	64.82	3.89	0.79	0.054

	Cell factors			Ratios		Other
Sample	Cell Volume (μm^3)	Aspect Ratio	Cell surface area (%)	ITO/ Binder	Solid/ Solvent	Dwell Time (s)
131	10026	0.58	79.79	3.89	0.79	0.054
132	8311	0.55	68.34	3.89	0.79	0.054
133	33044	0.25	80.33	3.89	0.79	0.054
134	22815	0.27	66.56	3.89	0.79	0.054
135	16070	0.51	80.37	3.89	0.79	0.054
136	12111	0.51	66.25	3.89	0.79	0.054
137	16427	0.35	79.46	3.89	0.79	0.07
138	13139	0.32	64.82	3.89	0.79	0.07
139	10026	0.58	79.79	3.89	0.79	0.07
140	8311	0.55	68.34	3.89	0.79	0.07
141	33044	0.25	80.33	3.89	0.79	0.07
142	22815	0.27	66.56	3.89	0.79	0.07
143	16070	0.51	80.37	3.89	0.79	0.07
144	12111	0.51	66.25	3.89	0.79	0.07
145	16427	0.35	79.46	3.89	0.79	0.198
146	13139	0.32	64.82	3.89	0.79	0.198
147	10026	0.58	79.79	3.89	0.79	0.198
148	8311	0.55	68.34	3.89	0.79	0.198
149	33044	0.25	80.33	3.89	0.79	0.198
150	22815	0.27	66.56	3.89	0.79	0.198
151	16070	0.51	80.37	3.89	0.79	0.198
152	12111	0.51	66.25	3.89	0.79	0.198
153	16427	0.35	79.46	3.89	0.79	0.0396
154	13139	0.32	64.82	3.89	0.79	0.0396
155	10026	0.58	79.79	3.89	0.79	0.0396
156	8311	0.55	68.34	3.89	0.79	0.0396
157	33044	0.25	80.33	3.89	0.79	0.0396
158	22815	0.27	66.56	3.89	0.79	0.0396
159	16070	0.51	80.37	3.89	0.79	0.0396
160	12111	0.51	66.25	3.89	0.79	0.0396
161	16427	0.35	79.46	2.27	0.56	0.066
162	13139	0.32	64.82	2.27	0.56	0.066
163	10026	0.58	79.79	2.27	0.56	0.066
164	8311	0.55	68.34	2.27	0.56	0.066
165	33044	0.25	80.33	2.27	0.56	0.066
166	22815	0.27	66.56	2.27	0.56	0.066
167	16070	0.51	80.37	2.27	0.56	0.066
168	12111	0.51	66.25	2.27	0.56	0.066
169	16427	0.35	79.46	6.43	1.08	0.066
170	13139	0.32	64.82	6.43	1.08	0.066
171	10026	0.58	79.79	6.43	1.08	0.066
172	8311	0.55	68.34	6.43	1.08	0.066
173	33044	0.25	80.33	6.43	1.08	0.066
174	22815	0.27	66.56	6.43	1.08	0.066

	Cell factors			Ratios		Other
Sample	Cell Volume (μm^3)	Aspect Ratio	Cell surface area (%)	ITO/ Binder	Solid/ Solvent	Dwell Time (s)
175	16070	0.51	80.37	6.43	1.08	0.066
176	12111	0.51	66.25	6.43	1.08	0.066
177	16427	0.35	79.46	3.18	0.85	0.066
178	13139	0.32	64.82	3.18	0.85	0.066
179	10026	0.58	79.79	3.18	0.85	0.066
180	8311	0.55	68.34	3.18	0.85	0.066
181	33044	0.25	80.33	3.18	0.85	0.066
182	22815	0.27	66.56	3.18	0.85	0.066
183	16070	0.51	80.37	3.18	0.85	0.066
184	12111	0.51	66.25	3.18	0.85	0.066
185	16427	0.35	79.46	5.00	0.72	0.066
186	13139	0.32	64.82	5.00	0.72	0.066
187	10026	0.58	79.79	5.00	0.72	0.066
188	8311	0.55	68.34	5.00	0.72	0.066
189	33044	0.25	80.33	5.00	0.72	0.066
190	22815	0.27	66.56	5.00	0.72	0.066
191	16070	0.51	80.37	5.00	0.72	0.066
192	12111	0.51	66.25	5.00	0.72	0.066
193	16427	0.35	79.46	3.89	0.79	0.066
194	13139	0.32	64.82	3.89	0.79	0.066
195	10026	0.58	79.79	3.89	0.79	0.066
196	8311	0.55	68.34	3.89	0.79	0.066
197	33044	0.25	80.33	3.89	0.79	0.066
198	22815	0.27	66.56	3.89	0.79	0.066
199	16070	0.51	80.37	3.89	0.79	0.066
200	12111	0.51	66.25	3.89	0.79	0.066
201	16427	0.35	79.46	3.89	0.79	0.066
202	13139	0.32	64.82	3.89	0.79	0.066
203	10026	0.58	79.79	3.89	0.79	0.066
204	8311	0.55	68.34	3.89	0.79	0.066
205	33044	0.25	80.33	3.89	0.79	0.066
206	22815	0.27	66.56	3.89	0.79	0.066
207	16070	0.51	80.37	3.89	0.79	0.066
208	12111	0.51	66.25	3.89	0.79	0.066
209	16427	0.35	79.46	3.89	0.79	0.066
210	13139	0.32	64.82	3.89	0.79	0.066
211	10026	0.58	79.79	3.89	0.79	0.066
212	8311	0.55	68.34	3.89	0.79	0.066
213	33044	0.25	80.33	3.89	0.79	0.066
214	22815	0.27	66.56	3.89	0.79	0.066
215	16070	0.51	80.37	3.89	0.79	0.066
216	12111	0.51	66.25	3.89	0.79	0.066
217	16427	0.35	79.46	3.89	0.79	0.066
218	13139	0.32	64.82	3.89	0.79	0.066

	Cell factors			Ratios		Other
Sample	Cell Volume (μm^3)	Aspect Ratio	Cell surface area (%)	ITO/ Binder	Solid/ Solvent	Dwell Time (s)
219	10026	0.58	79.79	3.89	0.79	0.066
220	8311	0.55	68.34	3.89	0.79	0.066
221	33044	0.25	80.33	3.89	0.79	0.066
222	22815	0.27	66.56	3.89	0.79	0.066
223	16070	0.51	80.37	3.89	0.79	0.066
224	12111	0.51	66.25	3.89	0.79	0.066
225	16427	0.35	79.46	2.73	0.69	0.09
226	13139	0.32	64.82	2.73	0.69	0.09
227	10026	0.58	79.79	2.73	0.69	0.09
228	8311	0.55	68.34	2.73	0.69	0.09
229	33044	0.25	80.33	2.73	0.69	0.09
230	22815	0.27	66.56	2.73	0.69	0.09
231	16070	0.51	80.37	2.73	0.69	0.09
232	12111	0.51	66.25	2.73	0.69	0.09

Table C.11: Fundamental parameters for sheet resistance and transparency, part 1

	Process Parameters		Material Properties			Responses	
Sample	Linear Pressure (lb/in.)	Speed (m/min)	Dynamic Viscosity (mPa-s)	Surface Tension dynes/cm	Density (g/cm^3)	Thick_ave (nm)	Ra_ave (nm)
1	35	10	0.24	23.55	1.25	675	90
5	35	10	0.24	23.55	1.25	841	109
14	45	10	0.24	23.55	1.25	681	112
19	35	20	0.24	23.55	1.25	524	81
20	35	20	0.24	23.55	1.25	437	71
33	35	10	0.34	23.76	1.41	764	237
34	35	10	0.34	23.76	1.41	581	140
37	35	10	0.34	23.76	1.41	999	238
41	45	10	0.34	23.76	1.41	743	157
42	45	10	0.34	23.76	1.41	588	132
45	45	10	0.34	23.76	1.41	849	194
46	45	10	0.34	23.76	1.41	826	125
47	45	10	0.34	23.76	1.41	793	157
50	35	20	0.34	23.76	1.41	536	87
51	35	20	0.34	23.76	1.41	590	104
52	35	20	0.34	23.76	1.41	452	84
60	45	20	0.34	23.76	1.41	461	90
61	45	20	0.34	23.76	1.41	827	99
63	45	20	0.34	23.76	1.41	648	124
65	35	10	0.12	23.67	1.19	603	83
69	35	10	0.12	23.67	1.19	717	78
74	45	10	0.12	23.67	1.19	471	67
77	45	10	0.12	23.67	1.19	688	84
78	45	10	0.12	23.67	1.19	774	69
82	35	20	0.12	23.67	1.19	497	60
84	35	20	0.12	23.67	1.19	398	60
87	35	20	0.12	23.67	1.19	595	76
89	45	20	0.12	23.67	1.19	599	63
91	45	20	0.12	23.67	1.19	506	73
97	35	10	0.14	18.28	1.40	767	163
101	35	10	0.14	18.28	1.40	1264	250
102	35	10	0.14	18.28	1.40	891	216
107	45	10	0.14	18.28	1.40	492	82
108	45	10	0.14	18.28	1.40	418	77
117	35	20	0.14	18.28	1.40	783	166
118	35	20	0.14	18.28	1.40	580	104
121	45	20	0.14	18.28	1.40	731	140
122	45	20	0.14	18.28	1.40	575	128
123	45	20	0.14	18.28	1.40	712	131
124	45	20	0.14	18.28	1.40	601	109
125	45	20	0.14	18.28	1.40	924	148
127	45	20	0.14	18.28	1.40	660	139

	Process Parameters		Material Properties			Responses	
Sample	Linear Pressure (lb/in.)	Speed (m/min)	Dynamic Viscosity (mPa-s)	Surface Tension dynes/cm	Density (g/cm^3)	Thick_ave (nm)	Ra_ave (nm)
129	30	15	0.29	29.04	1.36	692	127
132	30	15	0.29	29.04	1.36	450	91
135	30	15	0.29	29.04	1.36	712	139
138	50	15	0.29	29.04	1.36	643	112
170	40	15	0.20	22.60	1.49	731	138
171	40	15	0.20	22.60	1.49	780	112
172	40	15	0.20	22.60	1.49	650	109
173	40	15	0.20	22.60	1.49	1120	244
174	40	15	0.20	22.60	1.49	878	182
175	40	15	0.20	22.60	1.49	1052	276
176	40	15	0.20	22.60	1.49	756	129
177	40	15	0.30	27.46	1.30	548	84
181	40	15	0.30	27.46	1.30	793	101
183	40	15	0.30	27.46	1.30	682	84
184	40	15	0.30	27.46	1.30	546	68
185	40	15	0.07	27.29	1.28	641	90
187	40	15	0.07	27.29	1.28	491	66
188	40	15	0.07	27.29	1.28	408	63
190	40	15	0.07	27.29	1.28	560	89
193	40	15	0.29	29.04	1.36	697	128
195	40	15	0.29	29.04	1.36	569	113
199	40	15	0.29	29.04	1.36	624	148
201	40	15	0.29	29.04	1.36	758	138
203	40	15	0.29	29.04	1.36	615	122
208	40	15	0.29	29.04	1.36	596	118
209	40	15	0.29	29.04	1.36	758	193
211	40	15	0.29	29.04	1.36	587	153
212	40	15	0.29	29.04	1.36	518	104
215	40	15	0.29	29.04	1.36	692	176
217	40	15	0.29	29.04	1.36	624	79
219	40	15	0.29	29.04	1.36	518	76
221	40	15	0.29	29.04	1.36	732	93
225	35	10	0.24	23.55	1.25	667	103

Table C.12: Fundamental parameters for sheet resistance and transparency, part 2

	Cell factors			Ratios		Other
Sample	Cell Volume (μm^3)	Aspect Ratio	Cell surface area (%)	ITO/ Binder	Solid/ Solvent	Dwell Time (s)
1	16427	0.35	79.46	2.73	0.69	0.09
5	33044	0.25	80.33	2.73	0.69	0.09
14	22815	0.27	66.56	2.73	0.69	0.102
19	10026	0.58	79.79	2.73	0.69	0.045
20	8311	0.55	68.34	2.73	0.69	0.045
33	16427	0.35	79.46	4.44	0.96	0.09
34	13139	0.32	64.82	4.44	0.96	0.09
37	33044	0.25	80.33	4.44	0.96	0.09
41	16427	0.35	79.46	4.44	0.96	0.102
42	13139	0.32	64.82	4.44	0.96	0.102
45	33044	0.25	80.33	4.44	0.96	0.102
46	22815	0.27	66.56	4.44	0.96	0.102
47	16070	0.51	80.37	4.44	0.96	0.102
50	13139	0.32	64.82	4.44	0.96	0.045
51	10026	0.58	79.79	4.44	0.96	0.045
52	8311	0.55	68.34	4.44	0.96	0.045
60	8311	0.55	68.34	4.44	0.96	0.051
61	33044	0.25	80.33	4.44	0.96	0.051
63	16070	0.51	80.37	4.44	0.96	0.051
65	16427	0.35	79.46	3.33	0.64	0.09
69	33044	0.25	80.33	3.33	0.64	0.09
74	13139	0.32	64.82	3.33	0.64	0.102
77	33044	0.25	80.33	3.33	0.64	0.102
78	22815	0.27	66.56	3.33	0.64	0.102
82	13139	0.32	64.82	3.33	0.64	0.045
84	8311	0.55	68.34	3.33	0.64	0.045
87	16070	0.51	80.37	3.33	0.64	0.045
89	16427	0.35	79.46	3.33	0.64	0.051
91	10026	0.58	79.79	3.33	0.64	0.051
97	16427	0.35	79.46	5.71	0.89	0.09
101	33044	0.25	80.33	5.71	0.89	0.09
102	22815	0.27	66.56	5.71	0.89	0.09
107	10026	0.58	79.79	5.71	0.89	0.102
108	8311	0.55	68.34	5.71	0.89	0.102
117	33044	0.25	80.33	5.71	0.89	0.045
118	22815	0.27	66.56	5.71	0.89	0.045
121	16427	0.35	79.46	5.71	0.89	0.051
122	13139	0.32	64.82	5.71	0.89	0.051
123	10026	0.58	79.79	5.71	0.89	0.051
124	8311	0.55	68.34	5.71	0.89	0.051
125	33044	0.25	80.33	5.71	0.89	0.051
127	16070	0.51	80.37	5.71	0.89	0.051

	Cell factors			Ratios		Other
Sample	Cell Volume (μm^3)	Aspect Ratio	Cell surface area (%)	ITO/ Binder	Solid/ Solvent	Dwell Time (s)
129	16427	0.35	79.46	3.89	0.79	0.054
132	8311	0.55	68.34	3.89	0.79	0.054
135	16070	0.51	80.37	3.89	0.79	0.054
138	13139	0.32	64.82	3.89	0.79	0.07
170	13139	0.32	64.82	6.43	1.08	0.066
171	10026	0.58	79.79	6.43	1.08	0.066
172	8311	0.55	68.34	6.43	1.08	0.066
173	33044	0.25	80.33	6.43	1.08	0.066
174	22815	0.27	66.56	6.43	1.08	0.066
175	16070	0.51	80.37	6.43	1.08	0.066
176	12111	0.51	66.25	6.43	1.08	0.066
177	16427	0.35	79.46	3.18	0.85	0.066
181	33044	0.25	80.33	3.18	0.85	0.066
183	16070	0.51	80.37	3.18	0.85	0.066
184	12111	0.51	66.25	3.18	0.85	0.066
185	16427	0.35	79.46	5.00	0.72	0.066
187	10026	0.58	79.79	5.00	0.72	0.066
188	8311	0.55	68.34	5.00	0.72	0.066
190	22815	0.27	66.56	5.00	0.72	0.066
193	16427	0.35	79.46	3.89	0.79	0.066
195	10026	0.58	79.79	3.89	0.79	0.066
199	16070	0.51	80.37	3.89	0.79	0.066
201	16427	0.35	79.46	3.89	0.79	0.066
203	10026	0.58	79.79	3.89	0.79	0.066
208	12111	0.51	66.25	3.89	0.79	0.066
209	16427	0.35	79.46	3.89	0.79	0.066
211	10026	0.58	79.79	3.89	0.79	0.066
212	8311	0.55	68.34	3.89	0.79	0.066
215	16070	0.51	80.37	3.89	0.79	0.066
217	16427	0.35	79.46	3.89	0.79	0.066
219	10026	0.58	79.79	3.89	0.79	0.066
221	33044	0.25	80.33	3.89	0.79	0.066
225	16427	0.35	79.46	2.73	0.69	0.09

REFERENCES

[1] Gillett, E.K. (2003) *Gravure: Process and Technology*, GAA

[2] Yin, X. and S. Kumar (2006). "Flow visualization of the liquid emptying process in scaled-up gravure grooves and cells." Chemical Engineering Science 61(4): 1146-1156.

[3] Gamota, R.D., Brazis, P., Kalyanasundaram, K., Zhang, J., (2004) *Printed Organic and Molecular Electronics*, Kluwer Academic Publishers, Norwell, MA

[4] Benkreira, H. and R. Patel (1993). "Direct gravure roll coating." Chemical Engineering Science 48(12): 2329-2335.

[5] Hennig, G., K.-H. Selbmann, et al. (2006). "Laser engraving in gravure industry", Dresden, Germany, International Society for Optical Engineering, Bellingham WA, WA 98227-0010, United States.

[6] Leach, R. H., and R. J. Pierce, (1993) *The Printing Ink Manual, 5th Ed*., Blueprint, London, UK.

[7] Joyce, E. and G. L. Fuchs (1966). "Study of Gravure Ink Transfer." Paper Technology 10(2): 96-105.

[8] Bery, Y. A. (1985). "Mechanisms Governing Gravure Printing", TAPPI Press, Atlanta, GA, USA.

[9] Schwartz, L. W., P. Moussalli, et al. (1998). "Numerical modelling of liquid withdrawal from gravure cavities in coating operations." Chemical Engineering Research & Design, Transactions of the Institute of Chemical Engineers, Part A 76(A1): 22-28.

[10] Powell, C. A., M. D. Savage, et al. (2000). "Modeling the meniscus evacuation problem in direct gravure coating." Chemical Engineering Research and Design, Transactions of the Institute of Chemical Engineers, Part A 78(1): 61-67.

[11] Ahn, S. and Y. Na. (2007). "On the ink transfer process in gravure printing". Kuala Lumpur, Malaysia: Springer Verlag, Heidelberg, D-69121, Germany.

[12] Bohan, M. F. J., T. C. Claypole, et al. (1998). “Investigation into ink transfer in rotogravure printing”, Chicago, IL, USA, TAGA, Rochester, NY, USA.

[13] Bohan, M. F. J., T. C. Claypole, et al. (2000). "Effect of process parameters on product quality of rotogravure printing." Proceedings of the Institution of Mechanical Engineers, Part B: Journal of Engineering Manufacture 214(3): 205-219.

[14] Bohan, M. F. J., I. J. Fox, et al. (2002). Parametric study of the flow in printing and coating nips: The influence of non-Newtonian fluids, Asheville, NC, United States, Technical Association of the Graphic Arts.

[15] Benkreira, H. and O. Cohu (1998). "Direct forward gravure coating on unsupported web." Chemical Engineering Science 53(6): 1223-1231.

[16] Ederth, J., A. Hultaker, et al. (2002). "Electrical and optical properties of thin films prepared by spin coating a dispersion of nano-sized tin-doped indium oxide particles." Smart Materials and Structures 11(5): 675-8.

[17] Cairns, D. R. and G. P. Crawford (2005). "Electromechanical properties of transparent conducting substrates for flexible electronic displays." Proceedings of the IEEE 93(8): 1451-1458.

[18] Chen, Z., B. Cotterell, and W. Wang, “The fracture of brittle thin films on compliant substrates in flexible displays”. Engineering Fracture Mechanics, 2002. **69**(5): p. 597-603.

[19] Leterrier, Y. et al. “Mechanical Integrity of Transparent Conductive Oxide Films for Flexible Polymer-based Displays” Thin Solid Films vol. 460, pp.156-166, 2004

[20] Ederth, J., P. Heszler, et al. (2003). “Indium tin oxide films made from nanoparticles: Models for the optical and electrical properties”. Tokyo, Japan, Elsevier.

[21] Ederth, J., A. Hultaker, et al. (2002). "Electrical and optical properties of thin films prepared by spin coating a dispersion of nano-sized tin-doped indium oxide particles." Smart Materials and Structures 11(5): 675-8.

[22] Ederth, J., A. Hultaker, et al. (2005). "Thin porous indium tin oxide nanoparticle films: effects of annealing in vacuum and air." Applied Physics A (Materials Science Processing) A81(7): 1363-8.

[23] Ederth, J., G. A. Niklasson, et al. (2003). "Characterization of porous indium tin oxide thin films using effective medium theory." Journal of Applied Physics 93(2): 984-988.

[24] Ogi, T., F. Iskandar, et al. (2006). "Characterization of dip-coated ITO films derived from nanoparticles synthesized by low-pressure spray pyrolysis." Journal of Nanoparticle Research 8(3-4): 343-350.

[25] Ginley, D., M.A. Green, and R. Collins, (2008). "Solar energy conversion toward 1 terawatt". MRS Bulletin, 33(4): p. 355-364.

[26] Aernouts, T., T. Aleksandrov, et al. (2008). "Polymer based organic solar cells using ink-jet printed active layers." Applied Physics Letters 92(3): 033306.

[27] Claypole, Tim C. et al., (2004) "Micro-electronic printing: The state of the art, current research activities and the future potential". San Antonio, TX, United States: Technical Association of the Graphic Arts, Rochester, NY 14623-5604, United States.

[28] De Gans, B.-J. and U. S. Schubert (2004). "Inkjet printing of well-defined polymer dots and arrays." Langmuir 20(18): 7789-7793.

[29] Hoth, C. N., S. A. Choulis, et al. (2007). "High photovoltaic performance of inkjet printed polymer:Fullerene blends." Advanced Materials 19(22): 3973-3978.

[30] Schubert, U. S. (2006). "Inkjet printing of functional polymers and nanoparticles". Denver, CO, USA, Society for Imaging Science and Technology.

[31] Hagberg, J., M. Kittila, et al. (2002). "Fine line LTCC-structures by direct gravure printing (DGP) method", Denver, CO, United States, The International Society for Optical Engineering.

[32] Brabec, C. J. (2004). "Organic photovoltaics: Technology and market." Solar Energy Materials and Solar Cells 83(2-3): 273-292.

[33] Brabec, C. J., J. A. Hauch, et al. (2005). "Production aspects of organic photovoltaics and their impact on the commercialization of devices." MRS Bulletin 30(1): 50-52.

[34] Brabec, C. J., T. Nann, et al. (2004). "Nanostructured p-n junctions for printable photovoltaics." MRS Bulletin 29(1): 43-47.

[35] Pudas, M., N. Halonen, et al. (2005). "Gravure printing of conductive particulate polymer inks on flexible substrates." Progress in Organic Coatings 54(4): 310-316.

[36] Puetz, J., S. Heusing, et al. (2005). "Gravure printing of transparent conducting ITO coatings for display applications", Jena, Germany, International Society for Optical Engineering, Bellingham WA, WA 98227-0010, United States.

[37] Tuomikoski, M., R. Suhonen, et al. (2005). "Gravure printed optoelectronic thin films for flexible polymer LEDs and Microsystems", Oulu, Finland, Institute of Electrical and Electronics Engineers Computer Society, Piscataway, NJ 08855-1331, United States.

[38] Puetz, J., and M.A. Aegerter. (2008). "Direct gravure printing of indium tin oxide nanoparticle patterns on polymer foils". Thin Solid Films 516:4495–4501

[39] Ding, J.M., Vornbrock, A.F. et al. (2009). "Patternable polymer bulk heterojunction photovoltaic cells on plastic by rotogravure printing". Solar Energy Materials & Solar Cells 93:459–464

[40] Aernouts, T., P. Vanlaeke, et al. (2004). "Polymer solar cells: Screen-printing as a novel deposition technique", Strasbourg, France, International Society for Optical Engineering, Bellingham, WA 98227-0010, United States.

[41] Krebs, F.C. (2009). "Fabrication and processing of polymer solar cells: A review of printing and coating techniques" Solar Energy Materials & Solar Cells 93:394–412

[42] Sheats, J. R. (2004). "Manufacturing and commercialization issues in organic electronics." Journal of Materials Research 19(7): pp.1974-1989.

[43] Schmidt, G., H. Kempa, et al. (2006). "Challenges and perspectives of printed electronics", San Diego, CA, United States, International Society for Optical Engineering, Bellingham WA, WA 98227-0010, United States.

[44] Nanophase Technologies, (2009), *Products>>Main Catalog>>Nanoparticles*, Retrieved March 2009 from www.nanophase.com

[45] Bohan, M.F.J., et al. (2001). "Characterisation of gravure cylinders." Proceedings of the Technical Association of the Graphic Arts, San Diego, CA.

[46] Munson, B.R. et al. (2006), *Fundamentals of Fluid Mechanics, 5th Ed.* John Wiley & Sons, USA.

[47] Kutner, M.K., et al., (2004). *Applied Linear Statistical Models,* McGraw-Hill, New York, NY.

[48] ASTM F390, (2003), "Standard Test Method for Sheet Resistance of Thin Metallic Films With a Collinear Four-Probe Array", ASTM.

[49] Schroder, Dieter K. (2006), "Semiconductor Material and Device Characterization". 3rd Ed. Tempe, AZ

[50] Bery,Y.A., (1976), "Gravure Printing on Non-absorbing Materials". Technical Association of the Graphics Arts Proceedings.

[51] Hoth, C.N., et al., (2007). "High photovoltaic performance of inkjet printed polymer:Fullerene blends". Advanced Materials, 19(22): p. 3973-3978.

[52] Kim, D., S. Jeong, et al. (2006). "Direct writing of silver conductive patterns: Improvement of film morphology and conductance by controlling solvent compositions." Applied Physics Letters 89(26): 264101.

[53] Truskett, V.N. and K.J. Stebe, (2003) "Influence of surfactants on an evaporating drop: Fluorescence images and particle deposition patterns". Langmuir, 19(20): p. 8271-8279.

[54] Soltman, D. and V. Subramanian (2008). "Inkjet-printed line morphologies and temperature control of the coffee ring effect." Langmuir 24(5): 2224-2231.